

9-22-2017

# Material Characterization of Intermetallic Compound Formation with Respect to Thermosonic Bonding Duration

Mahin Khan

Santa Clara University, mmkhan@scu.edu

Follow this and additional works at: [https://scholarcommons.scu.edu/mech\\_mstr](https://scholarcommons.scu.edu/mech_mstr)



Part of the [Mechanical Engineering Commons](#)

---

## Recommended Citation

Khan, Mahin, "Material Characterization of Intermetallic Compound Formation with Respect to Thermosonic Bonding Duration" (2017). *Mechanical Engineering Master's Theses*. 18.  
[https://scholarcommons.scu.edu/mech\\_mstr/18](https://scholarcommons.scu.edu/mech_mstr/18)

This Thesis is brought to you for free and open access by the Engineering Master's Theses at Scholar Commons. It has been accepted for inclusion in Mechanical Engineering Master's Theses by an authorized administrator of Scholar Commons. For more information, please contact [rscroggin@scu.edu](mailto:rscroggin@scu.edu).

SANTA CLARA UNIVERSITY

Department of Mechanical Engineering

Date: September 22nd, 2017

I HEREBY RECOMMEND THAT THE THESIS PREPARED UNDER MY

SUPERVISION BY

**MAHIN M KHAN**

ENTITLED

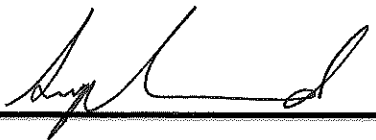
**MATERIAL CHARACTERIZATION OF INTERMETALLIC COMPOUND  
FORMATION WITH RESPECT TO THERMOSONIC BONDING DURATION**

BE ACCEPTED IN PARTIAL FULFILLMENT OF THE REQUIREMENTS

FOR THE DEGREE

OF

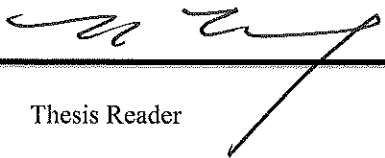
**MASTER OF SCIENCE IN MECHANICAL ENGINEERING**



---

Thesis Advisor

Dr. Panthea Sepehrband



---

Thesis Reader

Dr. Calvin Tszeng



---

Department Chair

Dr. Drazen Fabris

**MATERIAL CHARACTERIZATION OF INTERMETALLIC  
COMPOUND FORMATION WITH RESPECT TO THERMOSONIC  
BONDING DURATION**

By

Mahin M Khan

MASTER THESIS

Submitted in Partial Fulfillment of the Requirements

For the Degree of Master of Science

In Mechanical Engineering at

Santa Clara University, September 2017

Santa Clara, California

Dedicated to my wife Rehnuma and my family for their support.

## **ACKNOWLEDGMENTS**

I wish to express my gratitude to Dr. Sepehrband for her supervision and support. Her sincere guidance and patience helped provide me with an opportunity to learn in great depth. I would also like to express my gratitude to Tessera for their assistance in providing all the wire bonded samples analyzed in this thesis, Mr. Juwon Lee of AQS for providing his service with EDS analysis and Shawn Snyder of Center For Nanostructure (CNS) for her role in training me on SEM use.

This work was supported by Santa Clara University, School of Engineering. Resources for SEM Imaging were provided by Center For Nanostructure at Santa Clara University and sample preparation was performed in the materials lab.

## TABLE OF CONTENTS

<b>LIST OF TABLES</b> .....	<b>vii</b>
<b>LIST OF FIGURES</b> .....	<b>viii</b>
<b>NOMENCLATURE</b> .....	<b>xi</b>
<b>ABSTRACT</b> .....	<b>xiii</b>
<b>CHAPTER 1: INTRODUCTION</b> .....	<b>1</b>
<b>CHAPTER 2: LITERATURE SURVEY</b> .....	<b>3</b>
<b>2.1 Thermosonic Ball Bonding Process</b> .....	<b>3</b>
<b>2.2. Intermetallic Phases and material properties</b> .....	<b>4</b>
<b>2.3 Process of Diffusion</b> .....	<b>6</b>
2.3.1 Diffusion mechanism.....	6
2.3.2 Quantitative Definitions of Diffusion Coefficient .....	7
<b>2.4 Native Aluminum Oxide Layer</b> .....	<b>13</b>
<b>2.5 Bonding Parameters and their effects on IMC formation</b> .....	<b>14</b>
2.5.1 Ultrasonic power and IMC formation.....	14
2.5.2 Bonding duration and IMC formation .....	15
2.5.3 Thermal Aging of Copper-Aluminum bonds and IMC formation .....	16
<b>2.6 Micro-indentation test for IMC identification</b> .....	<b>19</b>
<b>2.5 Research Goal</b> .....	<b>19</b>
<b>CHAPTER 3: EXPERIMENTAL PROCEDURE AND CHARACTERIZATION TECHNIQUES</b> .....	<b>20</b>
<b>3.1 Specimen Preparation</b> .....	<b>20</b>
3.1.1. Cu-Al Wire-Bonds .....	20
3.1.2. Metallographic Specimen Preparation .....	21
3.1.2 Mounting.....	22
3.1.3 Sectioning and Cutting.....	22
3.1.4 Planar Grinding.....	22
3.1.5 Final Polishing.....	23
3.1.6 Charging Effect Neutralization.....	24
<b>3.3 IMC Thickness measurement</b> .....	<b>26</b>
3.3.1 Secondary Electron (SE) vs. Back Scattered Electron Imaging.....	26
3.3.2 Chemical Composition Analysis using Electron Dispersive Spectroscopy (EDS) .....	28
3.3.3 Sample ID Denotation .....	30
<b>3.4 Microhardness test at ball bond interface</b> .....	<b>31</b>
<b>CHAPTER 4: RESULTS AND DISCUSSION</b> .....	<b>34</b>
<b>4.1 BSE Images and IMC Measurement</b> .....	<b>34</b>
4.1.1 Specimen heat treated for 2 hours .....	34
<b>4.2 EDS Analysis of Ball Bond Interface</b> .....	<b>46</b>
4.2.2 Specimen heat treated for 4 hours at 250 ° C .....	52
<b>4.3.1 Indentation Region for samples annealed for 2 hours</b> .....	<b>58</b>
<b>4.3.2 Graphical Representation of Hardness Data for samples annealed for 2 hours</b> .....	<b>60</b>
<b>4.3.3 Indentation Region for samples annealed for 4 hours</b> .....	<b>63</b>

4.3.4 Graphical Representation of Hardness Data for samples annealed for 4 hours.....	65
<b>CHAPTER 5: CONCLUSION .....</b>	<b>69</b>
<b>5.1 Future work and Improvement .....</b>	<b>70</b>
<b>REFERENCES .....</b>	<b>71</b>
<b>APPENDIX A: Effect of anealing time on hardness evolution.....</b>	<b>75</b>

## LIST OF TABLES

Table 1 Properties of CuAl [5] .....	5
Table 2 Average Thickness of IMC based Visual Inspection of BSE Micrograph .....	45
Table 3 Summary of IMC thickness measured with BSE and EDS detection methods .....	57



## LIST OF FIGURES

Figure 1 Ball- Wedge wire bonding cycle [10].	4
Figure 2 Cu-Al Phase Diagram [11].	5
Figure 3 Schematic representations of (a) vacancy diffusion and (b) interstitial diffusion [13].	7
Figure 4 The activation energy Q required to move atoms past one another during diffusion. Substitutional atom requires more energy compared to interstitial atom [5].	8
Figure 5(a) IMC thickness versus annealing time (h). (b) IMC thickness versus annealing time <sup>1/2</sup> [16].	10
Figure 6 Edge and Screw Dislocation [18].	11
Figure 7 Diffusion through an edge dislocation [16].	12
Figure 8 TEM image showing a uniform amorphous native alumina over layer (~5 nm thick) enveloping an Al pad [17].	13
Figure 9 Cross-sectional BSE SEM of copper ball/Al metallization interfaces after aging at 250°C for: (a) 1 hours, (b) 25 hour; (c) 100 h; and (d) 169 hours [25].	15
Figure 10 schematic representations of the intermetallic morphology and evolution at Al-Cu wire-bonds as a function of a heat-treatment time [7].	16
Figure 11 Evolution of the Cu/Al IMC in the Copper bump bonds at 250 °C after aging for a) 1h, (b) 4hrs, (c) 16hrs, (d) 49hrs, (e) 64hrs, (f) 169hrs [24].	17
Figure 12 a) SEM image after 500 hours of annealing at 250 °C. b) Combined thickness for the three IMC phases Al <sub>4</sub> Cu <sub>9</sub> , AlCu and Al <sub>2</sub> Cu, which are observed over a larger temperature range, have been plotted over square root of anneal time [15].	18
Figure 13 Al pad containing 2 rows of Cu-Al ball-wedge bonds with 2.5-mil thick Pd coated Cu wire.	21
Figure 14 Kulicke & Soffa (K&S) iConn ball bonder [27].	21
Figure 15 a) Metallographic specimen encased in epoxy b) Specimen covered in adhesive copper tape to reduce charging effect and increase conductivity inside SEM chamber.	23
Figure 16 (a) Buehler MetaServ grinder/polisher (b) Buehler Isomet 1000 Precision cutter (c) Buehler Handimet 2 Roll Grinder [28].	24
Figure 17 Heating Tube Furnaces.	25
Figure 18 Tescan Mira 3 Scanning Electron Microscope (SEM) [29].	27
Figure 19 Examples of Micrographs of Cu-Al Bond Interface to compare clarity of SE vs. BSE image side by side. a) Image from SE Detector b) Image from BSE Detector.	27
Figure 20 Example showing how a BSE Micrograph scale bar is used to measure IMC thickness (this data does not represent actual sample data, used only for illustration).	28
Figure 21 Example of a BSE Image of Cu-Al interfacial region captured using EDS interface (this data does not represent actual sample data, used only for illustration). The spots on the sample are from plasma vapor deposit coating to reduce sample charging.	29
Figure 22 Example of how line-scan is performed and analyzed (this data does not represent actual sample data) on Cu-Al wire bond interface (a) Area being examined (b) Line-scan signals for each individual element and determination of IMC based on signal strength (b) line-scan spectrum with atomic percent data.	30

Figure 23 Example of a Micrograph that will be used in Results section to illustrate the different marked/numbered indentations and color-coded indentation individual sections (this data does not represent actual sample data and only used for illustration). .....	32
Figure 24 Example of a matlab plot of hardness data (this data does not represent actual sample data).....	33
Figure 25 Leco LM 248 AT Microhardness Tester.....	33
Figure 26 BSE SEM image of different sections of sample 20-250-2 (a) ball bond showing sections that are examined (b) enlarged view of section 1(c) enlarged view of section 2(d) enlarged view of section 3. ....	35
Figure 27 BSE SEM image of different sections of sample 40-250-2 (a) ball bond showing sections that are examined (b) enlarged view of section 1(c) enlarged view of section 2(d) enlarged view of section 3. ....	36
Figure 28 BSE SEM image of different sections of sample 60-250-2 (a) ball bond showing sections that are examined (b) enlarged view of section 1(c) enlarged view of section 2. ....	37
Figure 29 BSE SEM image of different sections of sample 80-250-2 (a) ball bond showing sections that are examined (b) enlarged view of section 1(c) enlarged view of section 2. ....	38
Figure 30 BSE SEM image of different sections of sample 100-250-2 (a) ball bond showing sections that are examined (b) enlarged view of section 1(c) enlarged view of section 2(d) enlarged view of section 3. ....	39
Figure 31 BSE SEM image of different sections of sample 20-250-4 (a) ball bond showing sections that are examined (b) enlarged view of section 1(c) enlarged view of section 2(d) enlarged view of section 3. ....	40
Figure 32 BSE SEM image of different sections of sample 40-250-4 (a) ball bond showing sections that are examined (b) enlarged view of section 1(c) enlarged view of section 2. ....	41
Figure 33 BSE SEM image of different sections of sample 60-250-4 (a) ball bond showing sections that are examined (b) enlarged view of section 1(c) enlarged view of section 2(d) enlarged view of section 3. ....	42
Figure 34 BSE SEM image of different sections of sample 80-250-4 (a) ball bond showing sections that are examined(b) enlarged view of section 1(c) enlarged view of section 2(d) enlarged view of section 3. ....	43
Figure 35 BSE SEM image of different sections of sample 100-250-4 (a) ball bond showing sections that are examined (b) enlarged view of section 1(c) enlarged view of section 2(d) enlarged view of section 3. ....	44
Figure 36 EDS scan results of sample 20-250-2 showing (a) cross-section of IMC analyzed with linescan (b) Intensity plot of line 1 (c) the energy spectrum results of line 1. ....	47
Figure 37 EDS scan results of sample 40-250-2 showing (a) cross-section of IMC analyzed with linescan (b) Intensity plot of line 1. ....	48
Figure 38 EDS scan results of sample 60-250-2 showing (a) cross-section of IMC analyzed with linescan (b) Intensity plot of line 1 (c) the energy spectrum results of line 1. ....	49
Figure 39 EDS scan results of sample 80-250-2 showing (a) cross-section of IMC analyzed with linescan (b) Intensity plot of line 1. ....	50
Figure 40 EDS scan results of sample 100-250-2 showing (a) cross-section of IMC analyzed with linescan (b) Intensity plot of line 1. ....	51

Figure 41 EDS scan results of sample 20-250-4 showing (a) cross-section of IMC analyzed with linescan (b) Intesity plot of line 1 .....	52
Figure 42 EDS scan results of sample 40-250-4 showing (a) cross-section of IMC analyzed with linescan (b) Intesity plot of line 1 .....	53
Figure 43 EDS scan results of sample 60-250-4 showing (a) cross-section of IMC analyzed with linescan (b) Intesity plot of line 1 .....	54
Figure 44 EDS scan results of sample 80-250-4 showing (a) cross-section of IMC analyzed with linescan (b) Intesity plot of line 1 .....	55
Figure 45 EDS scan results of sample 100-250-4 showing (a) cross-section of IMC analyzed with linescan (b) Intesity plot of line 1 .....	56
Figure 46 Micrographs showing micro indentations of all samples that are heat treated for 2 hours at 250 ° C(a) 20 ms bond duration(b) 40ms bond duration (c)60ms bond duration (d) 80ms bond duration (e)100ms bond duration. ....	59
Figure 47(a) Indentation hardness results for region L1 all samples that are heat treated for 2 hours at 250 ° C(b)Indentation location map.....	61
Figure 48(a) Indentation hardness results for region L2 all samples that are heat treated for 2 hours at 250 ° C. (b)Bare Aluminum coupon analyzed using SE Images. ....	62
Figure 49 Indentation hardness results for region L3 all samples that are heat treated for 2 hours at 250 ° C. ....	63
Figure 50 Micrographs showing microindentations of all samples that are heat treated for 4 hours at 250 ° C (a) 20 ms bond duration (b) 40ms bond duration (c) 60ms bond duration (d) 80ms bond duration (e) 100ms bond duration. ....	65
Figure 51 Indentation hardness results for region L1 all samples that are heat treated for 4 hours at 250 ° C. (b)Indentation location map.....	66
Figure 52 Indentation hardness results for region L2 all samples that are heat treated for 4 hours at 250 ° C. ....	67
Figure 53 Indentation hardness results for region L3 all samples that are heat treated for 4 hours at 250 ° C. ....	68

## NOMENCLATURE

Å Atomic Radius

at% Atomic percent

D Growth rate constant ( $\text{m}^2/\text{s}$ )

$D_0$  A temperature-independent Pre exponential factor ( $\text{m}^2/\text{s}$ )

J Diffusion flux per unit area and unit time

t time

R Gas Constant ( $8.31 \text{ J/mol}\cdot\text{K}$ )

$Q_v$  The Activation Energy for diffusion ( $\text{J/mol}$ )

T Annealing temperature (K)

X Intermetallic thickness

IMC Intermetallic Compound

gf Gram Force

SEM Scanning electron Microscope

BSE Back Scattered Electron

SE Secondary Electron

## EDS Energy Dispersive Spectroscopy

## ABSTRACT

Intermetallic Metallic Compounds (IMCs) formation is a common cause for wire bond failures. This research studied the effect of US vibration duration on IMC formation and growth in Copper-Aluminum (Cu-Al) wire bonded samples. Wire bonded samples, using 2.5 mil (63.5  $\mu\text{m}$ ) thick Palladium coated Copper wire, is ultrasonically bonded on a 2 cm thick Aluminum (1"x1") coupon. Segmented bonding technique using 200 gf force and 220 gf force are applied during segment 1 and segment 2 of the bonding respectively. Ultrasonic (US) vibration frequency of 115-117 khz and a bonding temperature of 175°C is used. A pair of 5 samples with bonding duration: 20 milliseconds (ms), 40ms, 60ms, 80ms, 100ms is created. Keeping the temperature constant at 250 °C, a tube furnace is used to annealing one set for 2 hours and the other set for 4 hours.

Backscattered Electrons (BSE) images were used to detect IMC growth. Backscattered images revealed formation of IMC at the Cu-Al bond interface, mostly around the center of and bond periphery. Using BSE images to identify location of IMC, Energy Dispersive Spectroscopy (EDS) linescans were then performed. Only EDS analysis was taken into account for final results assuming it was more accurate than visual inspection of BSE images.

EDS linescan analysis for 2 hour heat treated samples showed IMC thickness growing from 0.6  $\mu\text{m}$  to 1  $\mu\text{m}$  as bond duration increased from 20ms to 100ms. Linescan results for 4 hour samples had IMC thickness ranging from 0.8 $\mu\text{m}$  to 1.5  $\mu\text{m}$ , and hence showed an increase

with bond duration from 20ms to 100 ms.

Using micro indentations, hardness of both Cu ball and Al was measured. Change in hardness for Cu and Al was compared with bond duration and annealing time. Cu hardness decreased from 20ms to 60ms bond time and then increased in value from 80ms to 100ms bond time. When compared to anneal time, overall hardness in Cu increased with increase in annealing time. Overall hardness in Aluminum increased with increasing bond duration but decreased with increase in anneal time, such behavior is related to the concurrent effect of annealing and IMC growth.

## CHAPTER 1: INTRODUCTION

Ultrasonic (US) wire bonding is an interconnection technique that joins metal wires and bond pads (mainly Aluminum), known for having the lowest cost, and is the most flexible interconnect solution used by semiconductor industry. Every year 8 to 9 billion wire bonds are created [1]. Gold is the standard wire used for decades due to its high environmental stability and good electrical conductivity [2]. Gold being expensive, the industry is shifting focus on Copper as an alternative driven mostly by economic and technological considerations. Gold-Aluminum (Au-Al) bond is replaced by Copper-Aluminum (Cu-Al).

Major advantages of Copper wire: lower and more stable cost than gold, increased stiffness (minimizing wire sweep), improved electrical conductivity, lower resistivity and significantly reduced formation of Intermetallic Compounds (IMC) [3]. Copper however, is not a drop-in replacement for gold. The most significant concern is poor quality bond being made, due to small process window, caused by the less favorable mechanical properties of Copper [4]. Copper work hardens during bonding, which can cause: pad crack, pad peeling and Al splash. Oxidation of wire surface makes stitch side of bonding more challenging. It is prone to ball-neck fatigue failures in plastic encapsulation during temperature cycling. Despite Cu-Al bonds having lower IMC formation compared to Au-Al, growth of IMC remains as one of the most common causes for bond failure due to the high electric resistivity and brittleness of IMC.

In order to develop and optimize reliable Cu-Al wire bonds, a good assessment of the formation and growth mechanism of IMCs is crucial for the prediction and reduction in bond failures. Although US wire bonding process has been around for several decades, and there is extensive research on the topic, not enough reliable information is available on either initial bond



formation or how IMCs form and evolve in Al-CU systems. Due to short duration of bond formation, experimental analysis faces a significant obstacle during bonding [5]. Therefore, several post bond studies have been done to investigate IMC formation and growth. Major tests on bond include: morphological and compositional characterization, examining interfacial characteristics, destructive pull and shear tests, IMC coverage measurement, use of integrated micro sensors for bond process monitoring and also using molecular dynamics (MD) simulations [6][7][8][9]. Based on literature survey, it is implied that formation of IMC is controlled by rate of diffusion, during the short exposure to ultrasonic vibration during bonding period. However, there is still limited experimental analysis on IMC formation and, in particular, limited studies on quantitative models [9].

In this thesis, as part of a larger project to identify mechanisms of bond formation, experimental analysis is performed on Cu-Al bonds to analyze the effect of bonding time on formation and growth of IMC following post-annealing processes. Scanning electron microscope (SEM) is used to measure IMC coverage. Micro indentation is used to measure hardness and identify IMC locations around bond interfacial region. Chemical compositions of the interface region are studied using Energy Dispersive Spectroscopy (EDS) to confirm IMC formation. Varying only the bonding duration parameter, and using annealing at 250 ° C for 2 and 4 hours, wire bond samples ranging from 20ms to 100ms are analyzed.

## CHAPTER 2: LITERATURE SURVEY

### 2.1 Thermosonic Ball Bonding Process

The most widely used method of wire bonding is called Thermosonic ball bonding. The process combines ultrasonic energy with thermal energy to form bonds using a normal bonding force. The procedure is briefly illustrated in Figure 1. It can be divided into the following sequential steps:

1. A thin wire fed through a hole in the capillary, is melted using an electronic flame off (EFO) spark, forming a ball at the end of the wire.
2. The ball is then positioned and the capillary is lowered to the bond pad. The ball is then pressed against the bond pad and ultrasonic energy is applied, and a bond forms between Al and Cu.
3. The capillary tool is raised, leaving the ball bonded to the band pad.
4. A wire loop is formed as the wire moves with the capillary towards the second bond position.
5. The capillary tool is loaded to the second bond pad, to make a second bond. This bond is also called a stitch bond, crescent bond or wedge bond.
6. After the second bond is formed, the capillary tool is raised,
7. A wire clamp above the capillary tool pulls and breaks the wire free. The bonder then rises to EFO height and is ready to repeat the bonding cycle for the next wire [3].

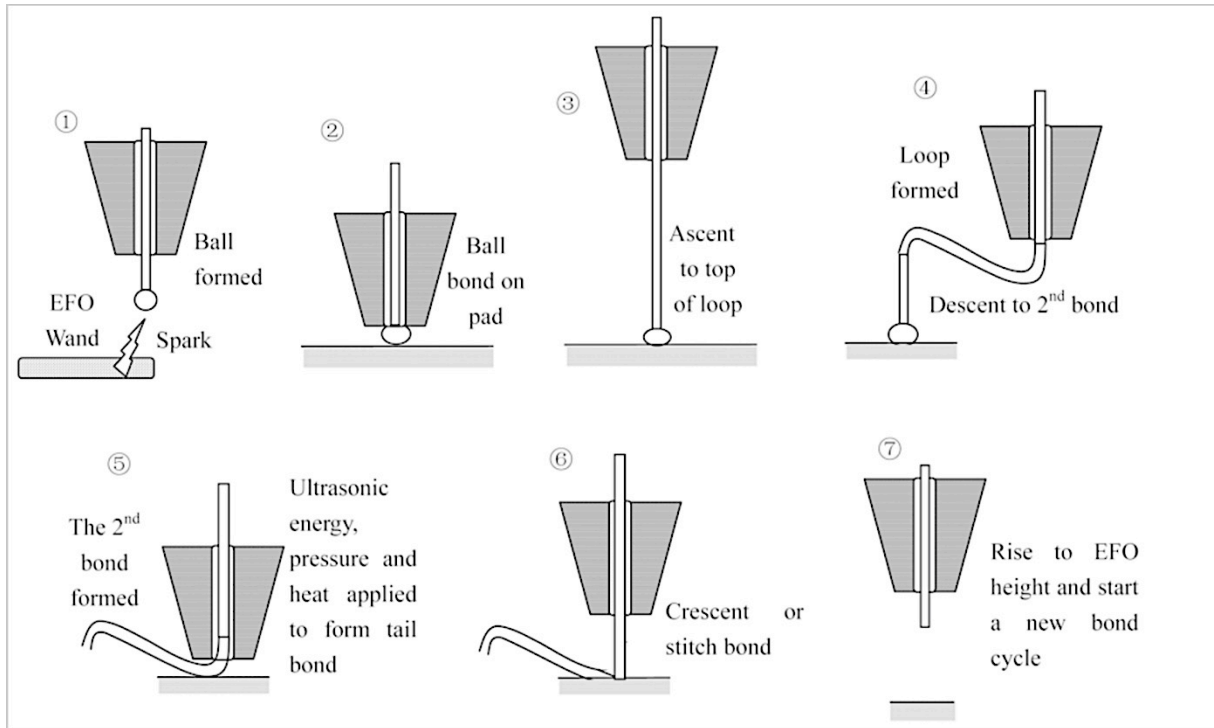


Figure 1 Ball- Wedge wire bonding cycle [10]. Permission to reprint not obtained

## 2.2. Intermetallic Phases and material properties

In order to identify IMC formation, knowledge of IMC phases and their composition is very important. The Cu-Al phase diagram, as shown in Figure 2, shows the existence of 5 IMCs that are known to form at temperatures of 300°C and above:  $\text{CuAl}_2$  ( $\theta$ ) has a cubic crystal structure,  $\text{CuAl}$  ( $\eta_2$ ) and  $\text{Cu}_4\text{Al}_3$  ( $\xi_2$ ) is based on monoclinic structure,  $\text{Cu}_3\text{Al}_2$  ( $\delta$ ) has a trigonal crystal structure and  $\text{Cu}_9\text{Al}_4$  ( $\gamma_1$ ) has a cubic crystal structure [5]. Table 1 gives the properties associated with each Cu-Al phase. For a better understanding of IMC formation and growth, the following sections of literature survey will focus on diffusion process, effects of ultrasonic vibration on native oxide layer rupturing and creating dislocations, and role of annealing on IMC formation and growth.

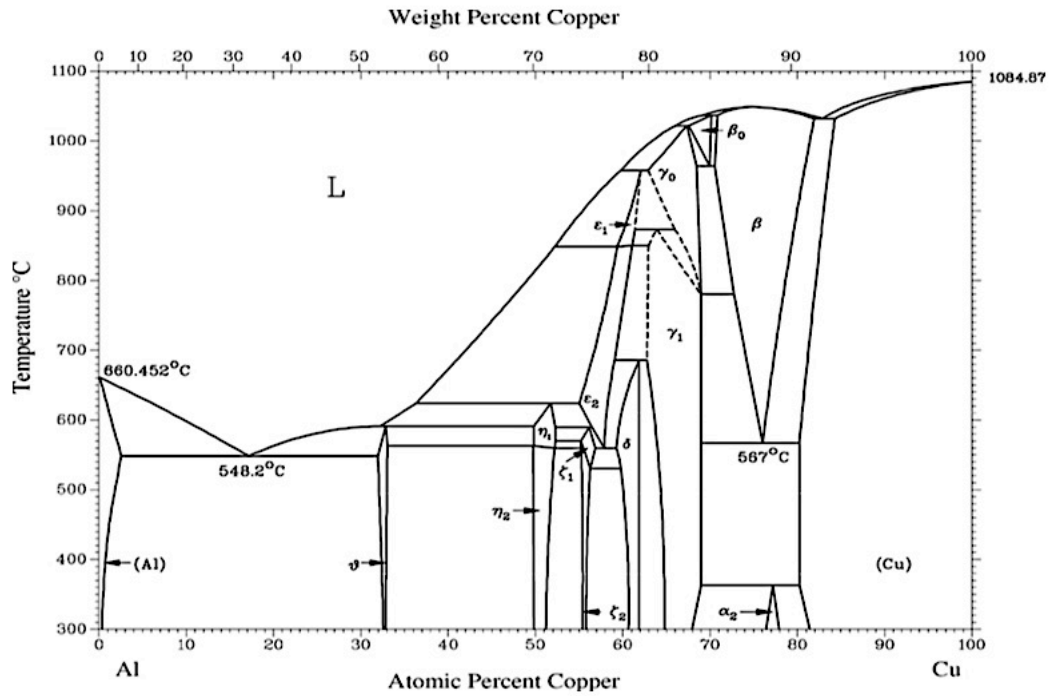


Figure 2 Cu-Al Phase Diagram [11]. Permission to reprint not obtained

Table 1 Properties of CuAl [5]

Phase	Notations	At.% Cu	Crystal Structure	Hardness HV	Resistivity ( $\mu\Omega$ cm)	CTE (ppm/ $^{\circ}$ C)	Density ( $g/cm^2$ )
Al		0 – 2.84	Cubic	20 - 50	2.4	2.35	2.7
CuAl <sub>2</sub>	$\theta$	31.9 - 33	Tetragonal	324	7.0 – 8.0	1.61	4.36
CuAl	$\eta_2$	49.8 52.3	– Monoclinic	628	11.4	1.19	2.7
Cu <sub>4</sub> Al <sub>3</sub>	$\xi_2$	55.2 56.3	– Monoclinic	616	12.2	1.61	NA

<b>Cu<sub>3</sub>Al<sub>2</sub> δ</b>	59.3 61.0	– Trigonal	558	13.4	1.51	NA
<b>Cu<sub>9</sub>Al<sub>4</sub> γ1</b>	62.5 - 69	Cubic	549	14.2 17.3	– 1.76	6.85
<b>Cu</b>	80.3 – 100	Cubic	60 - 100	2.0	1.73	8.93

## 2.3 Process of Diffusion

Diffusion is the phenomenon of material transport by atomic motion in the form of a net drift (flux) or transport of atoms from high to low concentration regions. The magnitude of this flux depends upon the concentration gradient and temperature. This section is dedicated to literature review on: diffusion mechanism, quantitative definition of diffusion, defects in polycrystalline materials, diffusion medium, dislocations, and ultrasonic vibration's effect on diffusion.

### 2.3.1 Diffusion mechanism

The two common mechanisms by which atoms can diffuse through solids are vacancy and interstitial diffusion, as shown in Figure 3. Vacancy diffusion mechanism involves the interchange of an atom from a normal lattice position to an adjacent vacant lattice site or vacancy. The extent to which vacancy diffusion can occur is a function of the number of these vacancies that are present. Interstitial diffusion involves atoms that migrate from an interstitial position to a neighboring one that is empty. No vacancies are required for this mechanism. In most metal alloys, interstitial diffusion occurs much more rapidly than diffusion by the vacancy

mode, because there are many more interstitial sites than vacancies. However, for metals that have similar atomic size, such as Cu-Al system, diffusion occurs through vacancy mechanism.

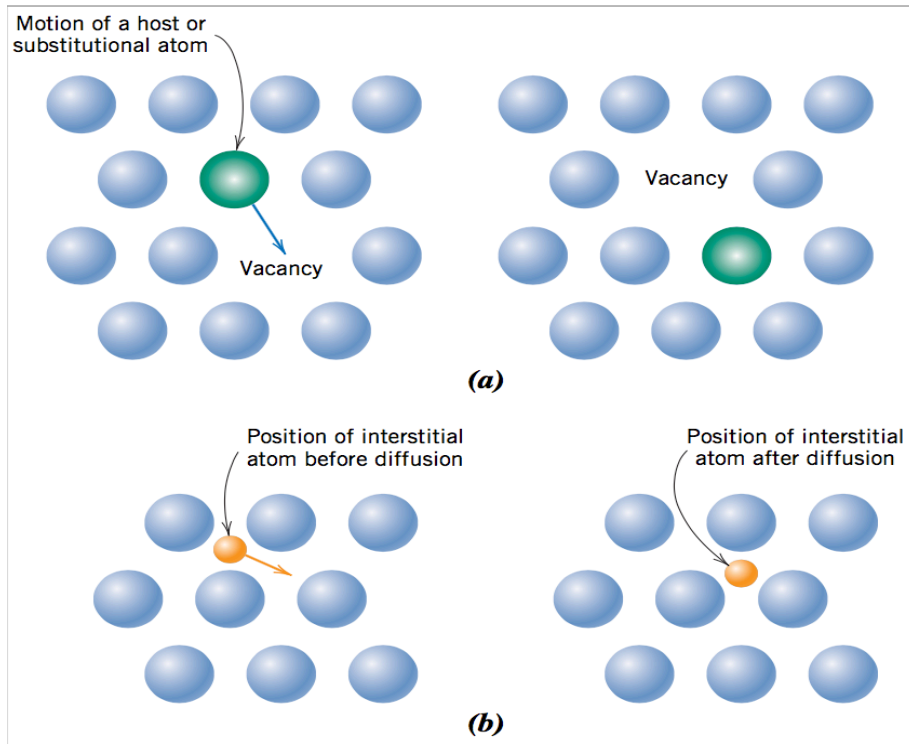


Figure 3 Schematic representations of (a) vacancy diffusion and (b) interstitial diffusion [13]. Permission to reprint not obtained

### 2.3.2 Quantitative Definitions of Diffusion Coefficient

For diffusion to take place, two conditions are required: the adjacent site needs to be empty, and there must be sufficient energy to cause lattice distortion during displacement by breaking the bonds with neighboring atoms. The energy barrier that an atom needs to overcome the attractive forces exerted on it by its neighboring atoms is also known as the activation energy  $Q_v$ , as shown

in the schematic diagram presented in Figure 4. The kinetics of diffusion strongly depends on temperature. Equation 1 represents the relationship between diffusion coefficients  $D$ , where  $D$  is assumed to be isotropic in all

$$D = D_0 \exp\left(-\frac{Q_v}{RT}\right) \quad (1)$$

directions, with activation energy  $Q_v$  and absolute temperature  $T$ .  $D_0$  is the diffusion constant and  $R$  is the Gas constant. According to works done by Kim et al [14] and Yik et al [17], thickness of all five IMC phases grow proportional to the square root of annealing time, indicating diffusion controlled growth kinetics. The growth rate of each individual IMC phases and of the total IMC stacks shows an exponential dependency on annealing temperature, indicating an Arrhenius like relation similar to Equation 2 [15].

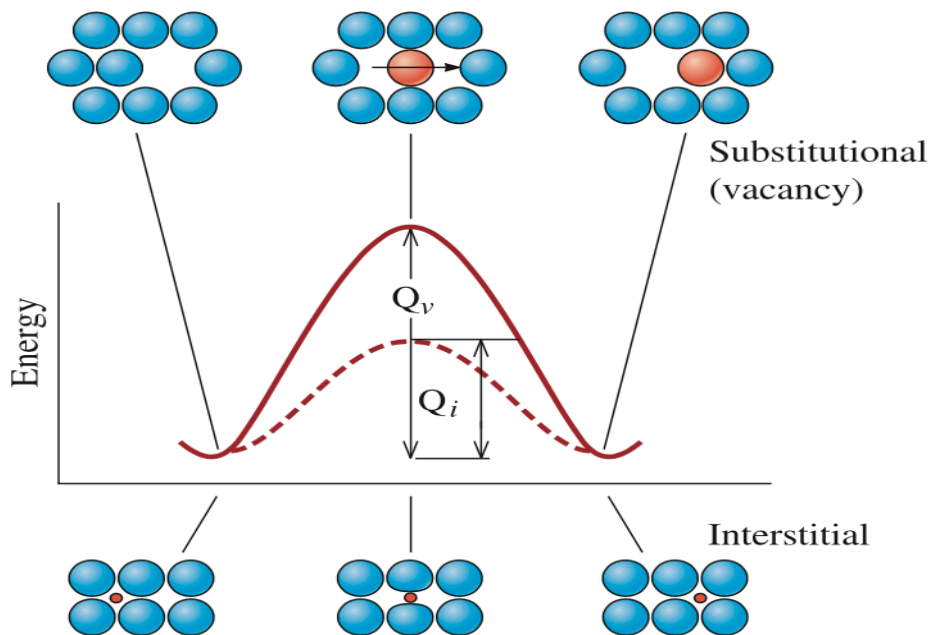


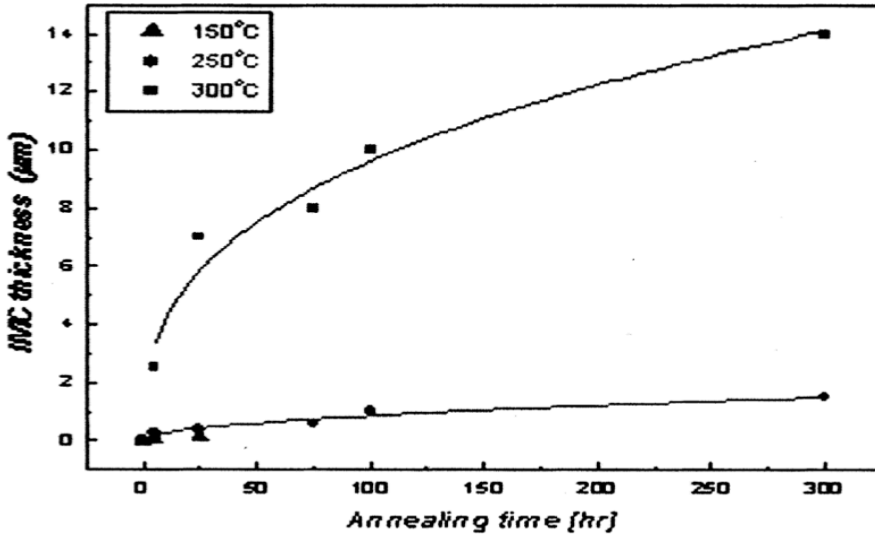
Figure 4 The activation energy  $Q$  required to move atoms past one another during diffusion.

Substitutional atom requires more energy compared to interstitial atom [5]. © 2004 IEEE

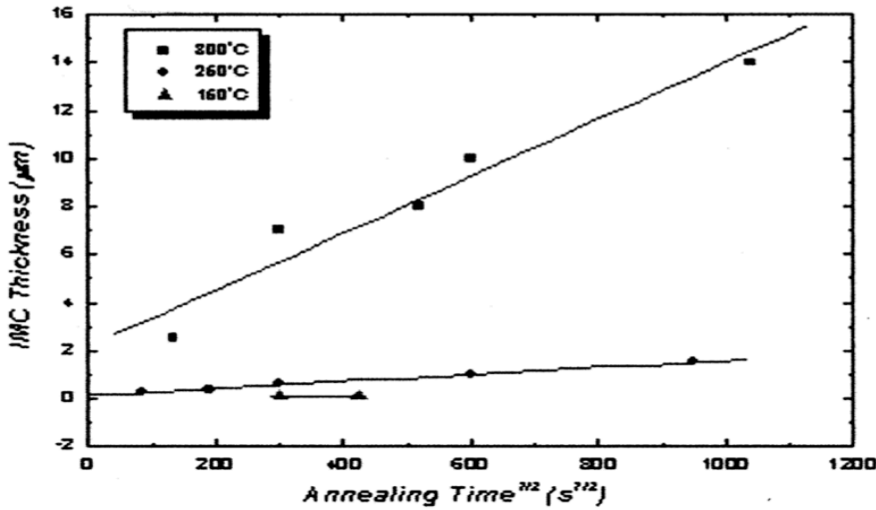
A graph of Kim et al's [14] work is shown in Figure 5. Fig. 5(a) shows the parabolic growth behavior of IMC, where IMC thickness grew fast at early stages of annealing. From the plots, it is observed that IMC thickness increases with increase in annealing time. Fig. 5(b) shows the relationship between IMC thickness and (annealing time)<sup>1/2</sup>. The thermal diffusion distance can be obtained from Equation 2 where  $t$  is the diffusion time, and IMC layer thickness  $x$  can be calculated using this equation.

$$x = \sqrt{Dt} \quad (2)$$





(a)



(b)

Figure 5(a) IMC thickness versus annealing time (h). (b) IMC thickness versus annealing time<sup>1/2</sup> [16].

### 2.3.3.1 Defects in crystalline materials

Many physical properties of solid materials are primarily based on the presence of different types of defects and imperfections. Specific material characteristics are often deliberately fashioned by introducing a controlled amount of particular defect. Classified by geometry or dimension of the defect, crystalline defects are categorized by (i) point defects,

which are related to a single or a few atomic positions, (ii) linear (or one- dimensional) defects, (iii) two-dimensional defects such as surfaces, interfaces, and different types of boundaries, and (iv) volume defects including inclusions, cracks, voids, and pores [18].

### 2.3.3.2 Dislocations

Dislocation is a defect or disarrangement within a crystal structure of a material. They typically are introduced into a crystal during solidification of the material or when the material is deformed permanently. The resulting distortion in the structure strongly influences many properties of materials. This thesis will be discussing dislocation enhanced diffusion process and therefore, for literature review, only linear defects are studied. Although there are many different types of dislocations, they all can be considered as combinations of the two fundamental types: edge and screw dislocations (Fig.6)

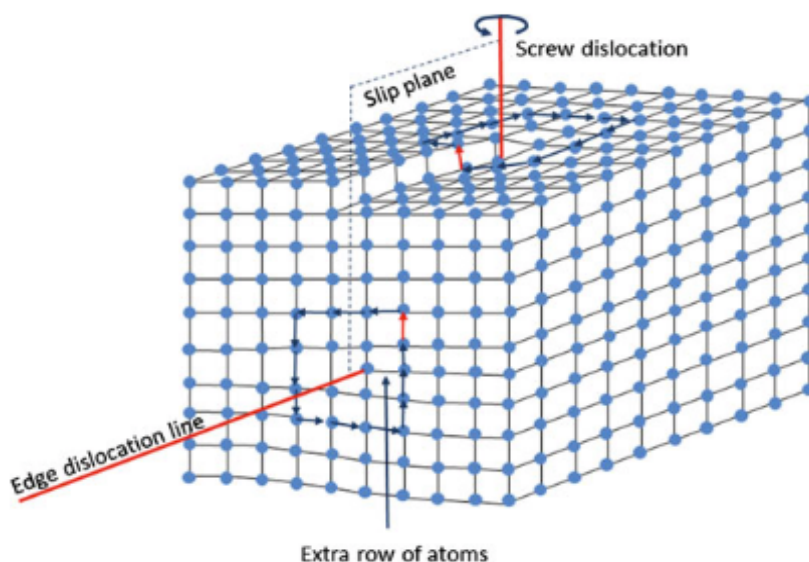


**Figure 6** Edge and Screw Dislocation [18]. Permission to reprint not obtained.

### 2.3.3.3 Diffusion through crystallographic defects

Most metals are found in polycrystalline form. Copper and Aluminum are no exception. The major types of diffusion, where both interstitial and substitutional diffusion can happen, and taking place in polycrystalline materials are: grain boundaries, surface, lattice and dislocations diffusion [16]. Grain boundary diffusion occurs when atoms can diffuse through grain boundaries. When diffusion occurs over the surface, it is called surface diffusion. This type of diffusion is also found through the cracks or pores in the material. In this case, the activation energy for diffusion is the lowest since there are no atoms above the atom of interest, which exchanges position with the vacancy. So, diffusion rate is the highest compared to other diffusion mechanisms. When diffusion occurs through the lattice inside a grain by point defects, it is called lattice diffusion or volume diffusion. Dislocation diffusion is when diffusion occurs via edge dislocation. It is also called pipe diffusion since it appears like movement of atoms through a pipe as seen in Figure 7.

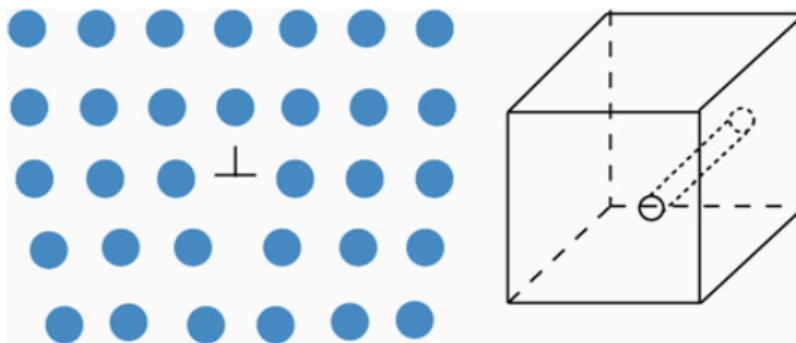


*Figure 7 Diffusion through an edge dislocation [16]. Permission to reprint not obtained.*

Ultrasonic power, during wire bond process, causes a strong plastic deformation in both the Copper ball and aluminum pad. This plastic deformation leads to a local increase in dislocations,

slip bands and vacancy density [17]. Presence of these defects decreases the activation energy of the metal atoms for diffusion [19,20]. Therefore, diffusion is now aided along these distortions in the metal lattice and is beneficial for IMC formation.

## 2.4 Native Aluminum Oxide Layer

Utilizing dual-beam focused ion beam (FIB) and high-resolution transmission electron microscopy (TEM), in a study done by Xu et al [17], a native aluminum oxide layer (~5 nm thick) on the aluminum pad is observed (Fig. 8). This uniform layer of aluminum oxide acts as a barrier to the diffusion of Cu and Al, so IMCs are unlikely to form in regions with uniform aluminum oxide layers. However, IMCs form in areas where the oxide layer is fragmented during bonding [3]. Therefore, in order to form wire bonds, application of ultrasonic power is required for wire bonding[6].

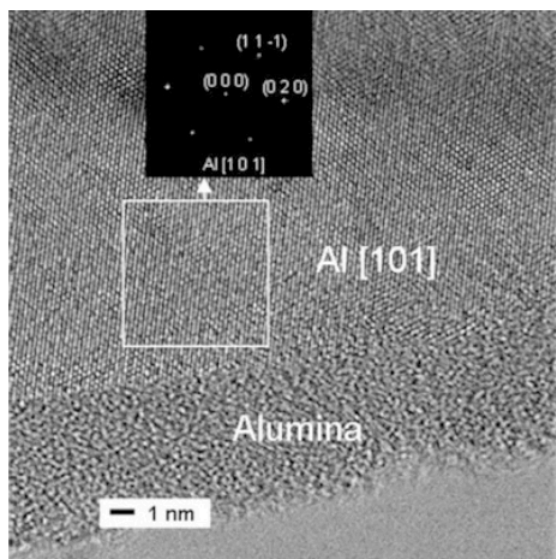


*Figure 8 TEM image showing a uniform amorphous native alumina over layer (~5 nm thick) enveloping an Al pad [17]. © 2014 IEEE*

## **2.5 Bonding Parameters and their effects on IMC formation**

In wire bonding, a total of four parameters have an influence in the formation of IMC. The parameters are: ultrasonic power, bonding force, bonding duration and substrate temperature. Considering the focus of the analysis in this research, the only relevant parameter for literature study is bonding duration. However, ultrasonic power and its effects are also briefly studied as its application plays an important role in IMC formation by rupturing Alumina layer as well as creating dislocations.

### **2.5.1 Ultrasonic power and IMC formation**

In thermosonic bonding process, Ultrasonic vibration plays a crucial role in the formation of IMC. It is applied by vibrating the bonding tool while it is in contact with the wire. Heat and ultrasonic energy soften the wire and pad metallization, and the bonding wire is deformed with the bonding tool against the pad metallization. This strong mechanical effect causes plastic deformation of the Cu ball as well as the Aluminum pad. This creates a local increase in dislocation, slip bands and vacancy density as a consequence and hence provides faster diffusion channels according to Rainer et al [22, 23]. Ultrasonic vibration under certain pressure and heat also partially fragments the oxide barrier (mentioned earlier). The level of ultrasonic energy affects the fracture process in the oxide, determining the quantity of initial IMCs and, therefore, affecting the bonding strength. Though the initial formation of IMCs relies on fracture of the native oxide layer, the growth of IMCs is sustained by diffusion of Cu and Al through the IMC layer [6].

### 2.5.2 Bonding duration and IMC formation

Ultrasonic metal-to-metal bonding duration is within several milliseconds [1]. During its relative short period, the bonding duration influences alumina fragmentation in Cu-Al wire bonds. A long bonding duration breaks the alumina layer throughout the interface and thus affects IMC formation [20][8]. Although it has been shown that ultrasonic duration affects IMC formation, but there is a lack of systematic investigation on quantitatively analyze the effect of bond duration time on IMC thickness.

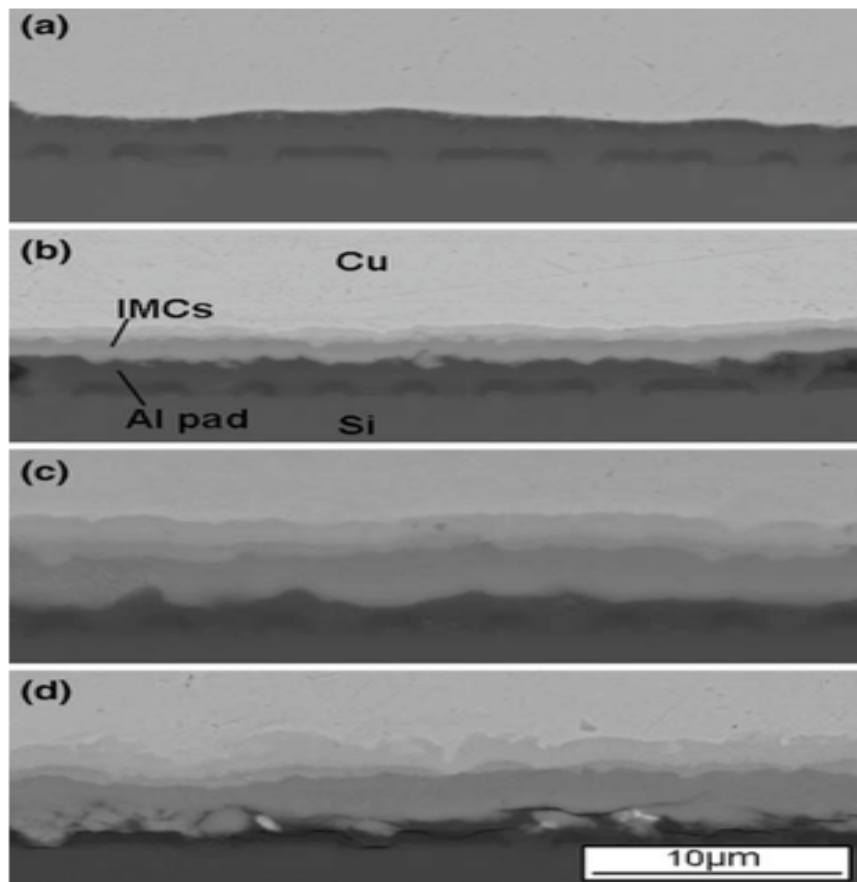


Figure 9 Cross-sectional BSE SEM of copper ball/Al metallization interfaces after aging at 250°C for: (a) 1 hours, (b) 25 hour; (c) 100 h; and (d) 169 hours [25].

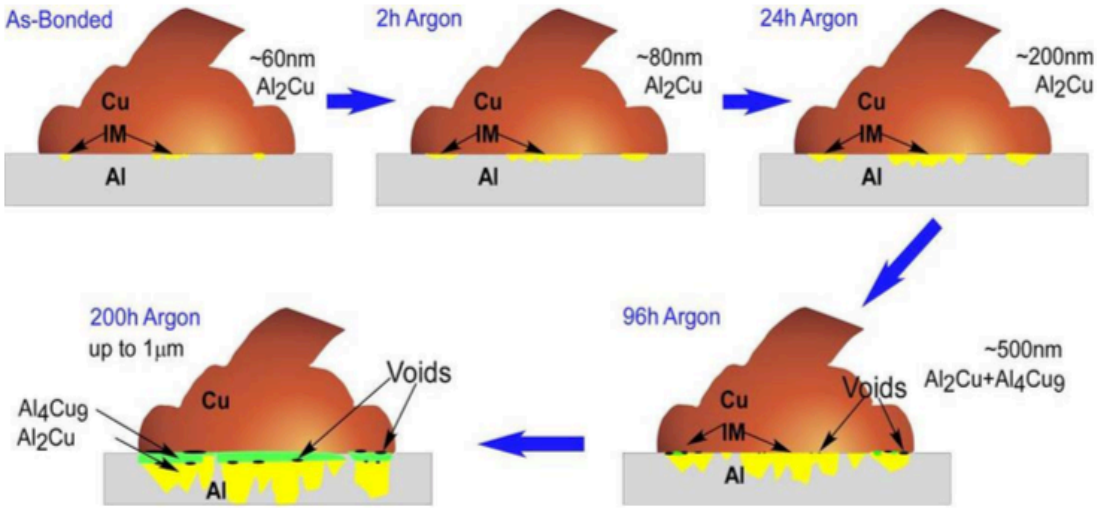


Figure 10 schematic representations of the intermetallic morphology and evolution at Al-Cu wire-bonds as a function of a heat-treatment time [7]. Permission to reprint not obtained.

Initiated at the peripheral regions of the ball/pad contact interface and extended inwards with an increase in bonding duration. Formation of IMC is thus accelerated.

### 2.5.3 Thermal Aging of Copper-Aluminum bonds and IMC formation

There is a common agreement that IMC layers, although confirmed by many researchers, are difficult to detect and measure at as bonded state. Work done by Xu et al [25] in Figure 8 shows trace amounts of IMC formed after 1 hour of annealing. This explains why it would be even harder to detect and measure them at the as bonded stage. From Maria et al's work [7] in Figure 10, the schematic representation also gives a clear visualization of how little IMC forms at as bonded stage. Therefore, taking the difficulty of identifying IMC in as bonded samples into consideration; only heat-treated samples are considered for experimental analysis.

Extensive amount of research work has been done in the past to show the relationship between thermal aging time and temperature with IMC growth. From Xu et al's work, it can be seen how thermal aging helps to grow a uniform and thicker layer of IMC (Figure 9). IMC coverage increase is directly proportional to aging time and temperature. Further literature study of works done by Tian et al (Figure 11) [24] and Yik et al (Figure 12) [ 15] shows IMC growth with increase in aging time. These findings justify the use of Equation 1 and Equation 2, to find IMC thickness 'x' as it varies with Temperature and Time.

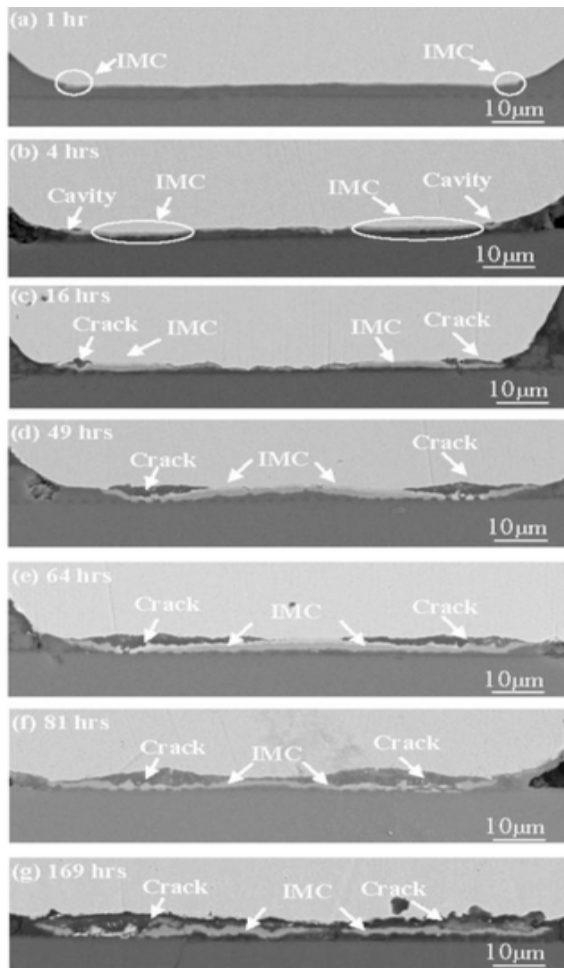


Figure 11 Evolution of the Cu/Al IMC in the Copper bump bonds at 250 °C after aging for a)1h, (b) 4hrs, (c) 16hrs, (d) 49hrs, (e) 64hrs, (f) 169hrs [24].



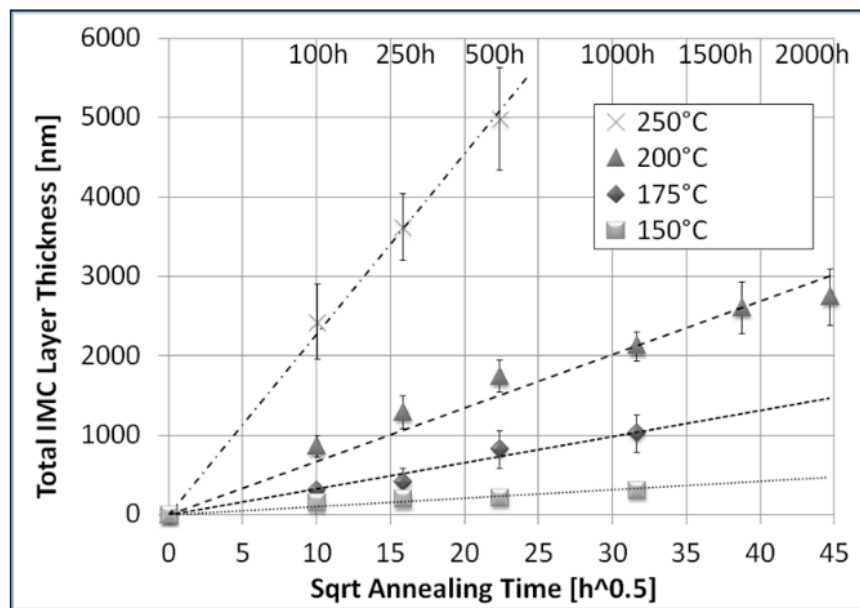
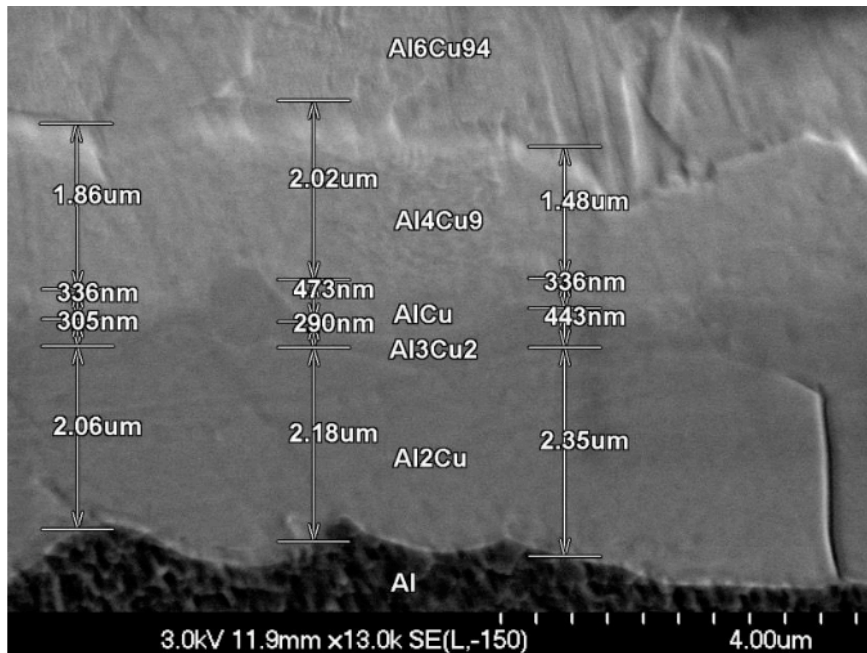


Figure 12 a) SEM image after 500 hours of annealing at 250 °C. b) Combined thickness for the three IMC phases  $Al_4Cu_9$ ,  $AlCu$  and  $Al_2Cu$ , which are observed over a larger temperature range, have been plotted over square root of anneal time [15]. © 2015 IEEE

## **2.6 Micro-indentation test for IMC identification**

Microindentation test on Cu-Al bond interface can be out to identify the intermetallic layers present in copper wire bonded samples. IMC layers in Al-Cu system are very thin [25], and therefore difficult to be detected. Based on the hardness data of the IMCs in Table 1, it is clear the IMC layers have a higher hardness than either Copper or Aluminum. Therefore, in order to cross check Cu-Al IMC analysis using SEM and EDS, microhardness test is a good test to confirm IMC by measuring hardness.

## **2.5 Research Goal**

The main goal of this research is to provide experimental analysis on IMC formation with respect to bond duration. The results will be beneficial for defining bonding parameter to reduce IMC thickness and improve bond reliability. The following techniques are used to measure and confirm IMC formation:

1. Scanning electron microscope (SEM) is used to measure IMC coverage.
2. Micro indentation is used to measure hardness and identify IMC locations around bond interfacial region.
3. Chemical compositions of the interface region are studied using Energy Dispersive Spectroscopy (EDS) to confirm IMC formation.

## **CHAPTER 3: EXPERIMENTAL PROCEDURE AND CHARACTERIZATION TECHNIQUES**

### **3.1 Specimen Preparation**

#### **3.1.1. Cu-Al Wire-Bonds**

A set of wire bonded samples are prepared using 2.5mil (63.5  $\mu\text{m}$ ) thick Copper wire, coated with Palladium, on a 2 cm thick Aluminum (1"x1") coupon, as shown in Figure 13. To create the thermosonic bonds a Kulicke & Soffa (K&S) iConn ball bonder that is shown in Figure 14, is used. A process called segmented bonding is used to create ball bonds as it allows bonding time to be independently varied for each segment. Segmented bonding consists of two basic stages: (i) contact stage and (ii) bonding stage. During the contact stage, a high bonding force and a low ultrasonic power is employed to cause big plastic deformation of the balls; during the bonding stage, a low bonding force and a high ultrasonic power is used to ensure robust bonds.

For each bond duration, one half of the total duration is used for contact stage or segment 1 and the remaining half for bonding stage or segment 2. The only exception is during 20ms bond duration where segment 1 is set at 0ms and segment 2 is set at 20 ms because it is difficult to form bonds when either segment is set at 10ms. During segment 1 the force applied is 200 gf and during segment 2 a force of 220 gf is applied to the Al pad. The frequency of ultrasonic vibration used is 115-117 khz. The substrate is preheated to 125 °C and reached a temperature of 175°C after bond completion. A set of samples, from bond duration of 20ms to 100ms, is created for analysis.

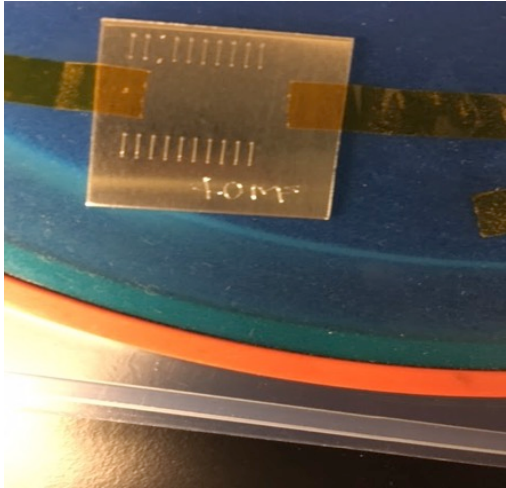


*Figure 13 Al pad containing 2 rows of Cu-Al ball-wedge bonds with 2.5-mil thick Pd coated Cu wire.*



*Figure 14 Kulicke & Soffa (K&S) iConn ball bonder [27].*

### **3.1.2. Metallographic Specimen Preparation**

For both optical and electron microscopy, good quality specimen preparation is crucial. The basic concern in specimen preparation is that it needs be a true representative of the sample.

Therefore, metallography is a critical process that is required to prepare materials for accurate characterization. Although metallographic specimen preparation can be quite a straightforward process, but for this project fragile wire bonded samples created some challenge. Therefore, special care had to be taken to prevent damage to the ball bonds while also creating good quality metallographic specimen. The basic steps for preparation included: mounting in epoxy molding, sectioning, planar grinding with simultaneous microscopic analysis and, final polishing.

### **3.1.2 Mounting**

Due to the fragile nature of the Ball bonds, the mounting operation is used to accomplish proper sectioning/grinding of the sample without causing any damage to the bond. Acrylic based castable mounting resin is used to encapsulate the specimen, before sectioning the top portion of the specimen to expose the Cu-Al ball bond joints. Figure 15a shows a sample mounted in clear epoxy resin.

### **3.1.3 Sectioning and Cutting**

Most metallographic samples need to be sectioned to the area of interest and for easier handling. Proper sectioning is required to minimize damage to samples, which may alter the microstructure and produce false metallographic characterization. For Cu-Al ball bonds, sectioning operation is done using Buehler Isomet 1000 Precision cutter as seen in Figure 16 b. A diamond wafer saw is used as the blade and water-based coolant is used to cool the blades during operation.

### **3.1.4 Planar Grinding**

This technique is required to planarize the specimen and to reduce the damage created by sectioning. Grinding is performed by manually rubbing the samples against abrasive grit papers

with varying grits, in one direction with uniform speed. A Buehler Handimet 2 Grinder, as shown in Figure 16c, is used for this purpose. A uniform planar grinding is accomplished by increasing the abrasive grit sequentially to obtain surface finishes that are ready for polishing. Care is taken to avoid being too abrasive in this step, and actually creating greater specimen damage than produced during cutting.

### 3.1.5 Final Polishing

The purpose of final polishing is to remove only surface damage. Fastick polishing cloths are used with Alumina abrasives. Polishing abrasives used ranged from  $5\mu\text{m}$  to  $0.05\mu\text{m}$ . For polishing purposes a Buehler MetaServ grinder/polisher is used as shown in Figure 16a.

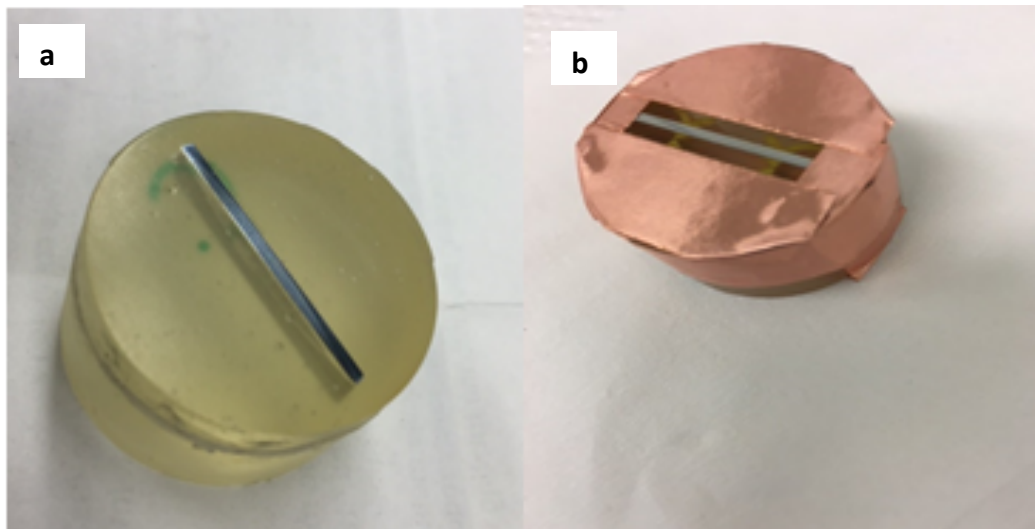


*Figure 15 a) Metallographic specimen encased in epoxy b) Specimen covered in adhesive copper tape to reduce charging effect and increase conductivity inside SEM chamber.*

a



b



c



Figure 16 (a) Buehler MetaServ grinder/polisher (b) Buehler Isomet 1000 Precision cutter (c) Buehler Handimet 2 Roll Grinder [28].

### 3.1.6 Charging Effect Neutralization

Standard metallographic specimen created with acrylic based epoxy creates a lot of charging effect when inserted inside an SEM chamber. In order to reduce charging effect and improve specimen conduction, the specimen is semi cloaked in double sided Copper tapes as shown in Figure 15b.

### 3.2 Cu- Al bond heat treatment process

Our research is focused on a quantitative analysis of the IMC layer thickness as a function of bonding duration. Initial research plan is to study IMC layer thickness in both as bonded and heat-treated bonds. Initial attempts are made to study the as-bonded sample but due to the small size of the IMC, it is not detectable with the available tools. Therefore, only annealed samples, heat-treated at 250 °C for 2 hours and 4 hours respectively, are studied. A tube furnace is used for annealing as shown in Figure 17. A pair of heat-treated samples, heated at two and four hours respectively, are created for each set of bonds bonded at specific bond durations: 20ms, 40ms, 60ms, 80ms and 100ms. To ensure accuracy of heat treatment duration and to avoid heating longer than intended hours, the samples are taken out at exactly two or four-hour mark after being heated at 250 °C.



*Figure 17 Heating Tube Furnaces.*



### **3.3 IMC Thickness measurement**

As the primary objective of our research, the IMC layer needs to be measured. Due to its miniature nature, it is a common practice to analyze IMC layers using SEM. The SEM used is shown in Figure 18. Both SE and BSE detectors are used to obtain imaging at the beginning. A comparison is then made between the two images to see which one provides more clarity, as shown on Figure 19

#### **3.3.1 Secondary Electron (SE) vs. Back Scattered Electron Imaging**

The SE signal derives its contrast primarily from the topography of the sample. For the most part, areas facing the detector tend to be slightly brighter than the areas facing away from the SE detector, and holes or depressions tend to be very dark while edges and highly tilted surfaces are bright. These electrons are of a very low energy and very easily influenced by voltage fields. BSE images display compositional contrast that results from different atomic number elements and their distribution. By observing micrographs obtained using BSE detector, the IMC layer can be identified as it appears in a different shade as compared to either Copper or Aluminum. Figure 20 shows a comparison of micrographs of Cu-Al bond interface using both SE (Figure 20a) and BSE (Figure 20b) signals using identical SEM conditions such as accelerating voltage and probe current. Based on the better clarity of the images, only BSE images are considered for IMC visual analysis purposes throughout the research. In order to measure the IMC coverage of Cu-Al wire bonds from BSE images, suspected IMC regions identified based on difference in contrast with both Cu ball as well as Al coupon. Figure 21 illustrates how the scale bars are used to measure IMC layer. The same process is used for visual inspection and measurement of IMC coverage for all 10 Cu-Al wire bonded samples.



*Figure 18 Tescan Mira 3 Scanning Electron Microscope (SEM) [29].*

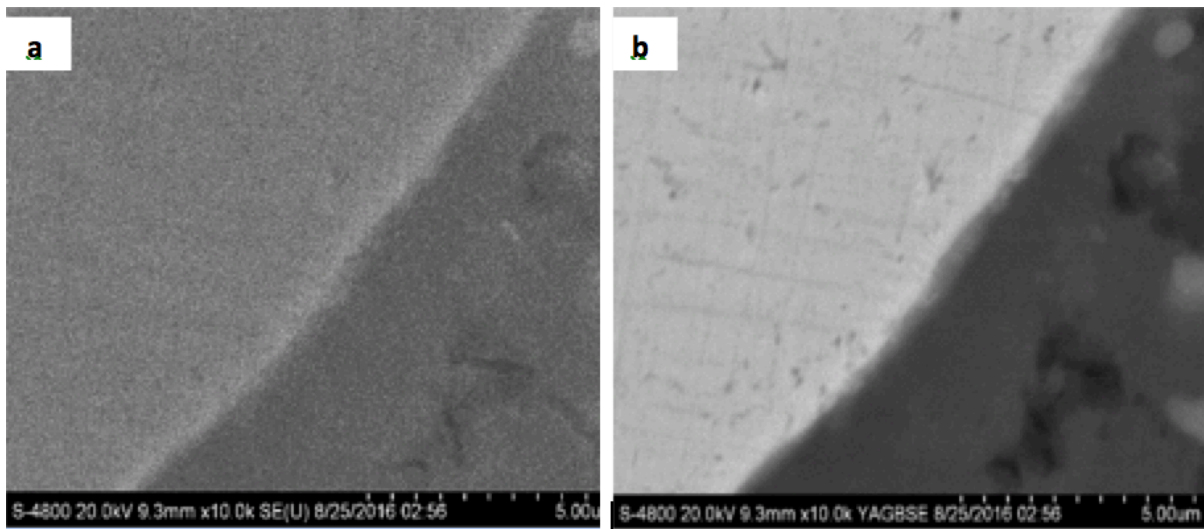


*Figure 19 Examples of Micrographs of Cu-Al Bond Interface to compare clarity of SE vs. BSE image side by side. a) Image from SE Detector b) Image from BSE Detector.*

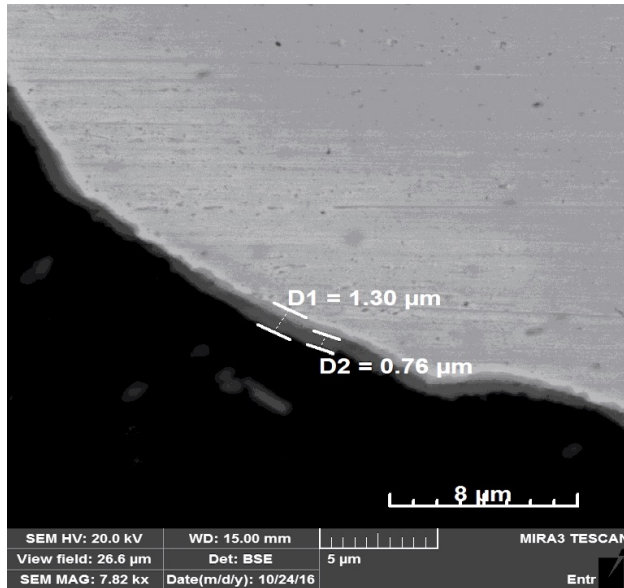
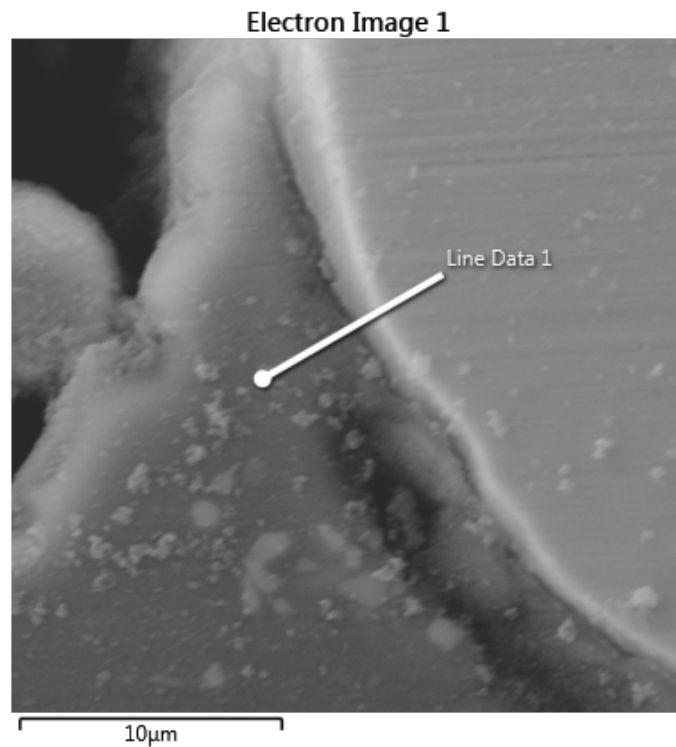


Figure 20 Example showing how a BSE Micrograph scale bar is used to measure IMC thickness (this data does not represent actual sample data, used only for illustration).

### 3.3.2 Chemical Composition Analysis using Electron Dispersive Spectroscopy (EDS)

A major limitation in using BSE imaging is that IMC regions can be visually identified but not confirmed as it's hard to figure out the elemental composition at bond interface using only visual inspection. Therefore, micrographs from the BSE alone are not sufficient to confirm IMC layer. In order to accurately determine the concentration profile for ultrasonically consolidated Cu–Al, the bond interface is studied using Energy Dispersive Spectroscopy (EDS) detector. Using the Oxford Instrument EDS interface, linescans are performed on BSE images and elemental identification and quantitative thickness of IM is obtained from intensity plots. An example of how this process is carried out, for all 10 samples, is shown in Figure 21. The line shows regions near the bond interface that are line-scanned. Using Intensity plot of line for each element, the region of IMC phase can be reasonably identified as shown as an example in Figure 22(b). At the bond interface, both Cu and AL are seen to have similar intensity. The square region marked in

Figure 22(b) can be considered having a high possibility of IMC formation. The thickness measured is then crosschecked with IMC measurements of BSE images.



*Figure 21 Example of a BSE Image of Cu-Al interfacial region captured using EDS interface (this data does not represent actual sample data, used only for illustration). The spots on the sample are from plasma vapor deposit coating to reduce sample charging.*

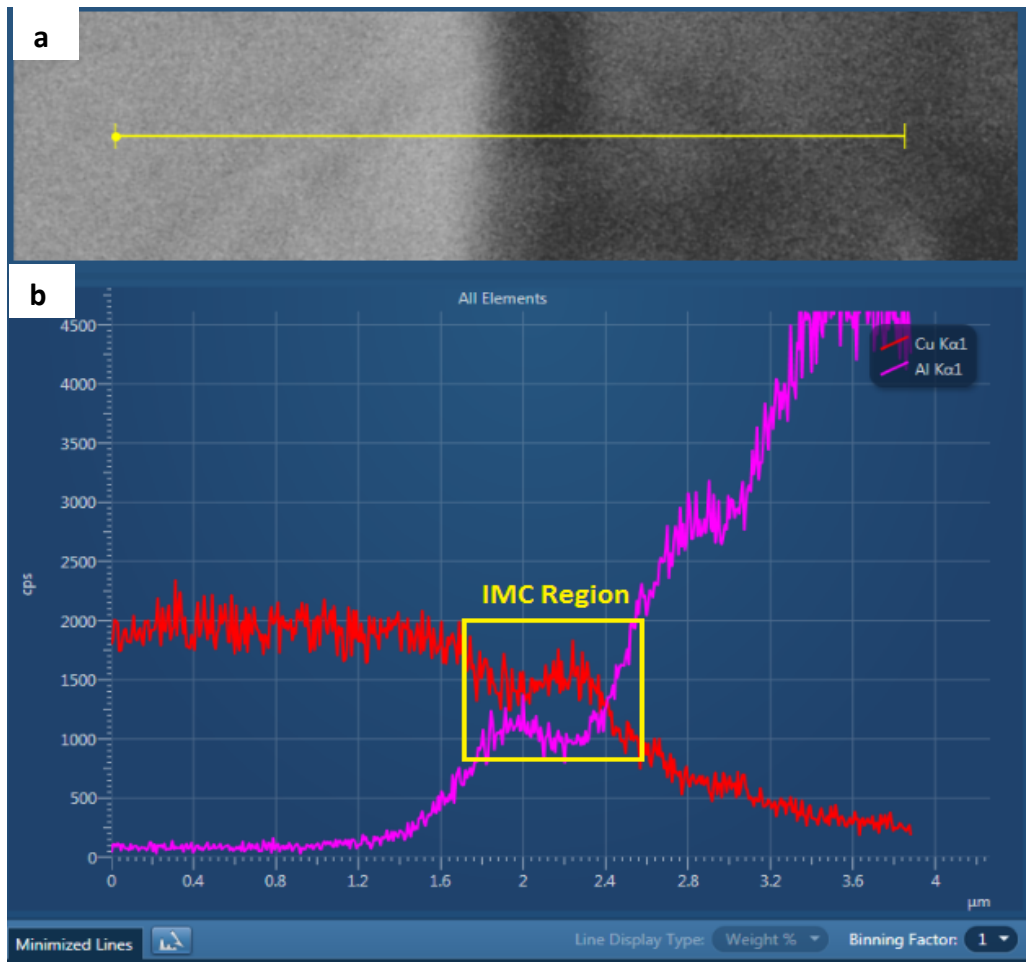


Figure 22 Example of how line-scan is performed and analyzed (this data does not represent actual sample data) on Cu-Al wire bond interface (a) Area being examined (b) Line-scan signals for each individual element and determination of IMC based on signal strength (b) line-scan spectrum with atomic percent data.

### 3.3.3 Sample ID Denotation

For the purpose of simplicity, to reduce typographical error and also to avoid confusion for the reader, a special coding system to name the samples has been applied in this thesis. For example, a sample with bond duration 20 milliseconds that have been annealed for 2 hours at 250 °C will

be referred to ID name 20-250-2 moving forward. Likewise, a sample with bond duration 100ms and annealed at 250 °C for 4 hours will be referred to as ID 100-250- 4.

### **3.4 Microhardness test at ball bond interface**

To measure hardness of Copper ball and Aluminum pad as well as the bond interface, Vickers hardness indentations are performed around the bond interface region. The Vickers Pyramid Number (HV) denotes the unit of hardness of a certain location. For guidance purposes an example of the region of the sample, along which indentations are performed, is shown in Figure 23. The regions are divided into 3 sections, 2 horizontal sections (L1 and L2) and 1 vertical sections (L3) to the bond interface. The regions are color coded for a better contrast so that they can be readily identified. The individual indentation for L1 and L2 are marked with indentation numbers from 1 through 3, starting from the left-hand side. The reasoning behind choosing these regions is to examine how hardness changes near the bond interface for both metals as well as how hardness changes as we move away from the bond interface. Plots similar to sample matlab plot in Figure 24 will help understand the change in hardness along a particular array near bond interface. The indentation number and their corresponding symbols are presented on the plot as Legends. This process is repeated for all 10 samples. Every effort is made to keep equal distance between indents in all the samples. The purpose of conducting this test is to quantify effects of different bonding duration and annealing times on hardness of the bond interface on both Copper and Aluminum as well as Copper ball. The hardness value also helps understand if an area has IMC nearby IMC regions are brittle and therefore have a higher hardness than either Copper or Aluminum. The microhardness tests are done using a Leco LM 248 AT (Figure 25). A load of 5

gf is used to avoid making bigger indents as well as avoiding damage to the bond. The hardness is then measured using the indenter microscope and viewing lens scale bar.

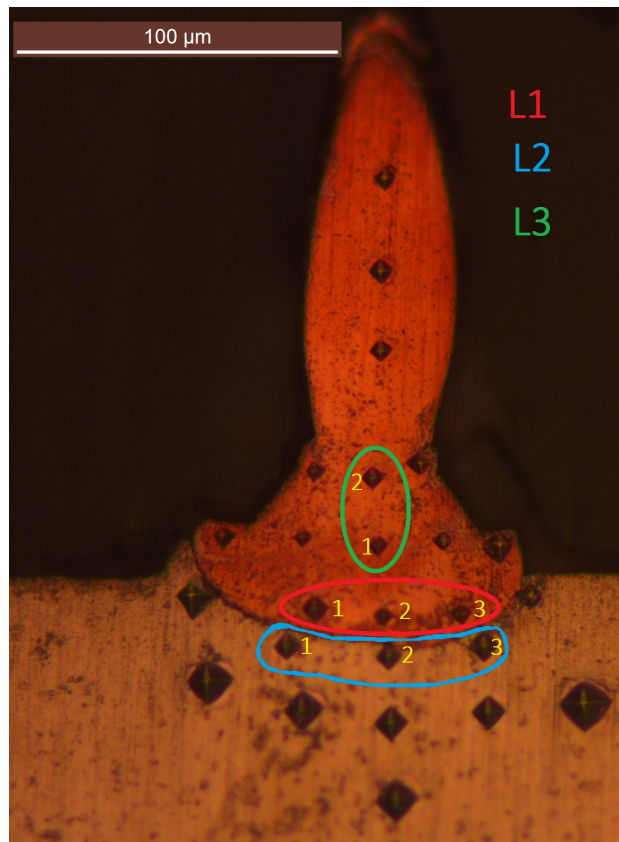


*Figure 23 Example of a Micrograph that will be used in Results section to illustrate the different marked/numbered indentations and color-coded indentation individual sections (this data does not represent actual sample data and only used for illustration).*

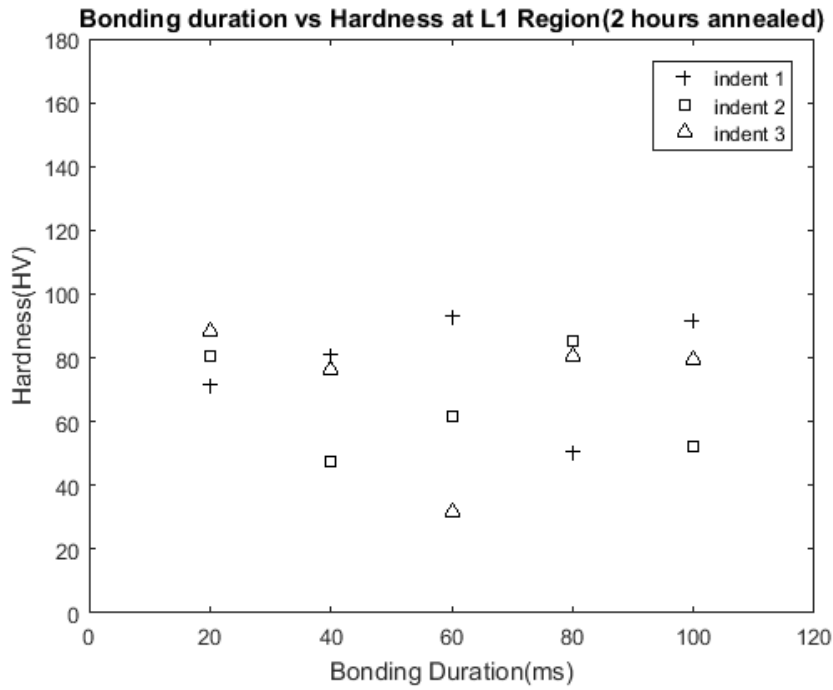


Figure 24 Example of a matlab plot of hardness data (this data does not represent actual sample data).

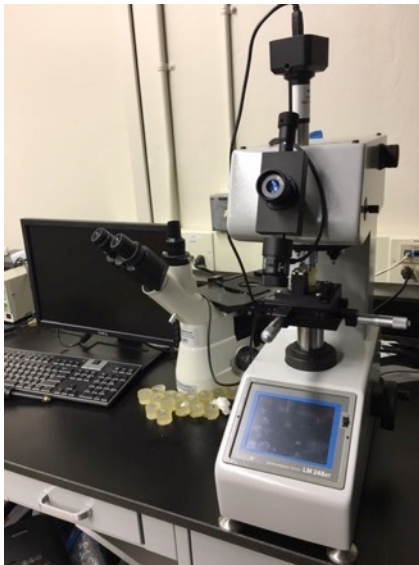


Figure 25 Leco LM 248 AT Microhardness Tester.



## CHAPTER 4: RESULTS AND DISCUSSION

In this chapter, the evolution and thickness of IMC of heat treated Cu-Al ball bonds, with respect to bonding duration, is presented and measured. BSE images are used for initial analysis of all 10 samples. In addition bond interface characterization, using EDS detector, for the same samples are done to further measure IMC thickness and the results are then compared. The EDS results are presented as energy spectrum of the characteristic x-rays from Copper and Aluminum at the bond interface. Using EDS system software, the intensity plots are then generated and The IMC thickness is then measured from these intensity plot.

### 4.1 BSE Images and IMC Measurement

For all ten samples, an image showing full ball bond is presented (marked by letter 'a'). The areas, where the IMC thickness is observed and measured, are numbered and then presented subsequently (marked by alphabets following letter 'a').

#### 4.1.1 Specimen heat treated for 2 hours

Figure 26 presents the locations on a SEM BSE micrograph for a 20-250-2 sample where IMC measurement was attempted. Figure 25b, Figure 25c and Figure 25d shows zoomed in regions where the scale bar was used to measure the suspected IMC. The IMC layer appears discontinuous and extremely thin in nature, forming mainly around bond center. No IMC was observed at the bond periphery. BSE image contrast shows only one type of IMC. IMC thickness was measured using SEM scale bar. The IMC layers measured from all locations are averaged for all samples and provided in Table2

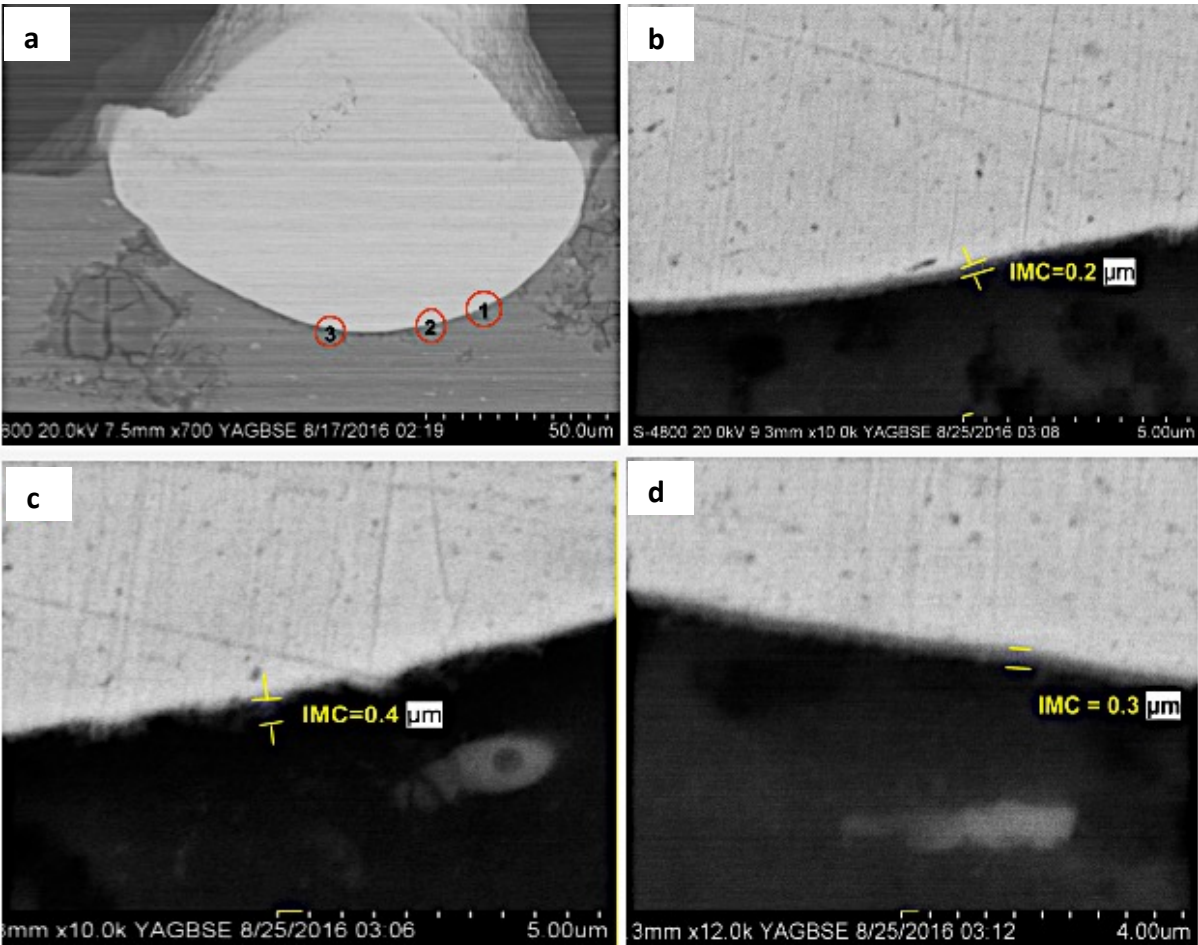


Figure 26 BSE SEM image of different sections of sample 20-250-2 (a) ball bond showing sections that are examined (b) enlarged view of section 1(c) enlarged view of section 2(d) enlarged view of section 3.

Figure 27a presents BSE Images for a 40-250-2 sample. A discontinuous, single type of IMC layer is detected (shown in Figure 26b, c, d), mainly around ball center. The IMC layer seems to be discontinuous and relatively thicker. Due to poor contrast in the image, it is hard to confirm whether IMC is actually part of Al pad or not.

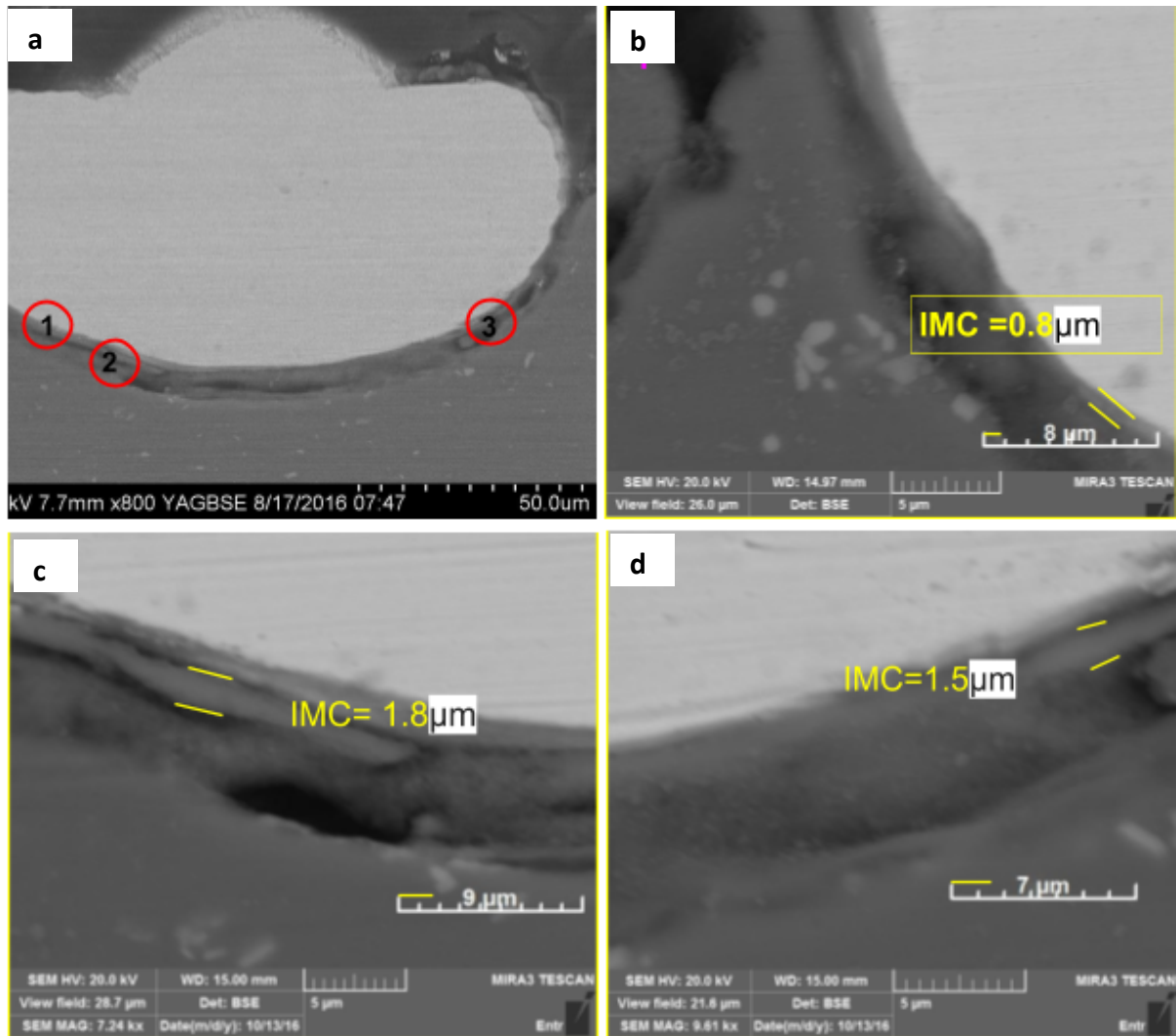


Figure 27 BSE SEM image of different sections of sample 40-250-2 (a) ball bond showing sections that are examined (b) enlarged view of section 1(c) enlarged view of section 2(d) enlarged view of section 3.

Figure 28 presents BSE Images for a 60-250-2 sample. The IMC layer, formed on either side of the bond center, appears discontinuous. Some voids can be observed, but there is a possibility that they may have been formed during specimen preparation and not during bond formation

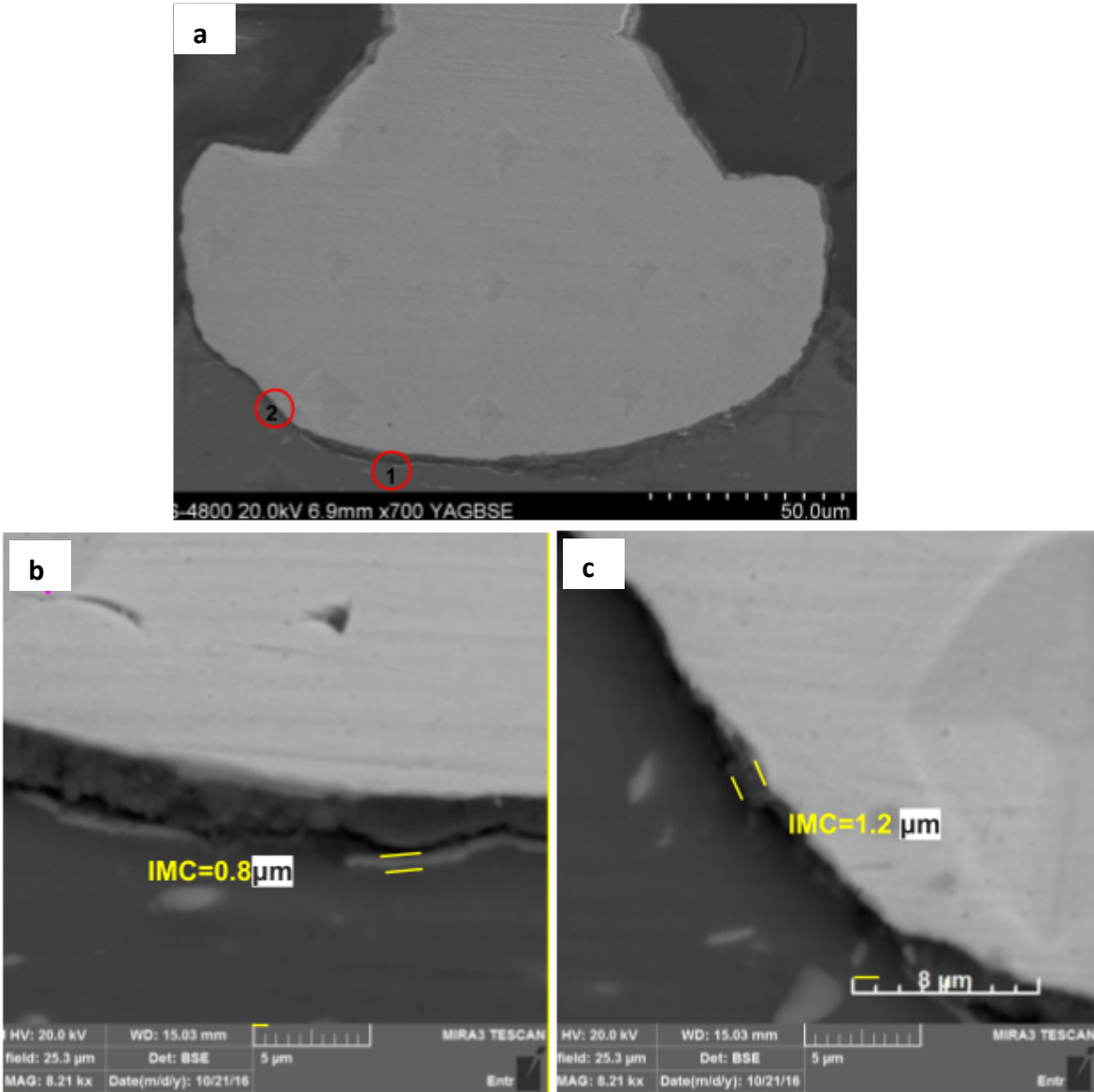


Figure 28 BSE SEM image of different sections of sample 60-250-2 (a) ball bond showing sections that are examined (b) enlarged view of section 1(c) enlarged view of section 2.

Figure 29 presents BSE Images for sample 80-250-2. The discontinuous IMC layer appeared around the ball center as well as the ball periphery this time compared to previous bonds. Micrograph Image contrast shows formation of one type of IMC layer.

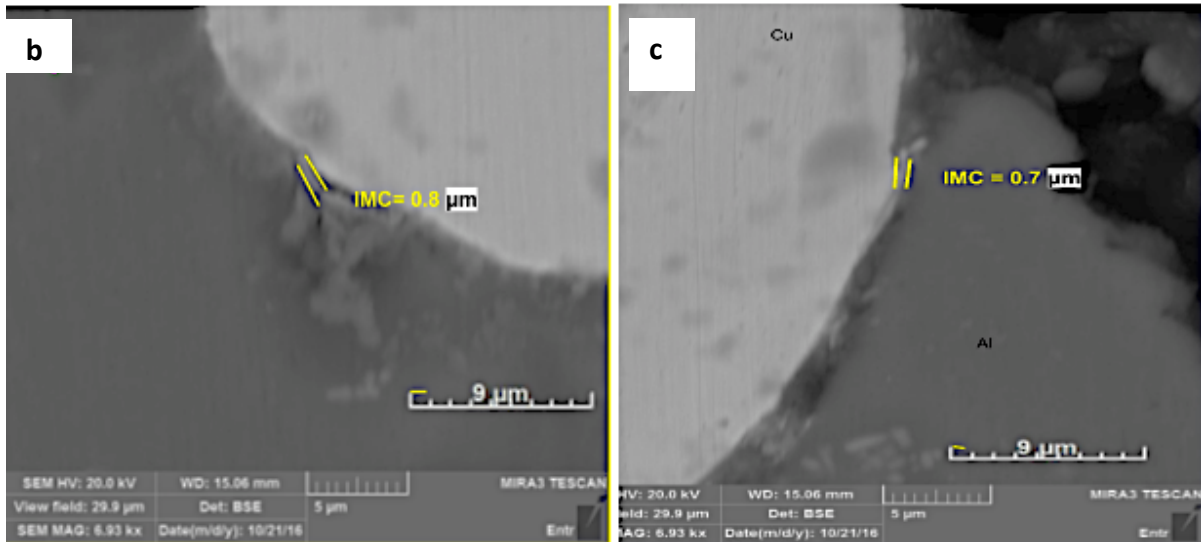
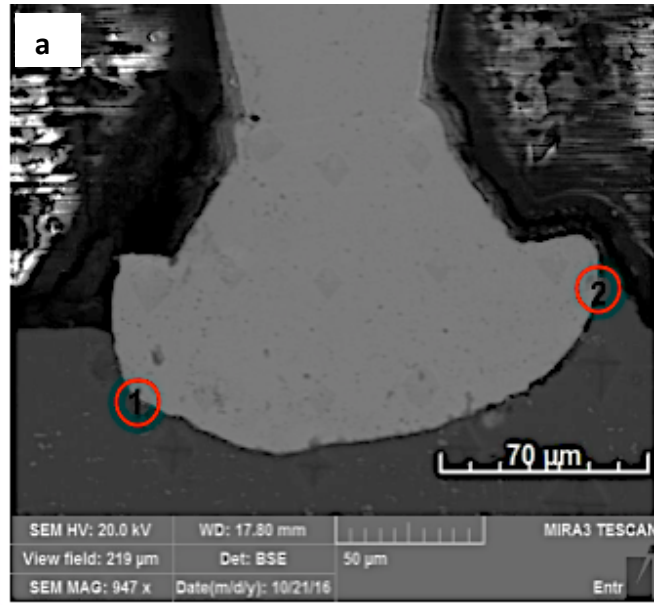


Figure 29 BSE SEM image of different sections of sample 80-250-2 (a) ball bond showing sections that are examined (b) enlarged view of section 1(c) enlarged view of section 2.

Figure 30 presents BSE Images for sample 100-250-2. The IMC layer around region 1 and 2 appear to be more uniform compared to region 3. Two different IMC layer can be seen to form as supported by BSE image contrast, compared to previous bonds. Small voids are also detected at the Al-Cu interface at the bond periphery.

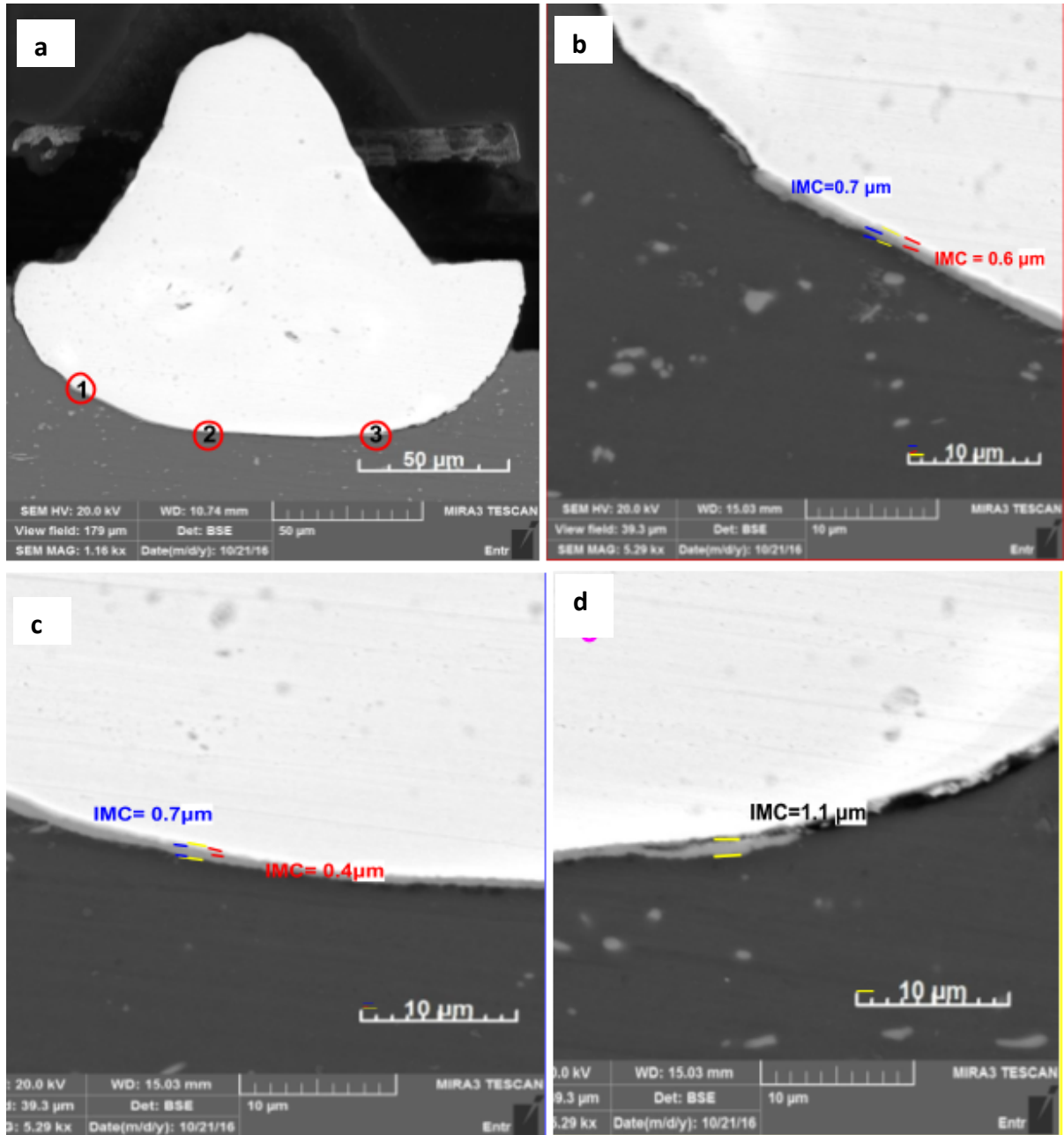


Figure 30 BSE SEM image of different sections of sample 100-250-2 (a) ball bond showing sections that are examined (b) enlarged view of section 1(c) enlarged view of section 2(d) enlarged view of section 3.

#### 4.1.2 Specimen heat treated for 4 hours

Figure 31 SEM BSE micrograph for sample 20-250-4. No IMC was observed. The edges that appeared to have a different contrast were actually part of the Copper ball that got detached from the Al pad during sample preparation. The difference in contrast may be due to a tilt on the edge when viewed top down.

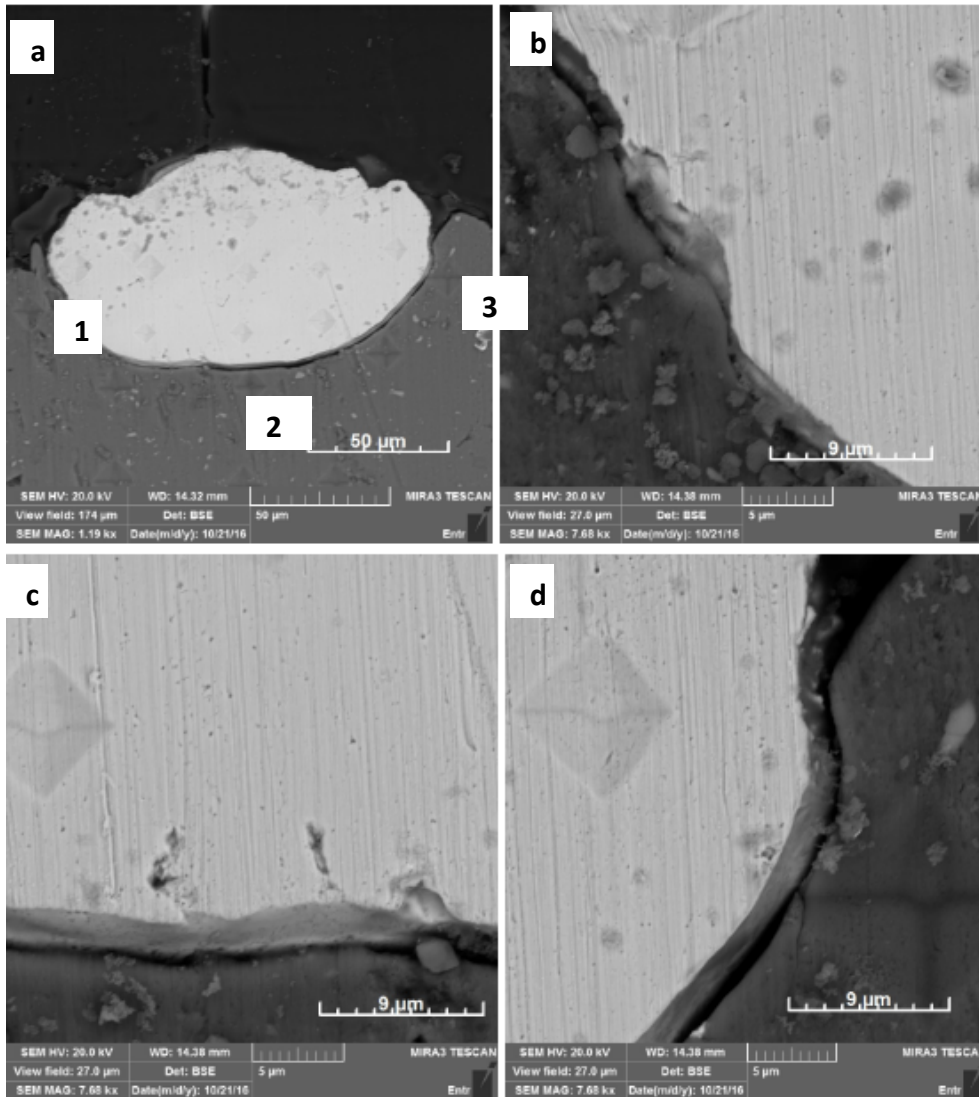


Figure 31 BSE SEM image of different sections of sample 20-250-4 (a) ball bond showing sections that are examined (b) enlarged view of section 1(c) enlarged view of section 2(d) enlarged view of section 3.

Figure 32 presents suspected IMC layer locations on a SEM BSE micrograph for sample 40-250-4. Once again discontinuous and very thin IMC layer appeared around the ball center as well as the ball periphery. Only one type of IMC, as shown by micrograph image contrast, is observed.

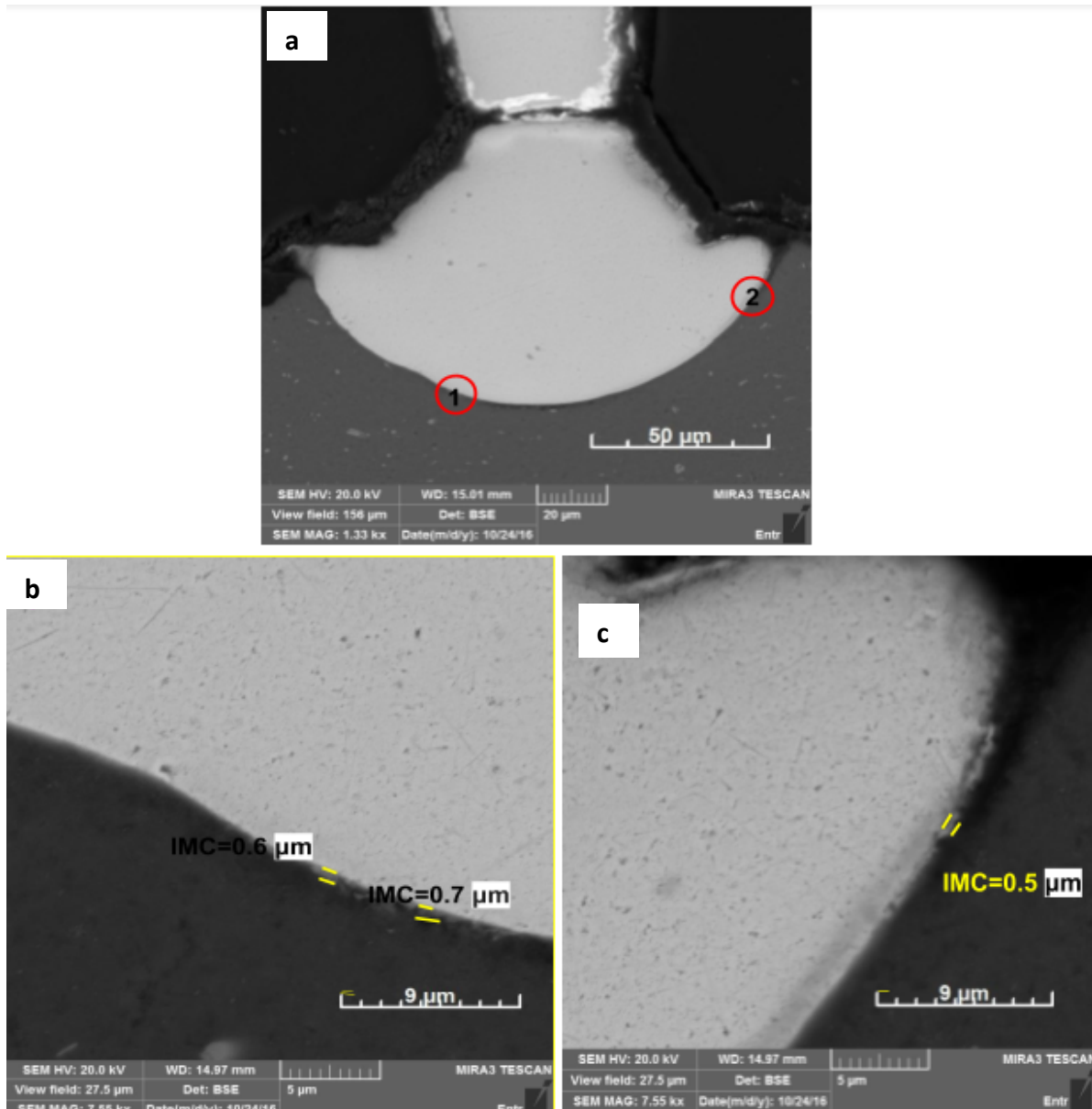


Figure 32 BSE SEM image of different sections of sample 40-250-4 (a) ball bond showing sections that are examined (b) enlarged view of section 1(c) enlarged view of section 2.



Figure 33, presents the locations with suspected IMC layer for sample 60-250-4. This entire specimen appears damaged where the Cu ball is detached from the Al pad. This may be caused by either during sample preparation or from formation of brittle IMC layers. Two different IMC layer can be seen to form as supported by BSE image contrast. The IMC layer appears discontinuous. in the regions shown in Figure 32b, c, d.

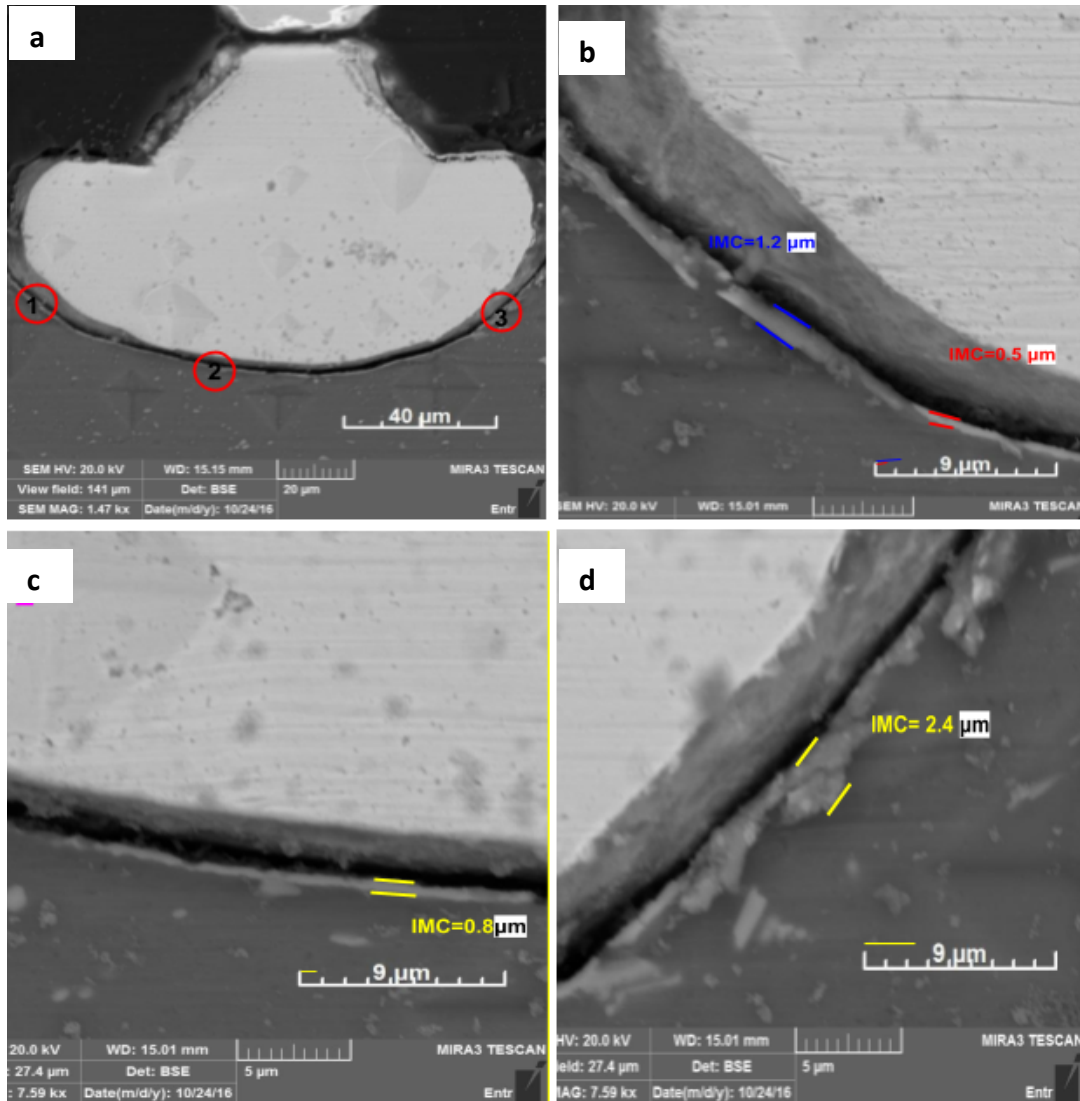


Figure 33 BSE SEM image of different sections of sample 60-250-4 (a) ball bond showing sections that are examined (b) enlarged view of section 1(c) enlarged view of section 2(d) enlarged view of section 3.

Figure 34, for sample 80-250-4, also shows two different IMC layer as seen in Figure 33b,c,d. They all formed around the center of the ball bond and also appeared much thicker and more uniform than any of the previous IMC layers of other samples. Some voids adjacent to the IMC layer is observed as well.

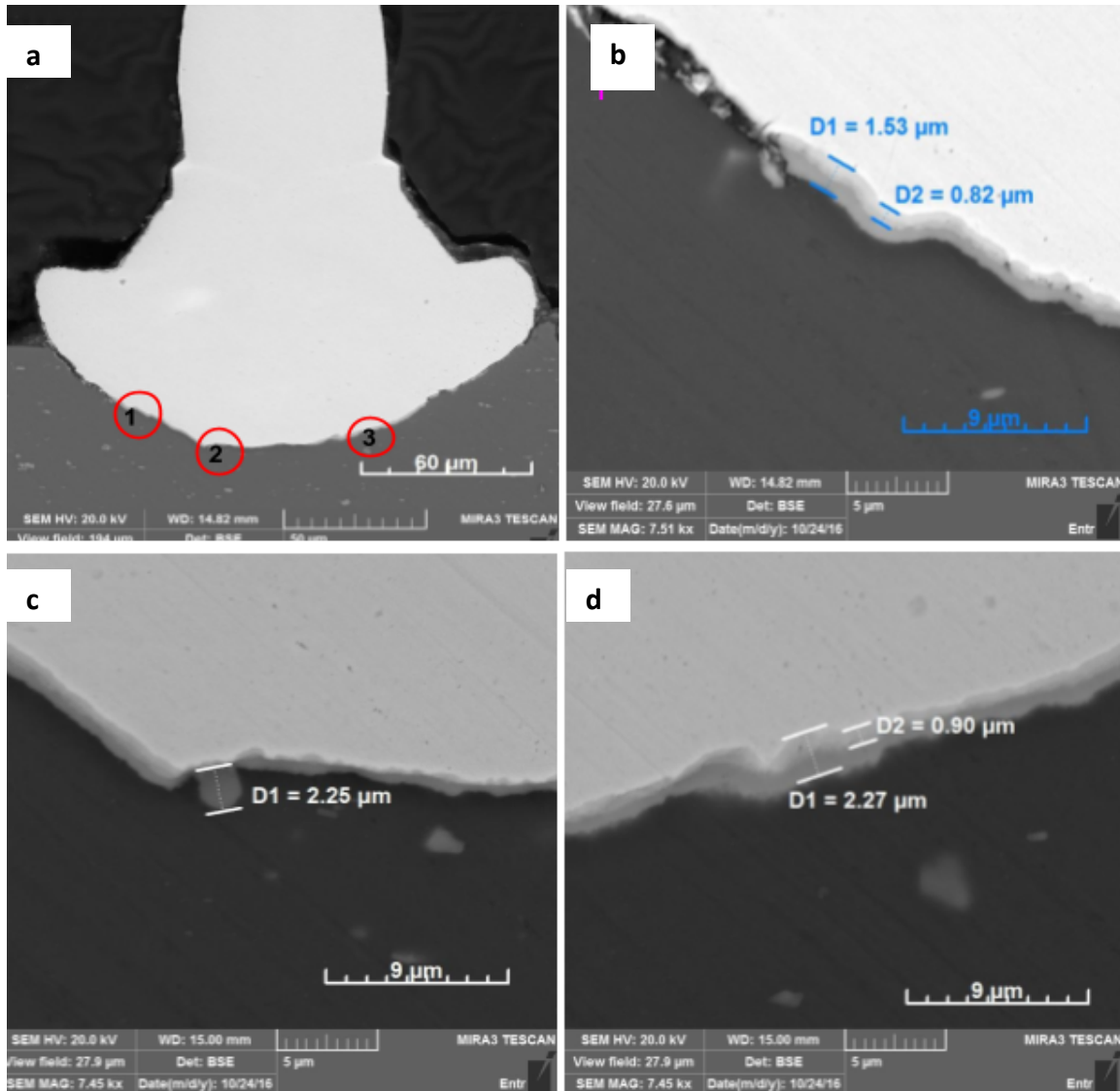


Figure 34 BSE SEM image of different sections of sample 80-250-4 (a) ball bond showing sections that are examined (b) enlarged view of section 1 (c) enlarged view of section 2 (d) enlarged view of section 3.

Figure 35, for sample 100-250-4, show two different IMC phase layer. The different IMC phase layer is similar to 100 ms bonds annealed at the same temperature but for 2 hours. They all formed around the center of the ball bond and appeared much thicker and more uniform than any of the previous IMC layers. Although some voids can be seen, but it is hard to assess if they are just damages caused during sample preparation or caused during bonding process.

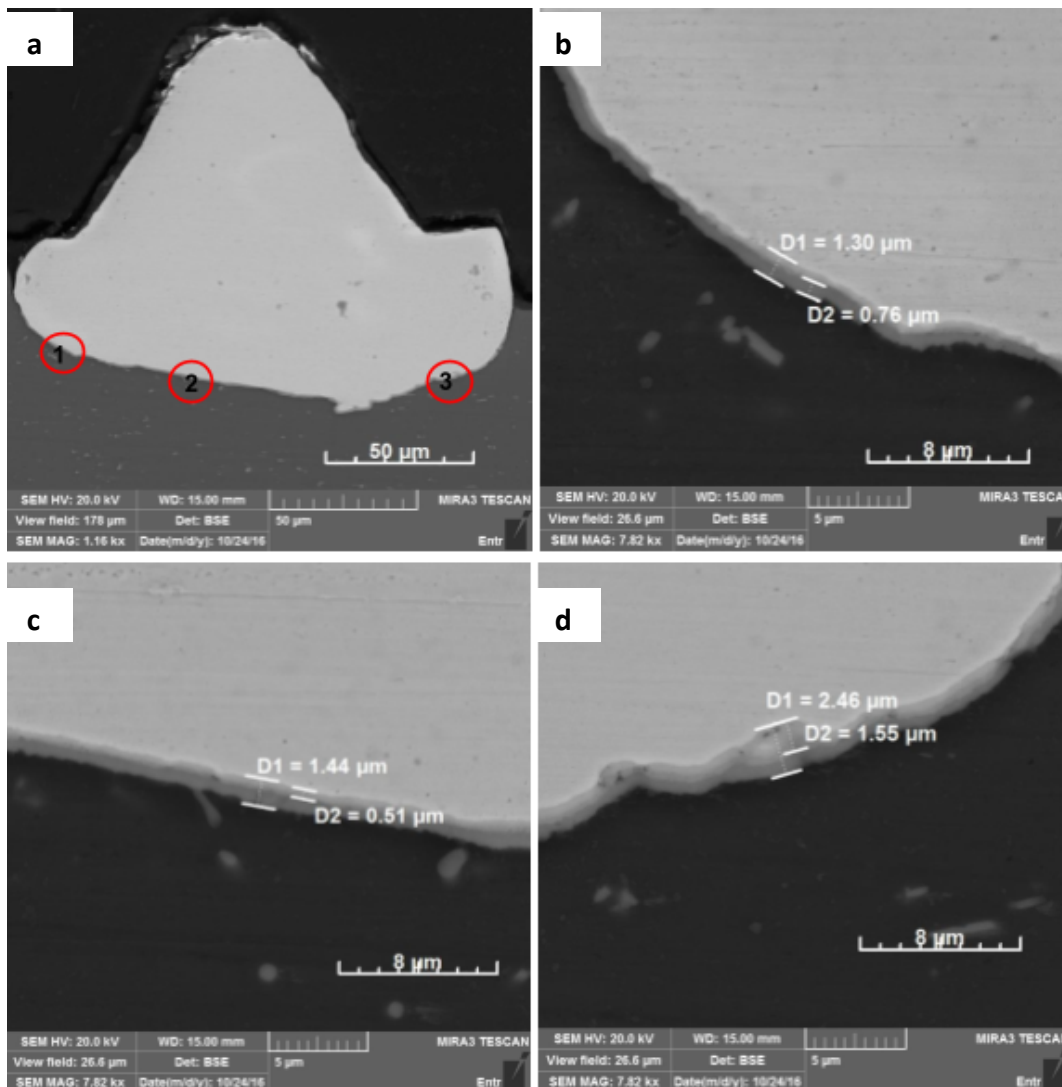


Figure 35 BSE SEM image of different sections of sample 100-250-4 (a) ball bond showing sections that are examined (b) enlarged view of section 1(c) enlarged view of section 2(d) enlarged view of section 3.

### 4.1.3 Discussion

Table 2 summarizes the result of average IMC as detected from BSE imaging. The IMC, when formed, were always discontinuous. Majority of the IMC were formed at the bond center compared to bond periphery. The IMC thickness does not increase proportionally with increased bond duration for samples annealed for 2 hours. The results are not in agreement with literature survey where it is established that duration of application of US vibration is directly proportional to IMC formation. The reason for the outliers could be due to some bond interfaces with edge of detached Copper ball, that looked similar to IMC layer in terms of contrast, got measured as IMC layer. However, for samples annealed at 4 hours, the thickness vs bond duration is more consistent with literature survey. The thickness increased with increase in bond duration. Overall thickness of IMC for samples annealed for 4 hours were thicker. This could be due to the bond interface being subjected to longer diffusion time.

**Table 2 Average Thickness of IMC based Visual Inspection of BSE Micrograph**

<b>Sample ID</b>	<b>Average IMC Thickness using BSE Analysis</b>
20-250-2	0.3 $\mu\text{m}$
40-250-2	1.36 $\mu\text{m}$
60-250-2	1 $\mu\text{m}$
80-250-2	0.75 $\mu\text{m}$
100-250-2	1.16 $\mu\text{m}$
20-250-4	0

40-250-4	0.6 $\mu\text{m}$
60-250-4	1.225 $\mu\text{m}$
80-250-4	2.01 $\mu\text{m}$
100-250-4	1.73 $\mu\text{m}$

## 4.2 EDS Analysis of Ball Bond Interface

In this segment of analysis, linescan data of one region of the Cu-Al bond is presented in the main body of thesis. Only reliable linescan data are provided in the thesis. Linescans were performed at regions with the most promising layer of IMC. The region where the intensity plots of Copper and Aluminum overlap, is considered to be IMC layer and the thickness is measured. Table 3 is then used to compare the results of IMC thickness found by BSE and EDS analysis.

### 4.2.1 Specimen heat treated for 2 hours at 250 ° C

#### 4.2.1.1 Specimen with 20 ms bond time

Figure 36 presents linescan results for sample 20-250-2, and it corresponds to the same region as Figure 25a. The Intensity plot shows IMC with thickness of 0.6  $\mu\text{m}$ . Based on Intensity plot, major portion of the line scan was on Al rich side.

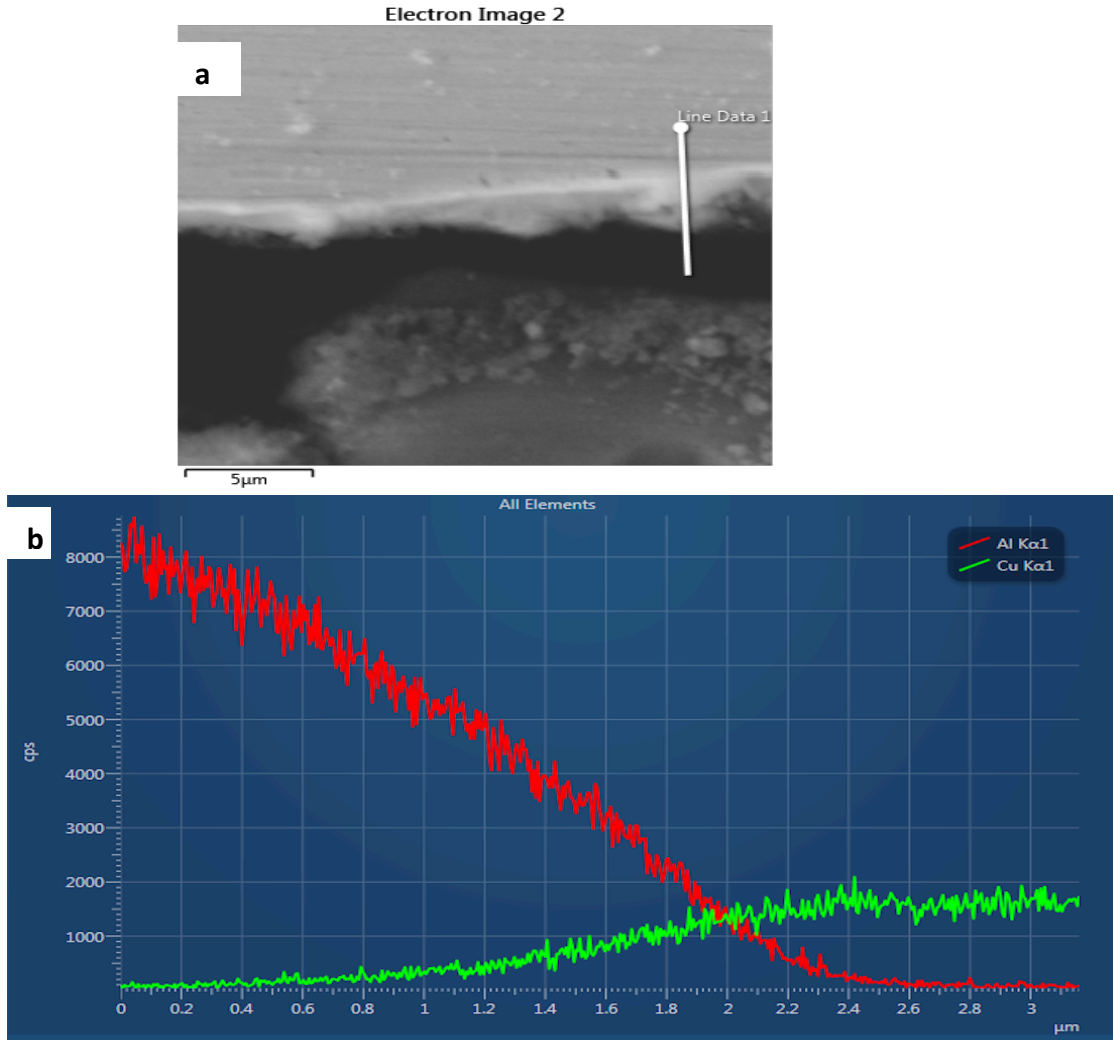


Figure 36 EDS scan results of sample 20-250-2 showing (a) cross-section of IMC analyzed with linescan (b) Intensity plot of line 1 (c) the energy spectrum results of line 1.

#### 4.2.1.2 Specimen with 40 ms bond time

Figure 37 presents linescan results for sample 20-250-2. The Intensity plot shows IMC with thickness of 1.5 µm. Based on Intensity plot, major portion of the line scan was on Cu portion of the bond interface.

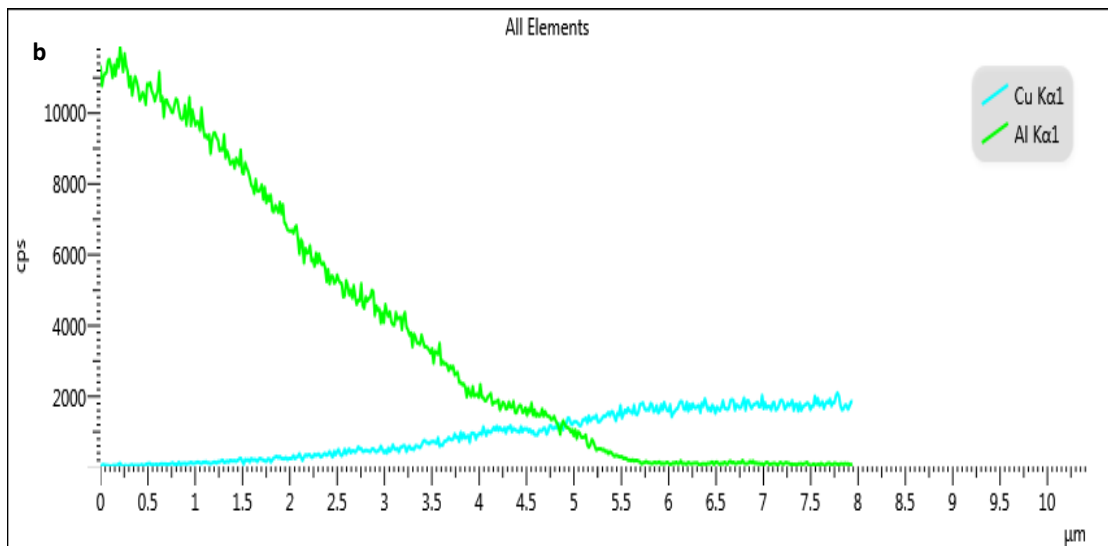
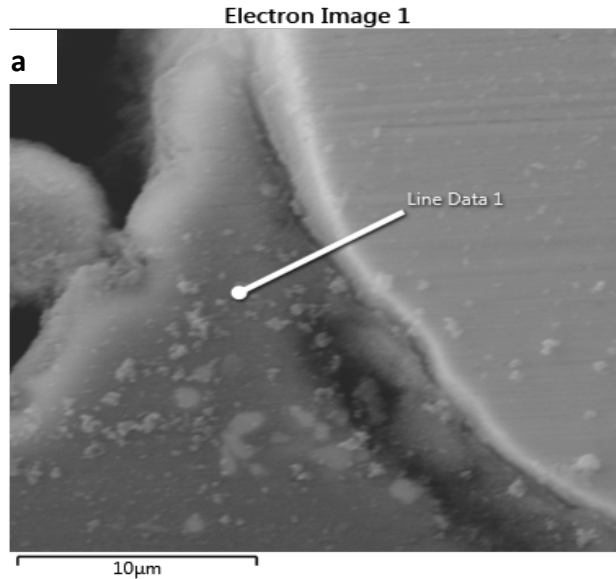


Figure 37 EDS scan results of sample 40-250-2 showing (a) cross-section of IMC analyzed with linescan (b) Intensity plot of line 1.

#### 4.2.1.3 Specimen with 60 ms bond time

Figure 38 presents linescan results for sample 60-250-2. The Intensity plot shows IMC with thickness of 0.8 μm. Based on Intensity plot, major portion of the line scan was on Cu portion of

the bond interface. The composition result of this scan does not correspond to any known composition of CuAl IMC.

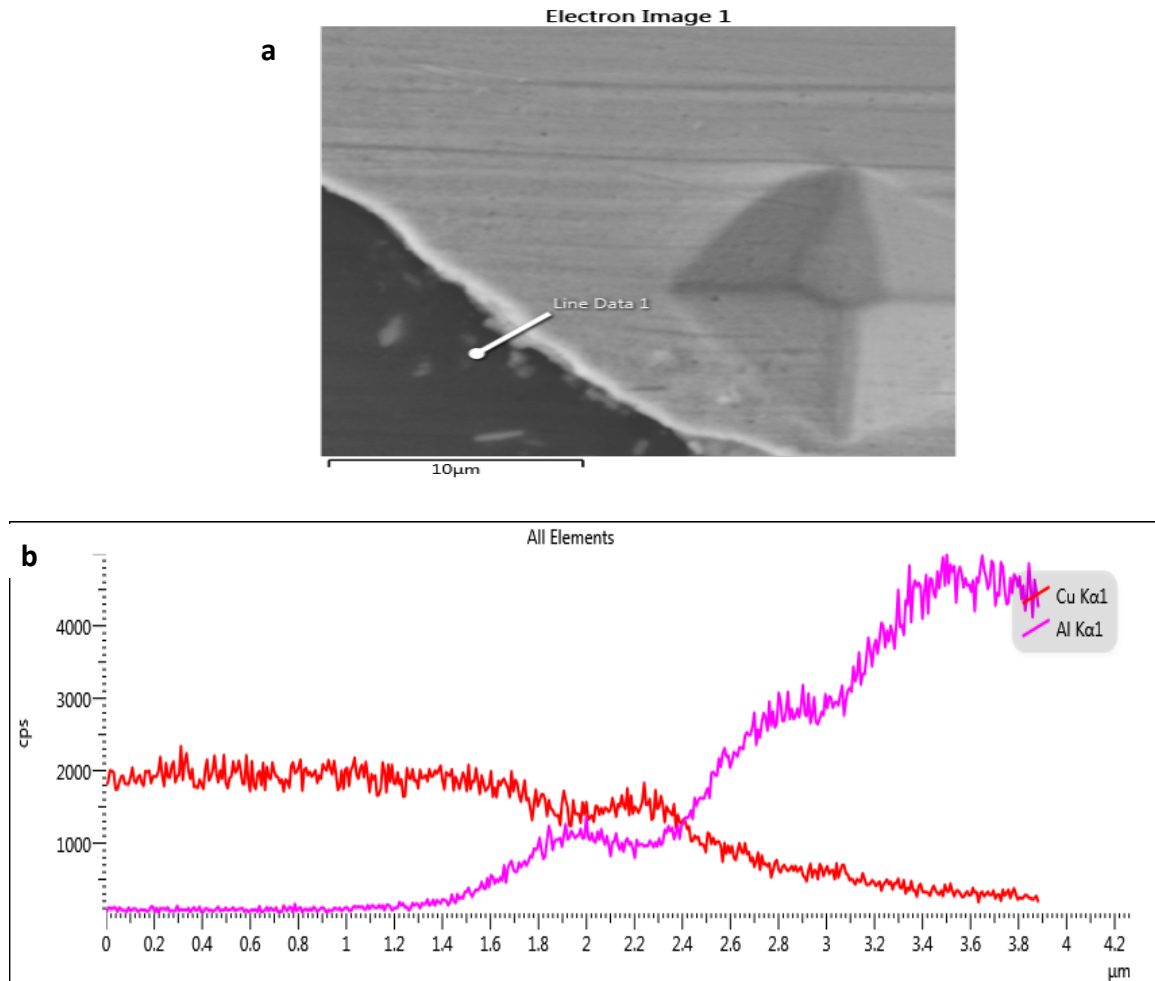


Figure 38 EDS scan results of sample 60-250-2 showing (a) cross-section of IMC analyzed with linescan (b) Intensity plot of line 1 (c) the energy spectrum results of line 1.

#### 4.2.1.4 Specimen with 80 ms bond time

Figure 39 presents linescan results for sample 80-250-2. The Intensity plot shows IMC with



thickness of 1.0  $\mu\text{m}$ . Based on Intensity plot, most of line scan was on Al portion of the bond interface.

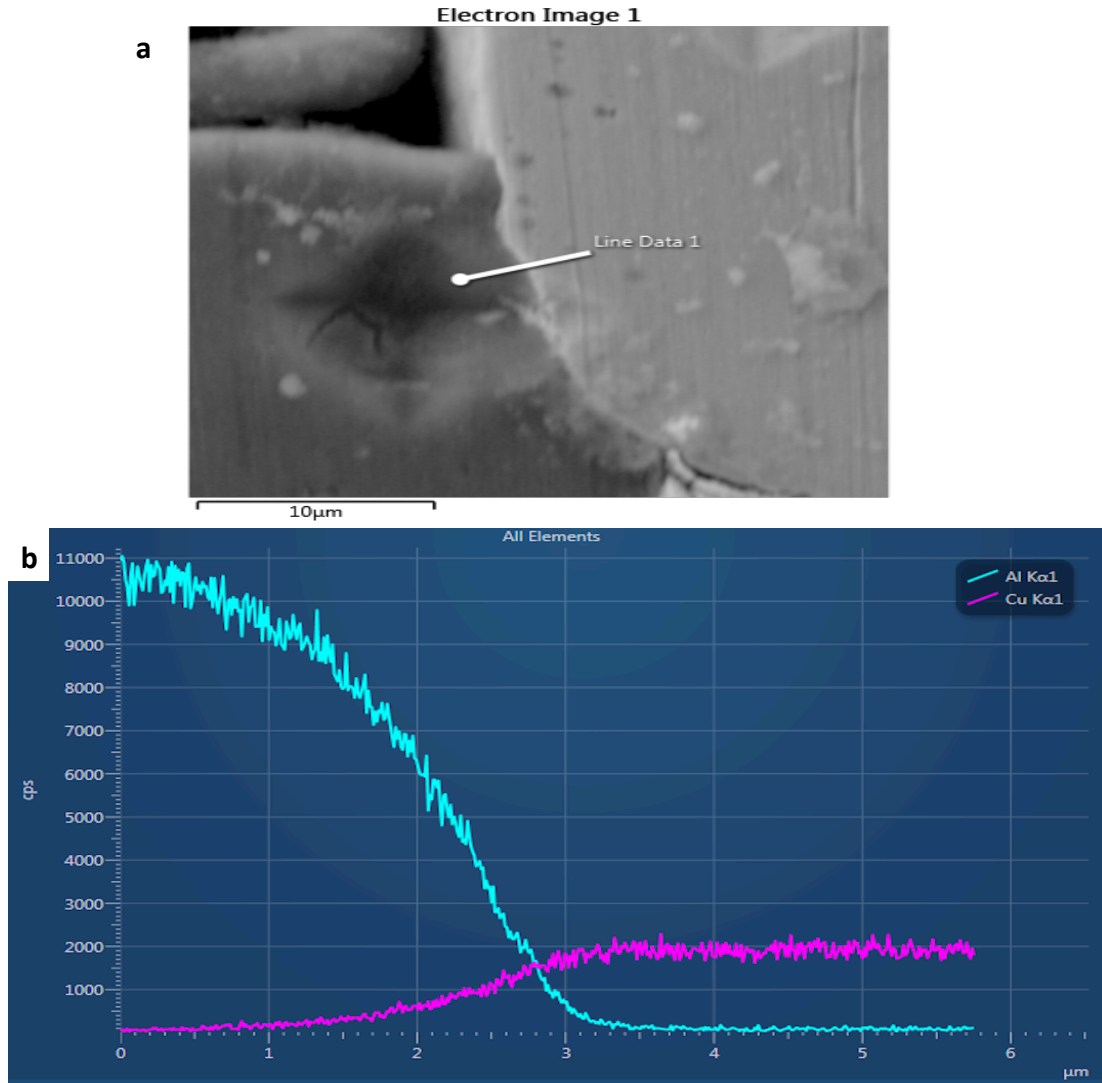


Figure 39 EDS scan results of sample 80-250-2 showing (a) cross-section of IMC analyzed with linescan (b) Intensity plot of line 1.

#### 4.2.1.5 Specimen with 100 ms bond time

Figure 40 presents linescan results for sample 100-250-2. The Intensity plot shows IMC with

thickness of around 1.0  $\mu\text{m}$ . Based on Intensity plot, major portion of the line scan was on Al region of bond interface.

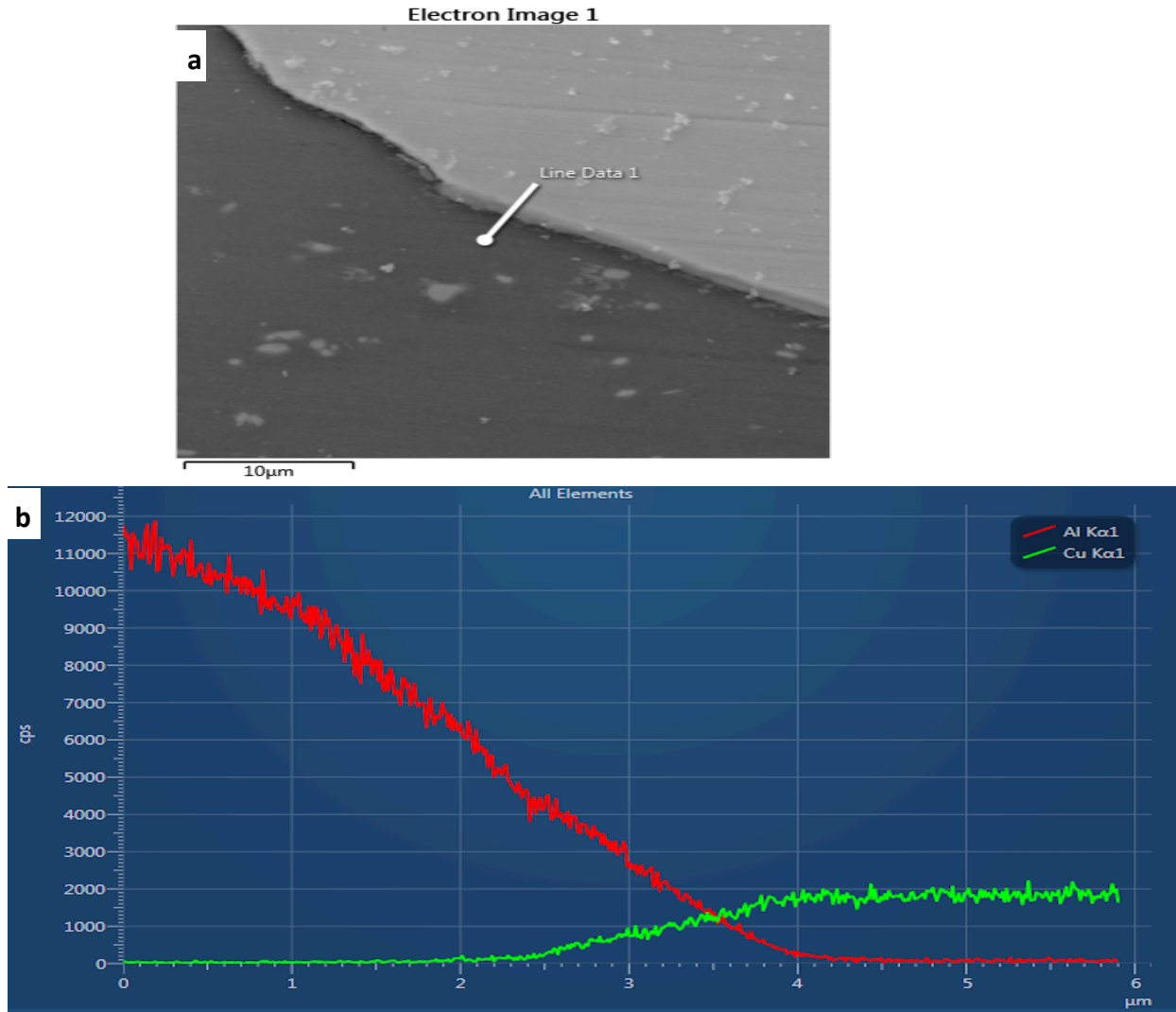


Figure 40 EDS scan results of sample 100-250-2 showing (a) cross-section of IMC analyzed with linescan (b) Intensity plot of line 1.

## 4.2.2 Specimen heat treated for 4 hours at 250 ° C

### 4.2.2.1 Specimen with 20 ms bond time

Figure 41 presents linescan results for sample 20-250-4. The Intensity plot shows IMC layer thickness of 0.8  $\mu\text{m}$ . A major portion of the intensity plot that is supposed to be IMC region is being ignored because a major portion (two thirds approx.) of the bond interface is void, according to the BSE image.

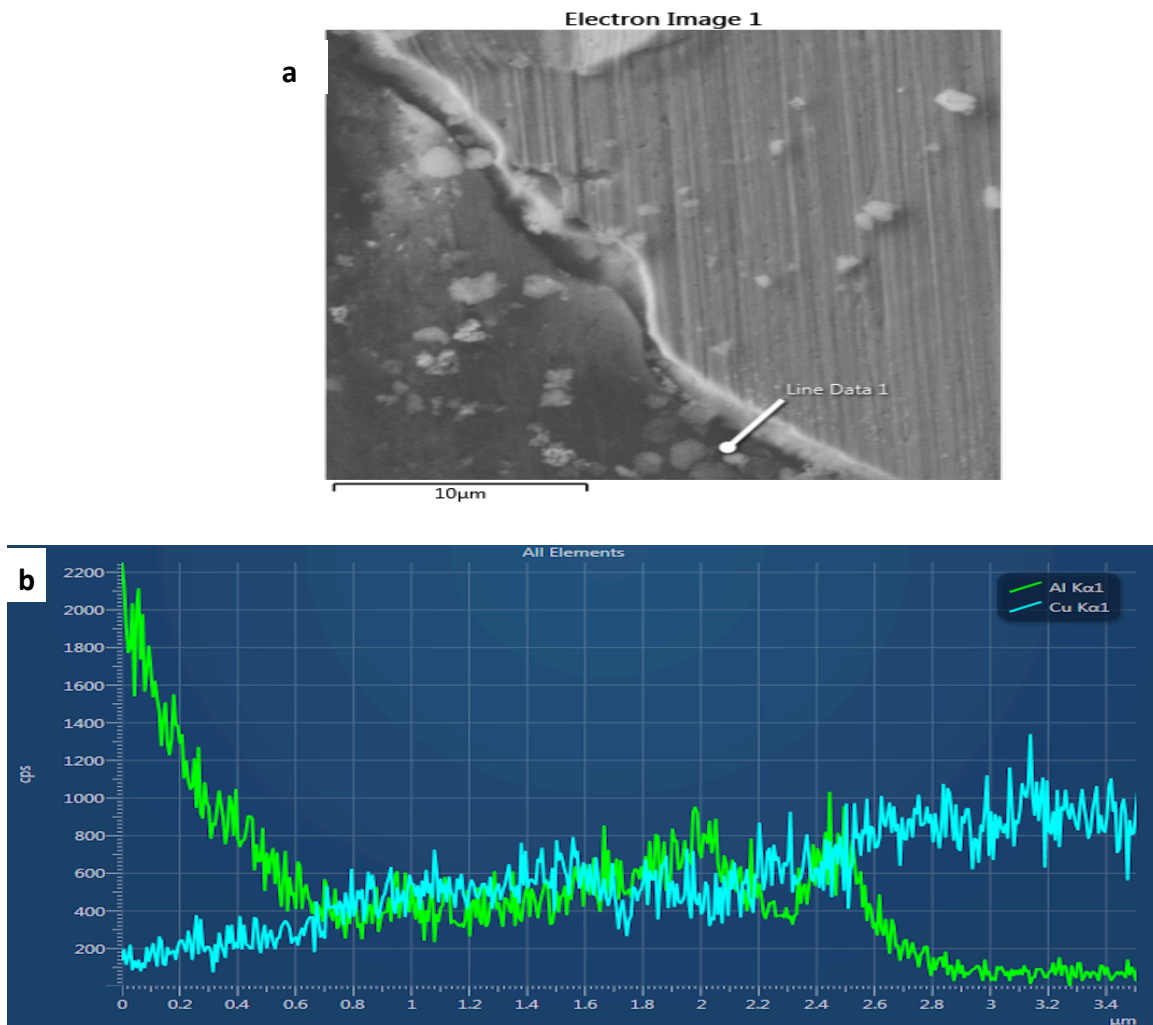


Figure 41 EDS scan results of sample 20-250-4 showing (a) cross-section of IMC analyzed with linescan (b) Intensity plot of line 1.

#### 4.2.2.2 Specimen with 40 ms bond time

Figure 42 presents linescan results for sample 40-250-4. The Intensity plot shows IMC with thickness less than 1  $\mu\text{m}$ . It also appears that the line scan was done right on bond interface and hence the signal strength difference between Al and Cu is not very large. The composition results of this scan do not correspond to any known composition of CuAl IMC.

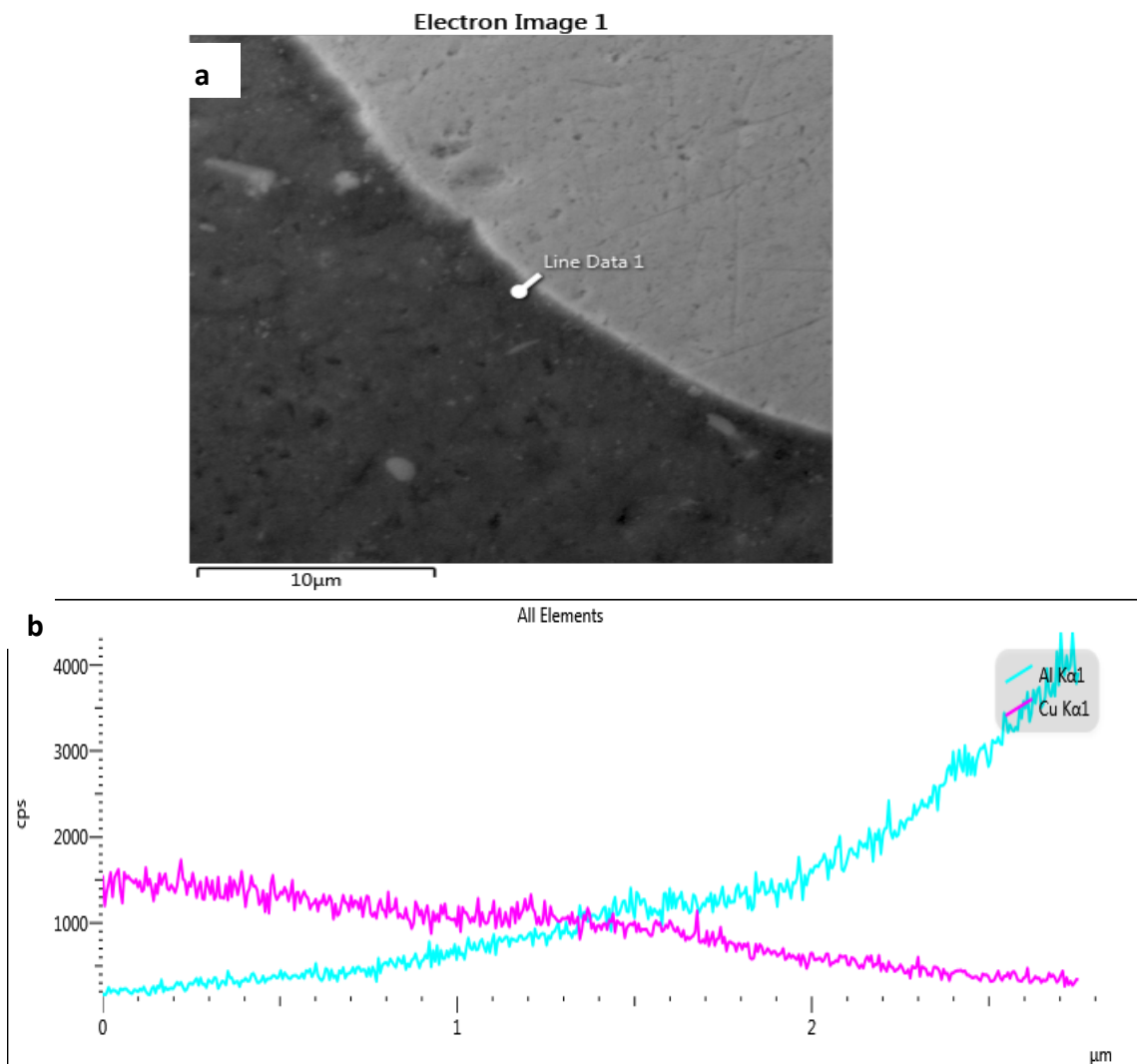


Figure 42 EDS scan results of sample 40-250-4 showing (a) cross-section of IMC analyzed with linescan (b) Intensity plot of line 1.

### 4.2.2.3 Specimen with 60 ms bond time

Figure 43 presents linescan results for sample 60-250-4. The Intensity plot shows IMC with thickness of 1.4 $\mu\text{m}$ . A big portion of the linescan, according to BSE image, falls on void region. The IMC region is attached to the Al Therefore, not all signals received by EDS are from Cu-Al bond interface. The voids may be a result of damage caused during specimen preparation or Brittle IMC formation.

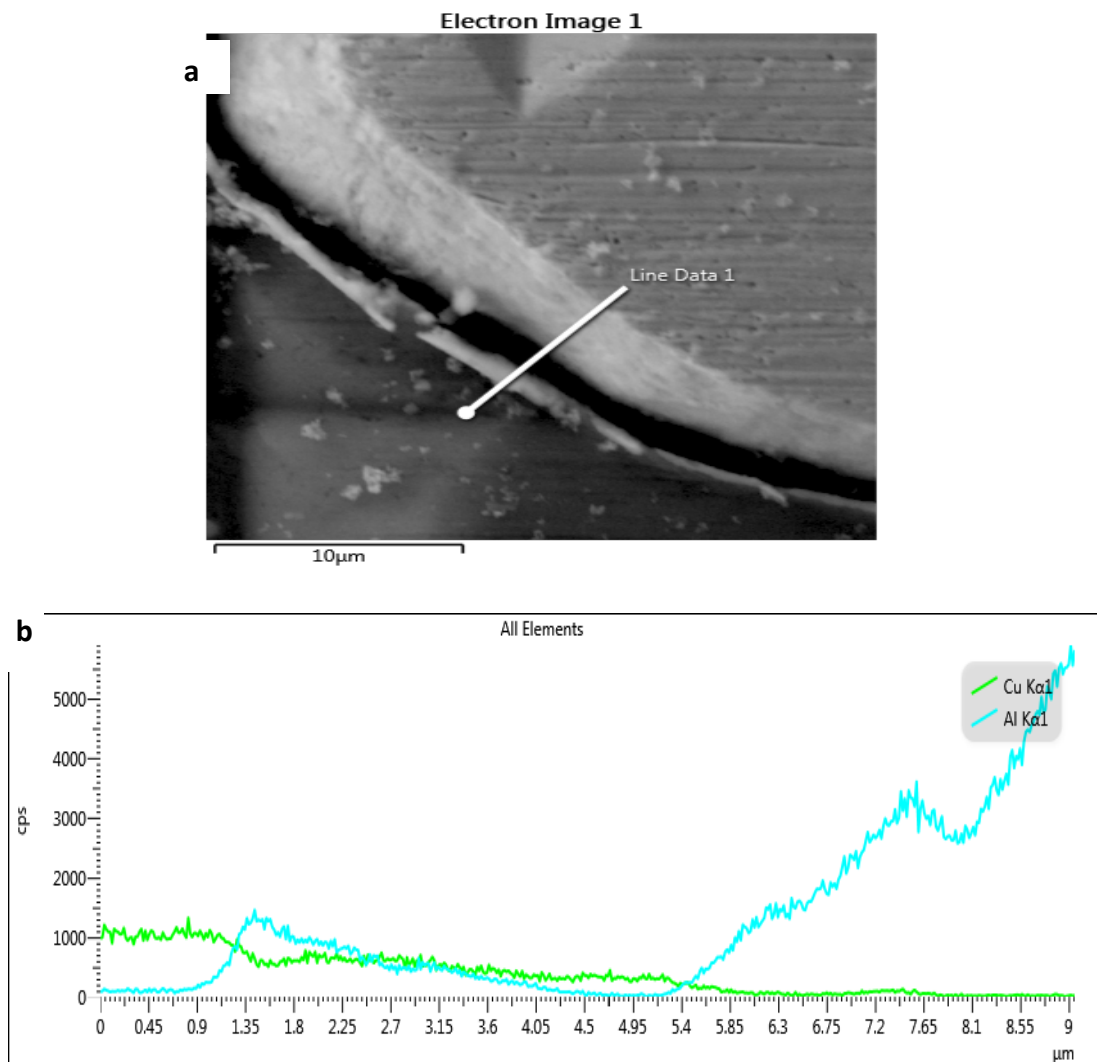


Figure 43 EDS scan results of sample 60-250-4 showing (a) cross-section of IMC analyzed with linescan (b) Intensity plot of line 1.

#### 4.2.2.4 Specimen with 80 ms bond time

Figure 44 presents linescan results for sample 80-250-4. The Intensity plot shows IMC with thickness of around 1.5  $\mu\text{m}$ . Based on Intensity plot, most of line scan was on Cu portion of the bond interface.

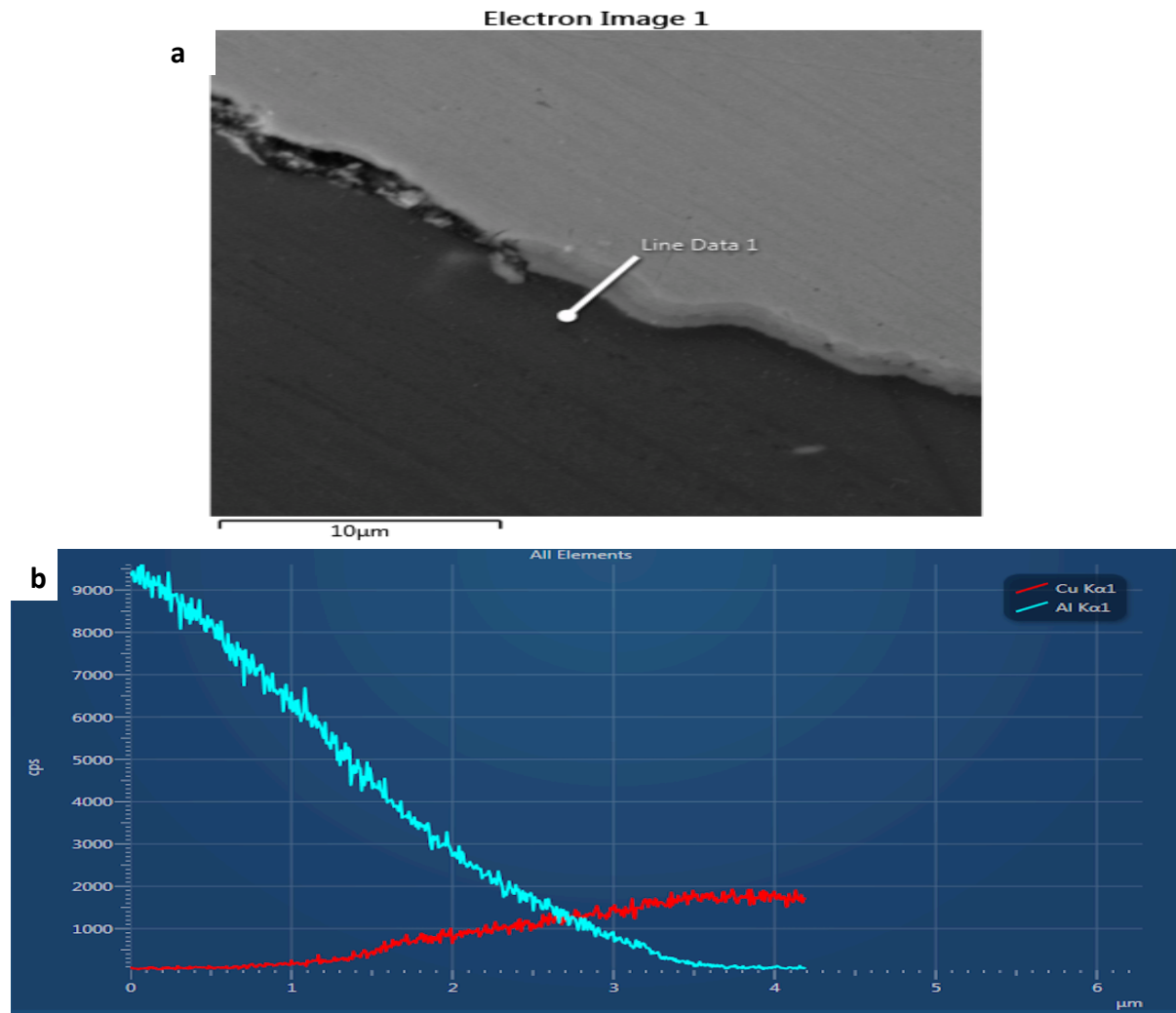


Figure 44 EDS scan results of sample 80-250-4 showing (a) cross-section of IMC analyzed with linescan (b) Intensity plot of line 1.

#### 4.2.2.5 Specimen with 100 ms bond time

Figure 45 presents linescan results for sample 100-250-4. The Intensity plot shows IMC with thickness of around 1.5  $\mu\text{m}$ . Based on Intensity plot, most of line scan was on Cu portion of the bond interface.

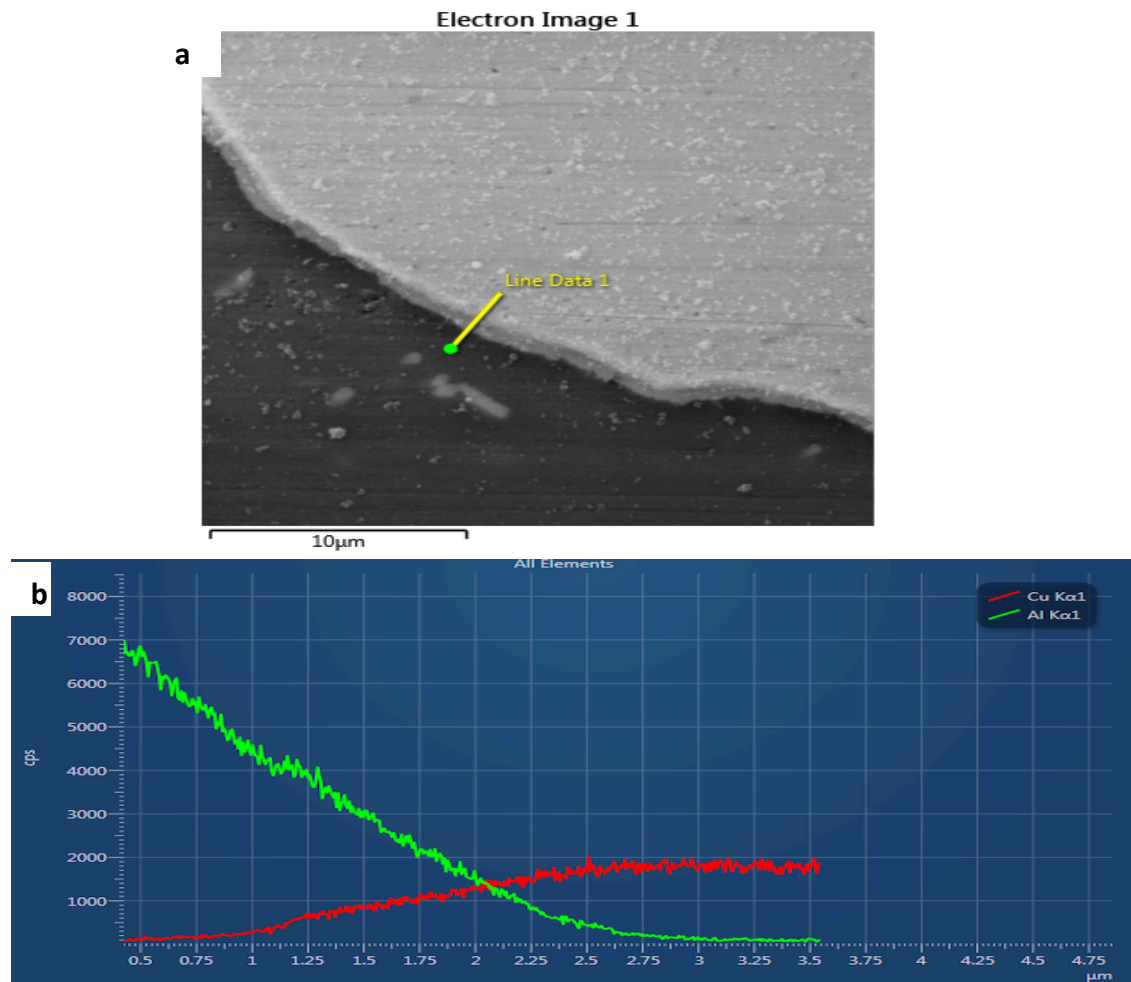


Figure 45 EDS scan results of sample 100-250-4 showing (a) cross-section of IMC analyzed with linescan (b) Intensity plot of line 1.

### 4.2.3 Discussion

The summary of EDS analysis, as well as IMC thickness data from BSE imaging, are given in Table 3. The trend observed in the plots is that as ultrasonic time is increased, for both annealing conditions, the IMC thickness increases. Ultrasonic power causes strong plastic deformation in both Cu and Al. Plastic deformation leads to local increase in dislocation, which then decreases activation energy needed for metal atoms to diffuse. Diffusion helps with IMC formation. Therefore, the longer the US vibration time, the more diffusion it leads to. US vibration also helps fragment the native oxide layer found in Al. IMCs, according to literature survey, IMC usually forms where the oxide layer is fragmented during bonding. Effects of annealing can be related directly to IMC growth by Equation 2. The longer the annealing time, the more diffusion occurs and therefore IMC thickness increases.

**Table 3 Summary of IMC thickness measured with BSE and EDS detection methods**

<b>Sample ID</b>	<b>Average IMC Thickness using BSE Analysis</b>	<b>IMC thickness/Cu-Al Phase</b>
20-250-2	0.3 $\mu\text{m}$	0.6 $\mu\text{m}$
40-250-2	1.36 $\mu\text{m}$	1.5 $\mu\text{m}$
60-250-2	1 $\mu\text{m}$	0.8 $\mu\text{m}$
80-250-2	0.75 $\mu\text{m}$	1 $\mu\text{m}$
100-250-2	1.16 $\mu\text{m}$	1 $\mu\text{m}$
20-250-4	0	0.8 $\mu\text{m}$



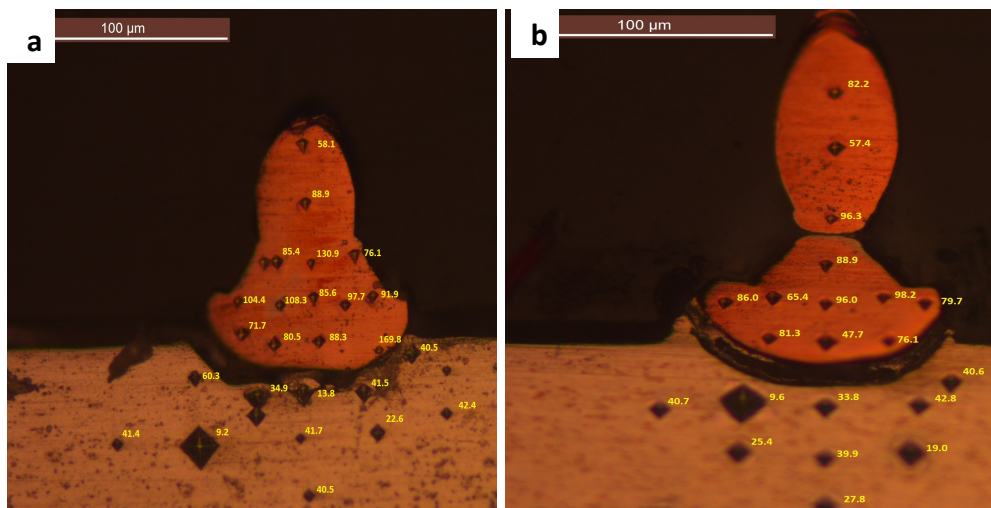
40-250-4	0.6 $\mu\text{m}$	1 $\mu\text{m}$
60-250-4	1.225 $\mu\text{m}$	1.4 $\mu\text{m}$
80-250-4	2.01 $\mu\text{m}$	1.5 $\mu\text{m}$
100-250-4	1.73 $\mu\text{m}$	1.5 $\mu\text{m}$

### 4.3 Microhardness Indentation of Copper-Aluminum Bond Interface

Data in this portion of research is present as micrographs of Cu-Al bonds with areas that underwent indentations for hardness test, as well as plots of bonding duration vs. hardness and bonding duration vs. annealing time.

#### 4.3.1 Indentation Region for samples annealed for 2 hours

The Micrographs in *Figure 46* shows the hardness value and indentation locations of all bonds annealed for 2 hours.



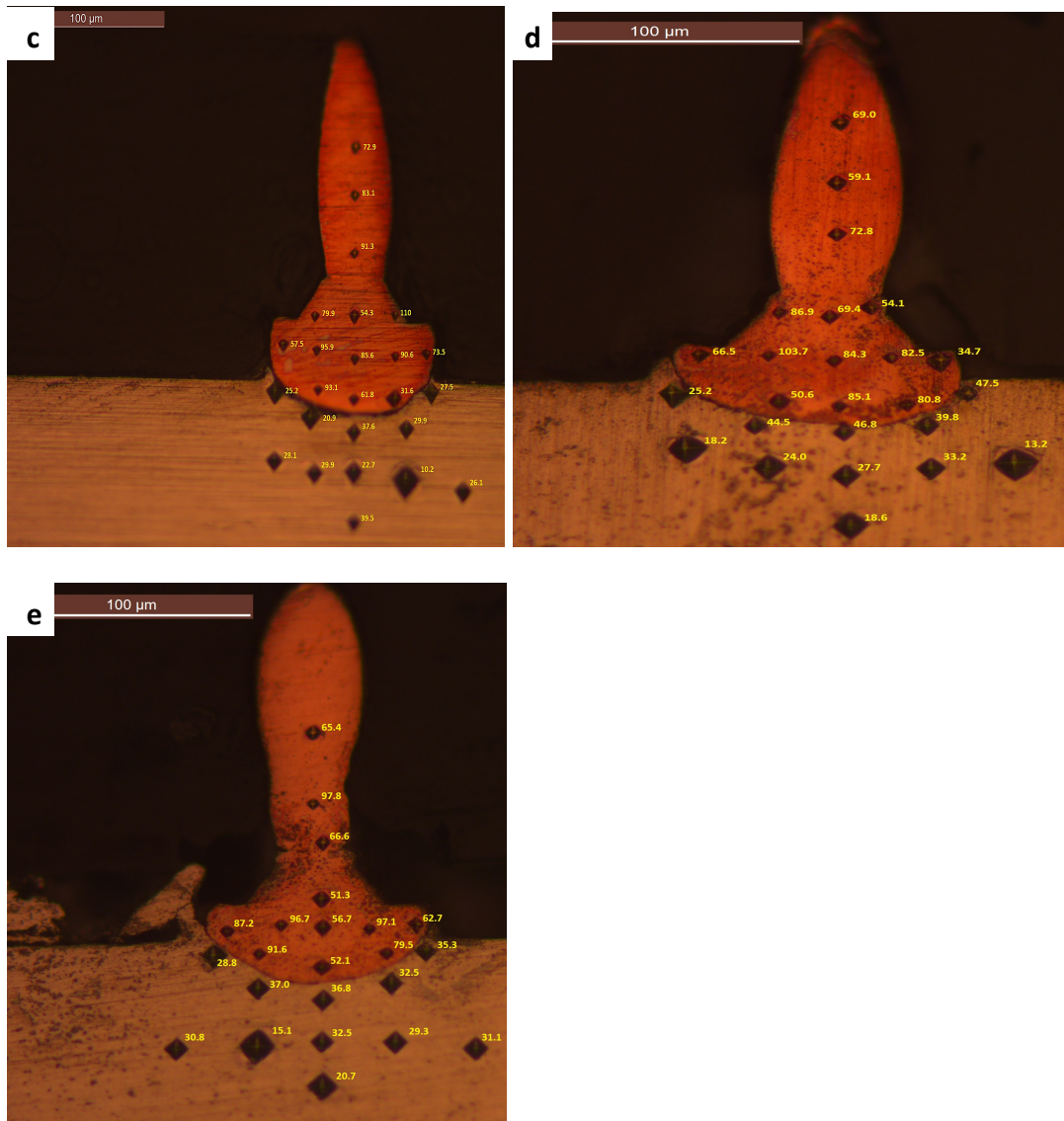


Figure 46 Micrographs showing micro indentations of all samples that are heat treated for 2 hours at 250 ° C(a) 20 ms bond duration(b) 40ms bond duration (c)60ms bond duration (d) 80ms bond duration (e)100ms bond duration.

### 4.3.2 Graphical Representation of Hardness Data for samples annealed for 2 hours

Relationship between hardness and bonding duration, for 2-hour annealed samples, is presented as plots in Figure 47 through Figure 49. Figure 47(b) can be used as a reference to identify the locations of indentation.

In Figure 47 the hardness for L1 region on Copper ball ranges from 30HV to 105HV. Pure Copper has hardness ranging from 60HV -100 HV. All the indentations reveal a hardness value within the range of pure Copper except indent 3 for 60 ms sample. Even after undergoing plastic deformation during US bonding, this region became softer instead of harder. The reason for this value could be due to presence of porosity on the Copper that results into an error in measurement or a softening effect of ultrasonic vibration due to dislocation detangling. Although all 3 indents for each of the five samples have similar property, the hardness value for most samples are very dissimilar. The reason for the hardness value being spread out for all samples could be due to microstructural inhomogeneities. Excluding all the outliers, a trend can be seen in how the hardness value changes with increase in bond duration. The overall hardness decreases from 20 ms to 60 ms samples. The hardness then starts to increase. The increase can be related to IMC formation, as have been also observed through SEM analysis.

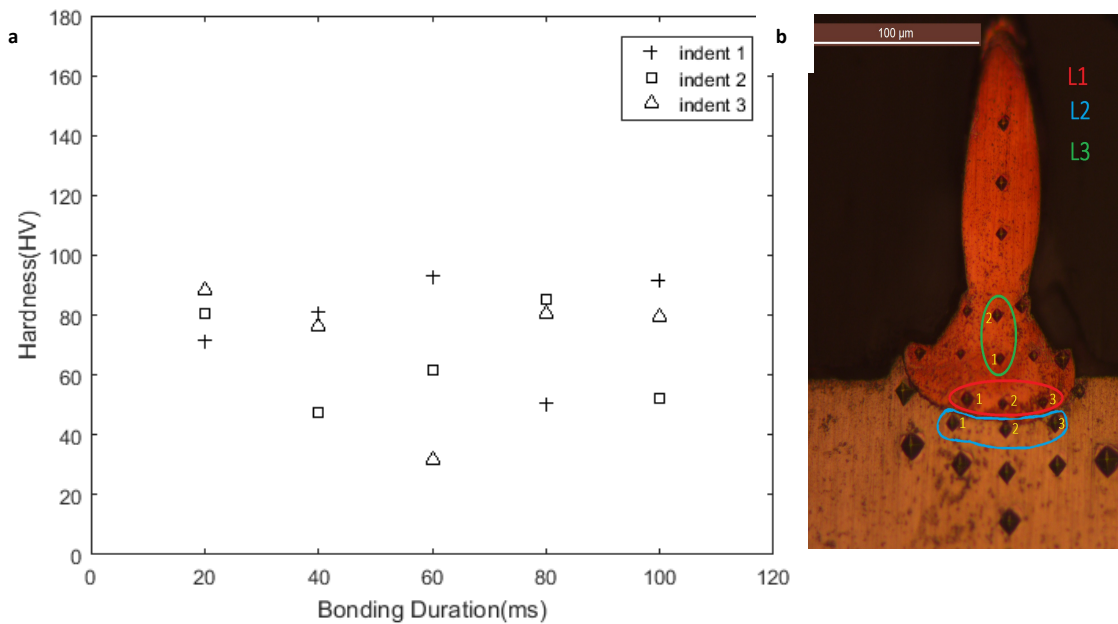


Figure 47(a) Indentation hardness results for region L1 all samples that are heat treated for 2 hours at 250 ° C (b) Indentation location map

The hardness data for L2 region is shown in Figure 48(a). The overall range for the hardness value in Aluminum is from 10HV to 50 HV. Pure Aluminum has hardness value range of 20HV-50HV. Both sample 20-250-2 and 40-250-2 has an indent each, indent 2 and indent 1 respectively, that is lower than the expected hardness of Al. The reason for this softness could be due to inhomogeneity of the Aluminum and porosities that have been detected through microscopical analysis. To properly study this, an empty Al coupon was analyzed using Secondary Electron(SE) imaging as shown in Figure 48(b). From the SE image of Al coupon, second phase Aluminum was observed and this explains some of the outlier value for Al hardness as well.

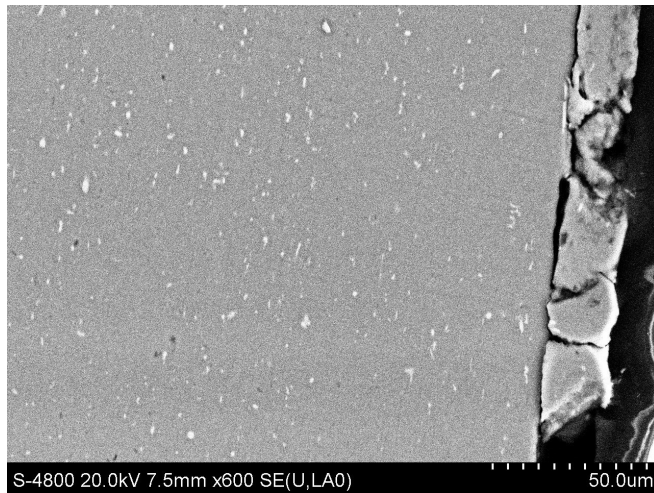
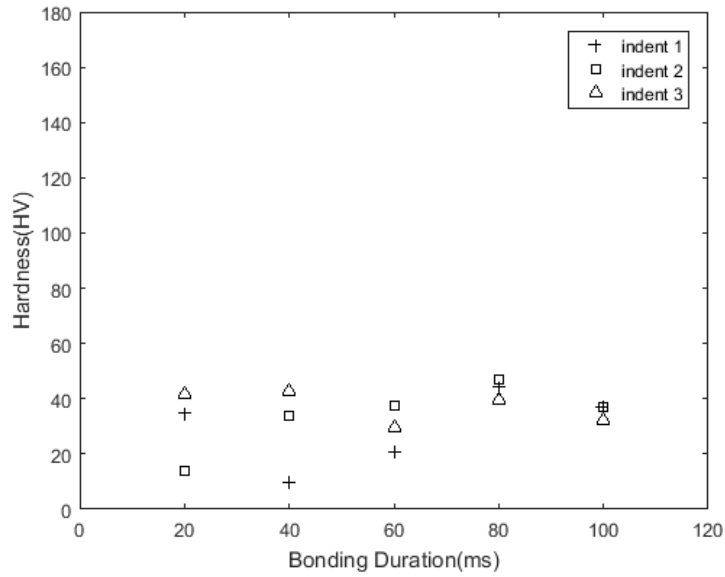
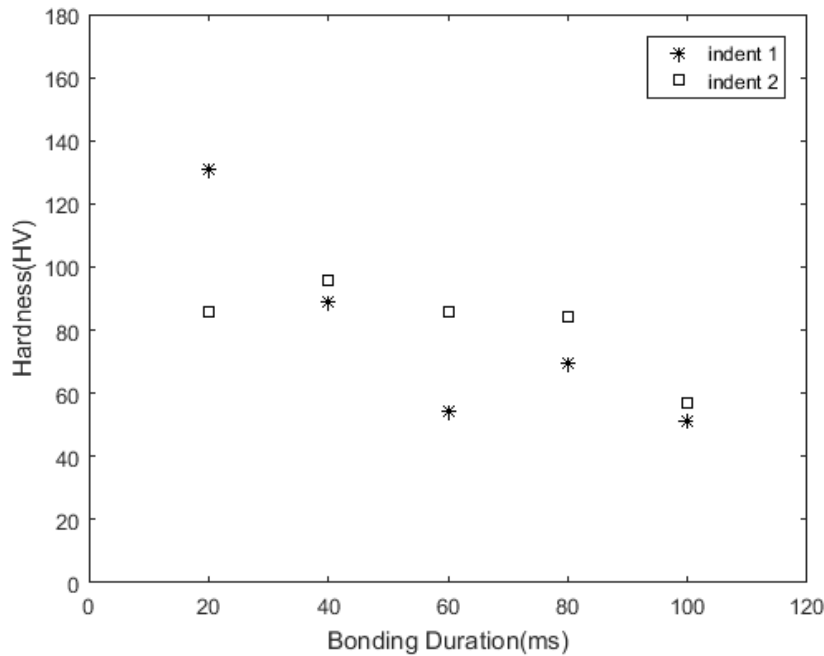


Figure 48(a) Indentation hardness results for region L2 all samples that are heat treated for 2 hours at 250 ° C. (b) Bare Aluminum coupon analyzed using SE Images.

The hardness data for L3 region is shown in Figure 49. The hardness for L3 region has a big range, between 50HV and 130HV. For indent 1 of sample 20-250-2, the hardness value is well beyond the range of HV for pure Copper. This could be due to an error in measurement. The hardness values for indent 1 and 2 across all bond duration range are also expected to be unchanged. The reason for that is L3 is away from the bond interface. Therefore, the hardness

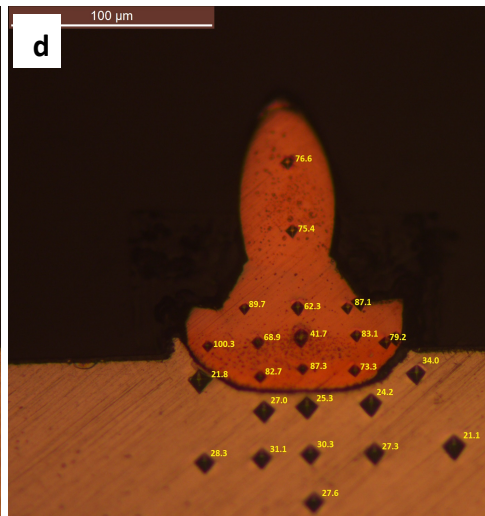
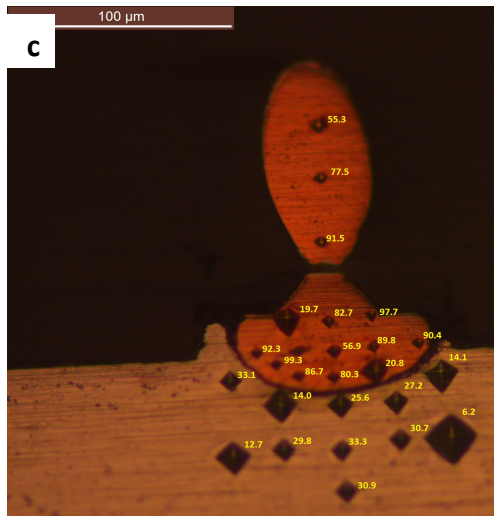
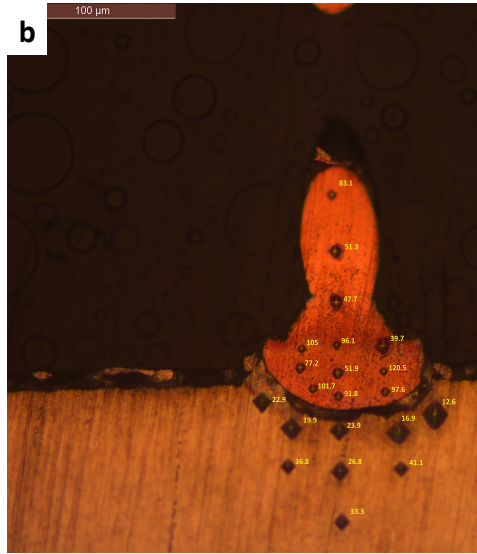
value in this region, among samples with different bond duration, should not be affected by formation of IMC or from plastic deformation. However, hardness is seen to decrease with increase in bond duration. A possible reason for the softening of Copper could be due to the softening effect of US vibration, as have also been observed in the early stages of bonding in L1 region.



*Figure 49 Indentation hardness results for region L3 all samples that are heat treated for 2 hours at 250 ° C.*

#### **4.3.3 Indentation Region for samples annealed for 4 hours**

The Micrographs in Figure 50 shows the hardness value and indentation locations of all bonds annealed for 2 hours.



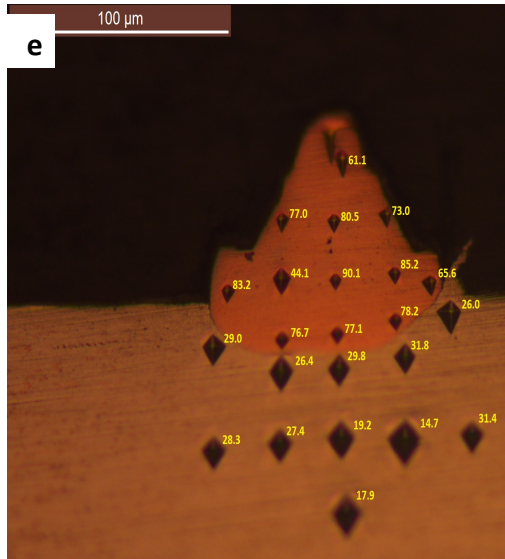


Figure 50 Micrographs showing microindentations of all samples that are heat treated for 4 hours at 250 ° C (a) 20 ms bond duration (b) 40ms bond duration (c) 60ms bond duration (d) 80ms bond duration (e) 100ms bond duration.

#### 4.3.4 Graphical Representation of Hardness Data for samples annealed for 4 hours

Figure 51 (b) can be used as a reference to identify the locations of indentation. The hardness data for region L1 has a range between 75HV to 120HV. Overall hardness for 4 hours annealed samples is greater than 2 hours annealed samples. The reason for this could be due to longer annealing time that leads to formation of larger IMC near the bond interface. Since the size of the indent is much larger than the size of the intermetallic particle, none of the indentation is expected to have same hardness as the IMC. Instead, a higher level of hardness is expected in the surrounding area of IMC, as is the case for this region. Unlike samples annealed for 2 hours, most of the hardness values of the indents also fall within a close range of each other, with the exception of indent 1 of sample 20-250-4. This shows overall higher accuracy in data



measurement for this region and the outlier could be due to an error in measurement. Excluding the outliers, the overall hardness seems to decrease for sample with higher bond duration.

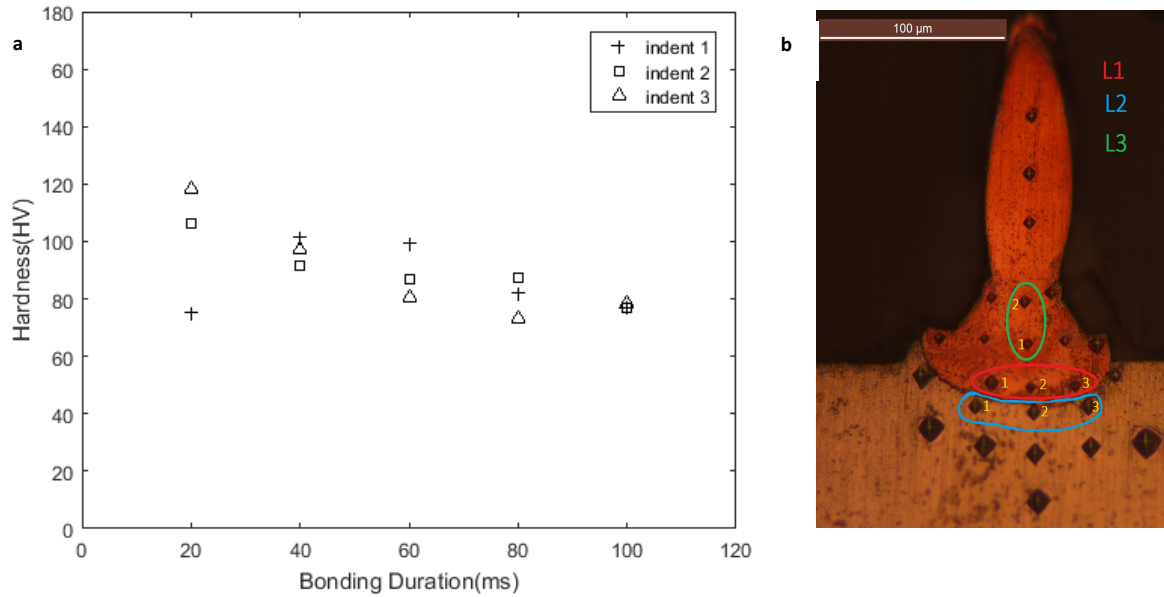


Figure 51 Indentation hardness results for region L1 all samples that are heat treated for 4 hours at 250 ° C. (b) Indentation location map

Figure 52 shows the hardness data for L2 region that has a range between 15HV to 55HV. All hardness value for sample 20-250-4 seems to be outliers for L2 region. The reason for high hardness could be due to presence of second phase Aluminum, as has been discussed earlier. The hardness values for each sample also lie within close range of each other. The overall hardness (starting from sample 40-250-4) seems to increase with increase in bond duration. This could be due to softening of the Al pad from longer exposure to US vibration.

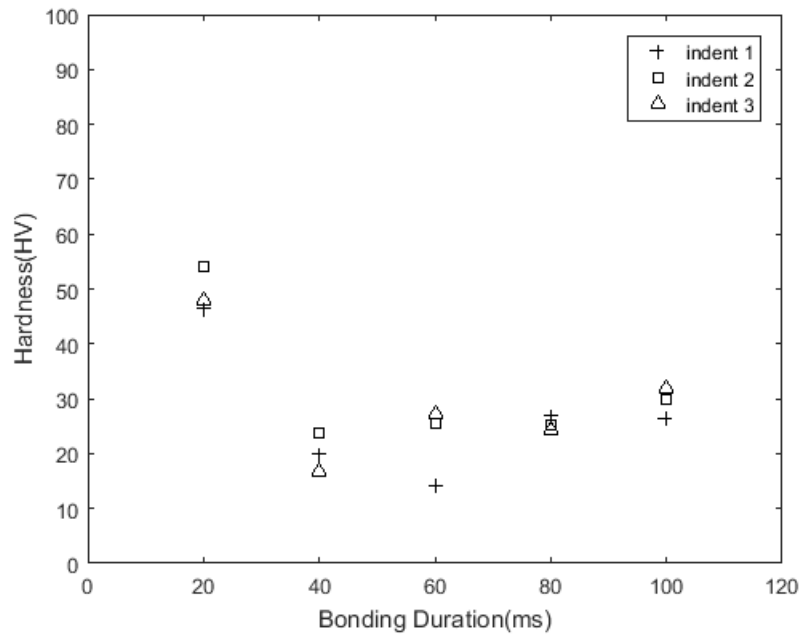
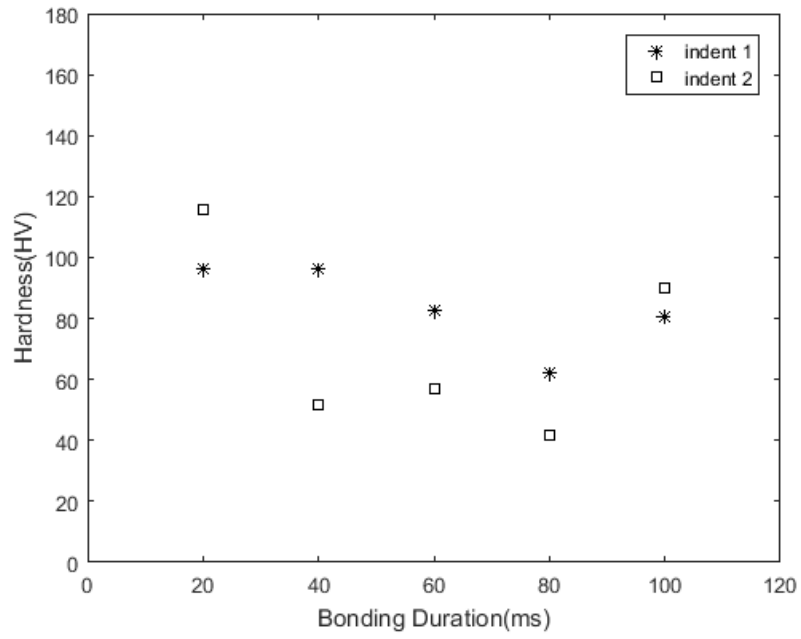


Figure 52 Indentation hardness results for region L2 all samples that are heat treated for 4 hours at 250 ° C.

Hardness plot for L3 in Figure 53 has a hardness value range between 40HV to 120HV. All values lie within the hardness value of pure Copper except sample 20-250-4. Indent 2 could be having a higher value due to possible IMC formation or higher plastic deformation. But this hypothesis is ruled out because this trend is not shared with the samples with higher bond duration, which have undergone greater plastic deformation and also have a higher chance of IMC formation. This can be considered an outlier due to measurement error. Overall hardness also seems to decrease for both indent locations of samples with 40ms, 60ms and 80 ms bond duration. The hardness then rises in value, showing possible formation of IMC.



*Figure 53 Indentation hardness results for region L3 all samples that are heat treated for 4 hours at 250 ° C.*

## CHAPTER 5: CONCLUSION

The purpose of this research is to investigate the effect of US bonding duration and annealing time on IMC formation and growth for Cu-Al wire bonds. This was to be done by quantitative analysis of Copper-Aluminum bonds with different bond duration to see impact of bonding duration on IMC formation. A set of samples, with bond duration ranging from 20 ms to 100 ms, was chosen. Due to the difficulty in measurement of IMC thickness in the bonded samples, all samples being analyzed were heat-treated to ensure formation of IMC. The samples were heat treated at 250 ° C for 2 and 4 hours. Three different characterization methods were used to confirm the presence of IMC layers: BSE detectors were used to measure IMC based on contrast in micrographs, EDS was used for compositional analysis, and indentation test were used to look for regions with higher hardness similar to IMC layers.

BSE imaging and measurement was done as a preliminary method to identify and measure regions of IMC based on difference in contrast in the image. The IMC layer detected on some samples showed an increase in growth with increase in bond duration and annealing time. Using the EDS interface, linescans were then performed on the same region where IMC were visually detected after BSE imaging. Using linescan intensity plot, the thickness of IMC was then measured. IMC layer was detected in both 2 hours as well as 4 hour samples. EDS scans followed the same trend as BSE images, showing IMC thickness increasing with ultrasonic bond time and annealing. Indentation was then performed on those regions to measure hardness values. Plotted results of hardness vs bond duration showed that hardness in Copper directly proportional to increase in US duration as well as annealing times. This was related to formation of IMC. In Aluminum, hardness increased with increase in US duration possibly due to IMC

formation. Aluminum hardness decreased in hardness with annealing time increased due to softening caused by annealing.

### **5.1 Future work and Improvement**

For future research on Cu-Al bond, the following processes can be used to improve results:

1. In order to prevent charging issue, epoxy resin may be avoided to mount samples. Instead ion milling can be used to prepare samples and then take cross sectional images of the bond interface
2. 2-hour samples could be first analyzed and then annealed further to examine the growth in the existing IMC
3. Better grinding tool to prevent sample damage.
4. Using better SEM tools so that samples can be zoomed to a higher magnification and EDS point ID scans can be performed for compositional analysis

This research work has laid the foundation to perform hardness analysis on Copper-Aluminum ball bonds. Since hardness of Copper is a major concern when using it in wire bonding, it will be interesting to study this topic in more details using techniques that allow investigating hardness evolution is smaller scales.

## REFERENCES

- [1] Harman, George G. "1." *Wire Bonding in Microelectronics*. 3rd ed. New York: McGraw-Hill, 2010. N. pag. Print.
- [2] Chen, Andrea, and Randy Hsiao-Yu Lo. "7." *Semiconductor Packaging: Materials, Interaction and Reliability*. Boca Raton: CRC, 2012. N. pag. Print.
- [3] Chauhan, Preeti S. "1." *COPPER WIRE BONDING*. Place of Publication Not Identified: Springer-Verlag New York, 2016. 3-5. Print.
- [4] Schneider-Ramelow, Martin, Ute Geißler, Stefan Schmitz, Wolfgang Gräßl, and Bernhard Schuch. "Development and Status of Cu Ball/Wedge Bonding in 2012." *Journal of Electronic Materials* 42.3 (2013): 558-95. Web.
- [5] Wulff, F.w., C.d. Breach, D. Stephan, Saraswati, and K.j. Dittmer. "Characterisation of Intermetallic Growth in Copper and Gold Ball Bonds on Aluminium Metallization." *Proceedings of 6th Electronics Packaging Technology Conference (EPTC 2004) (IEEE Cat. No.04EX971)* (n.d.): n. pag. Web.
- [6] Xu, H., C. Liu, V. V. Silberschmidt, M. Sivakumar, and Z. Chen. "Effect of Ultrasonic Energy on Interfacial Structure and Bond Strength in Copper Wire Bonding." *2010 Proceedings 60th Electronic Components and Technology Conference (ECTC)*(2010): n. pag. Web.
- [7] Drozdov, M., et al. "Detailed Investigation of Ultrasonic Al-Cu Wire-Bonds: II. Microstructural Evolution during Annealing." *Journal of Materials Science*, vol. 43, no. 18, 2008, pp. 6038–6048., doi:10.1007/s10853-008-2955-9.

- [8] Xu, Hui. "Thermosonic Ball Bonding: a Study of Bonding Mechanism and Interfacial Evolution." *Loughborough University Institutional Repository*, Loughborough University, 2010. *Research Student Office*.
- [9] Shah, Aashish Satish. "Mechanical and Tribological Aspects of Microelectronic Wire Bonding." *University of Waterloo*, 2010.
- [10] Yan, Tian-Hong, et al. "Design of a Smart Ultrasonic Transducer for Interconnecting Machine Applications." *Sensors*, vol. 9, no. 6, 2009, pp. 4986–5000., doi:10.3390/s90604986.
- [11] Funamizu, Y and K Watanabe. "Interdiffusion in the Al-Cu system." 12 (1971): 147-152.
- [12] Porter, David A., Kenneth E. Easterling and Mohamed Sherif. *Transformation in Metals and Alloys*. Third. Boca Raton: CRC Press, 2009. Print.
- [13] Callister, Jr, William D. and David G. Rethwisch. *Materials Science and Engineering*. 9. Wiley, 2013. Print.
- [14] Kim, Hyoung-Joon, et al. "Effects of Cu/Al Intermetallic Compound (IMC) on Copper Wire and Aluminum Pad Bondability." *IEEE Transactions on Components and Packaging Technologies*, vol. 26, no. 2, 2003, pp. 367–374., doi:10.1109/tcapt.2003.815121.
- [15] Tan, Yik Yee, et al. "Growth and Reactivity of Al-Cu Intermetallic Compounds under Ideal Conditions." *2015 IEEE 65th Electronic Components and Technology Conference (ECTC)*, 2015, doi:10.1109/ectc.2015.7159781.
- [16] Paul, Aloke. "Chapter 5." *Thermodynamics, Diffusion and the Kirkendall Effect in Solids*, Springer, Cham, Switzerland, 2014, pp. 167–170.

- [17] Pelzer, Rainer, et al. "Growth Behavior and Physical Response of Al-Cu Intermetallic Compounds." *2014 IEEE 16th Electronics Packaging Technology Conference (EPTC)*, 2014, doi: 10.1109/eptc.2014.7028259.
- [18] Murali, S, et al. "Grains, Deformation Substructures, and Slip Bands Observed in Thermosonic Copper Ball Bonding." *Materials Characterization* , 2003, pp. 39–50., [www.sciencedirect.com/science/article/pii/S1044580303001025](http://www.sciencedirect.com/science/article/pii/S1044580303001025). Accessed 20 Jan. 2017.
- [19] Tian, Yanhong, et al. "Evolution of Cu/Al Intermetallic Compounds in the Copper Bump Bonds during Aging Process." *2007 8th International Conference on Electronic Packaging Technology*, 2007, doi:10.1109/icept.2007.4441444.
- [20]. Xu, H., V.V. Silberschmidt, C. Liu, M. Sivakumar, Z. Chen, and J. Wei. "Effect of Bonding Duration and Substrate Temperature in Copper Ball Bonding on Aluminium Pads: A TEM Study of Interfacial Evolution." *Effect of Bonding Duration and Substrate Temperature in Copper Ball Bonding on Aluminium Pads: A TEM Study of Interfacial Evolution*. Elsevier, 15 May 2010. Web. 29 Mar. 2016. <[www.elsevier.com/locate/microrel](http://www.elsevier.com/locate/microrel)>.
- [21] Xu, H., et al. "A Micromechanism Study of Thermosonic Gold Wire Bonding on Aluminum Pad." *Journal of Applied Physics*, vol. 108, no. 11, 2010, p. 113517., doi:10.1063/1.3514005.
- [22] Langenecker, B. "Effects of Ultrasound on Deformation Characteristics of Metals." *IEEE Transactions on Sonics and Ultrasonics*, vol. 13, no. 1, 1966, pp. 1–8., doi: 10.1109/t-su.1966.29367.



- [23] H. Xu, C. Liu, V. V. Silberschmidt, S. S. Pramana, T. J. White, and Z. Chen, "A reexamination of the mechanism of thermosonic copper ball bonding on aluminum metallization pads," *Scripta Materialia*, vol. 61, pp. 165–168, Jul 2009.
- [24] Hang, C.j., et al. "Growth Behavior of Cu/Al Intermetallic Compounds and Cracks in Copper Ball Bonds during Isothermal Aging." *Microelectronics Reliability*, vol. 48, no. 3, 2008, pp. 416–424., doi:10.1016/j.microrel.2007.06.008.
- [25] Hui, Xu.,Liu, Changqing., Silberschmidt, V.V., Chen, Zhong., et al. "Growth of Intermetallic Compounds in Thermosonic Copper Wire Bonding on Aluminum Metallization." *Journal of Electronic Materials*, vol. 39, no. 1, 2009, pp. 124–131., doi:10.1007/s11664-009-0951-8.
- [26] Kouters, M.h.m., et al. "Characterization of Intermetallic Compounds in Cu-Al Ball Bonds: Mechanical Properties, Delamination Strength and Thermal Conductivity." *2012 13th International Thermal, Mechanical and Multi-Physics Simulation and Experiments in Microelectronics and Microsystems*, 2012, doi:10.1109/esime.2012.6191740.
- [27] "IConnPS High Performance Wire Bonder." *Kulicke & Soffa Products*. N.p., n.d. Web. 20 Oct. 2016. <<http://www.kns.com/enus/Pages/IConn.aspx?kns=TLFQStL4sfpp%2B18m5g2LJN4dyqqdm73wHCZ7c%2B5eNYTKum6GSSTqfw%3D%3D>>.
- [28] "IsoMet® 1000 Precision Cutter." *IsoMet® 1000 Precision Cutter | Buehler*. N.p., 09 Sept. 2011. Web. 11 Oct. 2016. <<https://shop.buehler.com/equipment/sectioning-equipment/precision-diamond-wafering-cutters/isomet-1000-precision-cutter>>.
- [29] "MIRA3." *Tescan*. N.p., n.d. Web. 11 Oct. 2016. <<http://www.tescan.com/enus/technology/sem/mira3>>.

## APPENDIX A: Effect of annealing time on hardness evolution

The effect of annealing is compared with changes in hardness for all samples. The following plots in Figure 54 through Figure 58 compares hardness vs annealing time for regions L1 and L2. Region L3 is omitted because no IMC formation occurs in that region. Therefore, effect of annealing time on hardness of L3 is limited to annealing phenomena that happens in the system, and this does not relate to this thesis. Figure A.1, to A.5 show hardness data for regions L1 and L2 of the samples bonded for 20ms, 40ms, 60ms, 80ms, and 100ms.

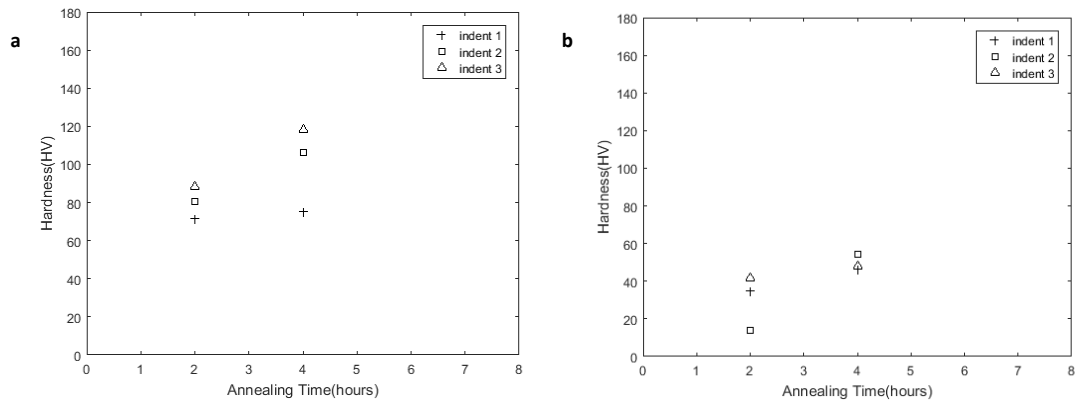


Figure A. 1 Plot showing relationship between hardness vs annealing for all 4 regions of samples 20-250-2 and 20-250-4(a) Region L1 (b) Region L2.

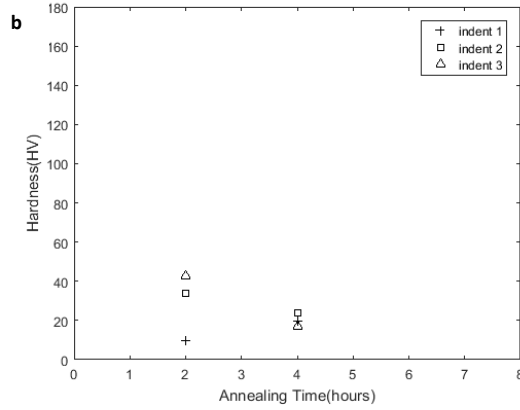
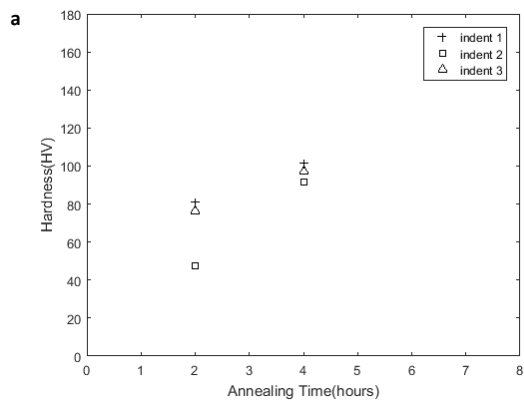


Figure A. 2 Plot showing relationship between hardness vs annealing for all 4 regions of samples 40-250-2 and 40-250-4(a) Region L1(b) Region L2.

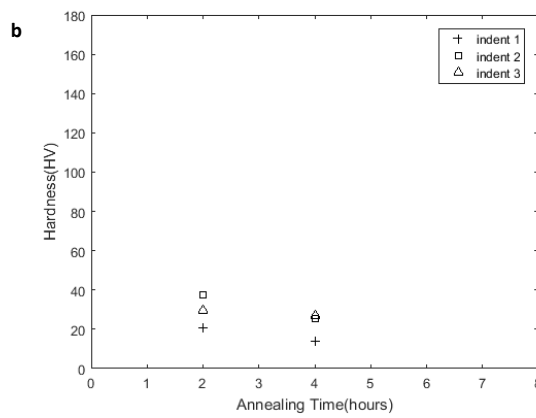
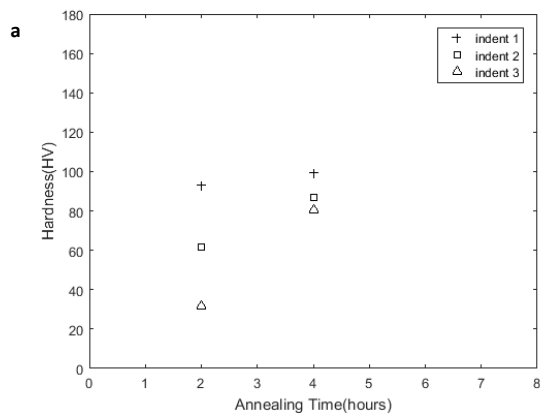


Figure A. 3 Plot showing relationship between hardness vs annealing for all 4 regions of samples 60-250-2 and 60-250-4(a) Region L1(b) Region L2.

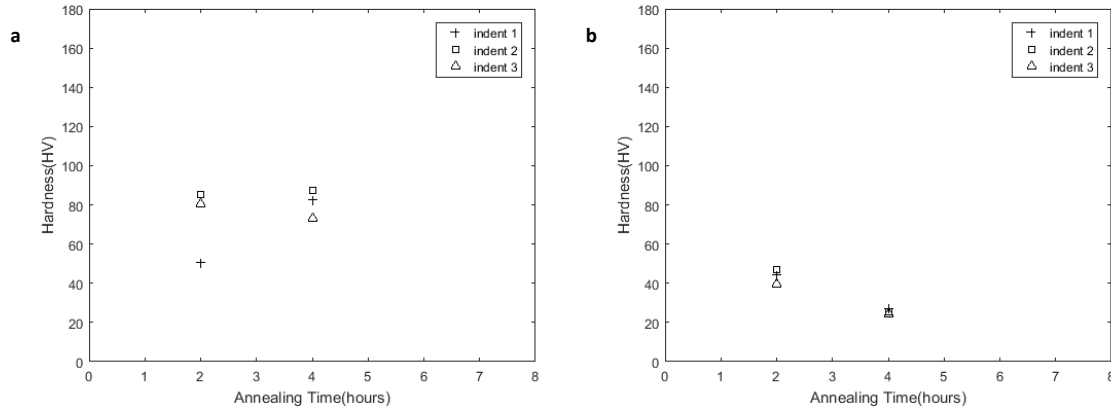


Figure A. 4 Plot showing relationship between hardness vs annealing for all 4 regions of samples 80-250-2 and 80-250-4(a) Region L1 (b) Region L2.

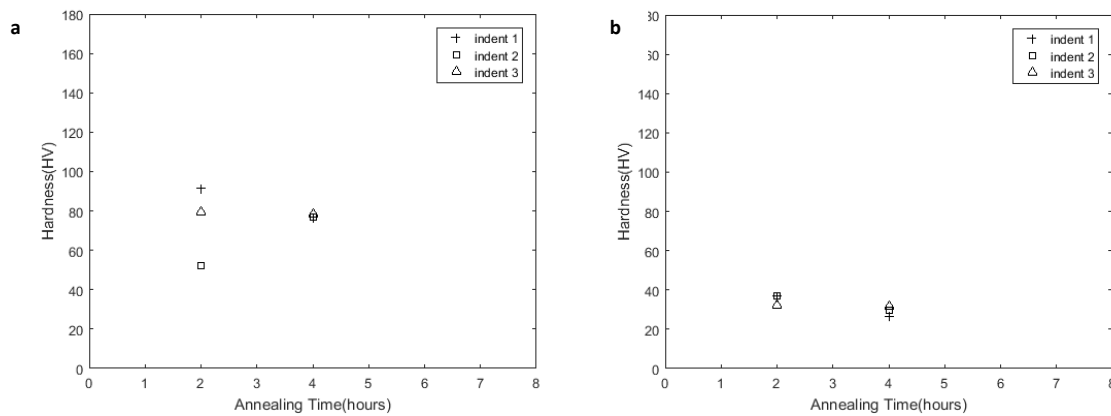


Figure A. 5 Plot showing relationship between hardness vs annealing for all 4 regions of samples 100-250-2 and 100-250-4(a) Region L1 (b) Region L2.

For regions L1 hardness increases as annealing time increases for all ultrasonic bond durations. L1 region is close to the bonding interface and so this increase can be related to IMC growth. SEM/EDS analysis done on these samples has shown an increase in IMC growth with increase in annealing time. Presence of IMC can increase the hardness in a metal and as the IMC region

grows, so does regions with higher hardness. This explains why hardness increases as a function of annealing time in this region.

For L2 region, with the exception of samples with 20ms bond duration, hardness decreases as annealing time increases for all samples. Changes in hardness in this case can be attributed to two phenomena happening concurrently, IMC growth, which causes increase in hardness and softening of metal that results during annealing process. Aluminum has a melting temperature of around 660 °C and Copper has a melting temperature of 1,085°C. Annealing temperature of 250 °C is about 0.4 of the melting temperature of Al whereas it is about 0.25 the melting temperature of Cu. Therefore, it is expected that annealing temperature would have a more dominant effect in Al region compared to Cu region. While formation and growth of IMC causes L1 region of Copper to increase in hardness, Al becomes softer with more annealing as is evident from the trend in plots (except for 20ms sample). From previous SEM and EDS analysis, 20 ms showed very small IMC formation as a result of annealing. Although softening also occurred, there is a possibility that the growth of IMC lead to an overall increase in hardness.